UNIVERSITÀ DEGLI STUDI DI MILANO

Corso di Dottorato in Chimica Industriale – XXIX ciclo

DESIGN, SYNTHESIS AND CHARACTERIZATION OF MAGNETIC BIO-INORGANIC NANOSYSTEMS WITH THERANOSTIC FEATURES

Tesi di Dottorato di:

Sara Mondini

Matricola R10574

Tutor: Prof.ssa Alessandra Puglisi

Co-tutor: Dott. Alessandro Ponti

Anno accademico 2015-2016

Ai miei genitori, Carmen e Giuliano

"Whatever you can do or dream you can, begin it.

Boldness has genius, power and magic in it!"

Johann Wolfgang von Goethe

TABLE OF CONTENTS

o Abstract

The aim of my PhD project is to obtain magnetic bio-inorganic nanosystems having both diagnostic and therapeutic functions. We have focused our attention on magnetic nanoparticles (NPs) since their properties allow to use them in diagnosis, as good MRI contrast agents and in therapy, as colloidal mediators for hyperthermia or carriers for drug delivery. Furthermore, their diagnostic properties could also allow one to monitor the response to therapy.

However, to achieve active targeting of magnetic nanocrystals in medical applications, we need to study in detail their interactions with biological systems. Indeed, when nanoparticles are injected into the bloodstream (we consider the parenteral administration because all cells receive supplies thanks to the blood circulation), circulating plasma proteins, opsonins, adsorbe on the NP surface forming a layer known as protein "corona". Such protein layer is recognized by the cells of the mononuclear phagocyte system (MPS), which remove the NPs from the blood by phagocytosis. Usually, the MPS concentrates the NPs in organs such as the liver and the spleen and prevents the NPs to reach their target. For this reason, one must rationally design nanosystems minimizing or delaying their internalization by MPS cells in order to increase their plasma half-life and consequently the ability to reach the desired organ/tissue by active targeting. Such NPs are known as "stealth NPs". The NP surface properties appear as more important than those of the core to escape phagocytosis, because the coating is in direct contact with blood and organs. In particular, during my PhD I have explored some examples of the two types of NP coating that, until now, have been mainly studied to prevent protein adsorption: the "conventional" polyethylene glycol (PEG) ligands and recently introduced small zwitterionic surfactants.

Therefore, in the first part of my PhD thesis, we reported on magnetic iron oxide NPs coated with zwitterionic dopamine sulfonate (ZDS), containing a sulfobetaine group that we have chosen among the zwitterionic groups used in nanomedicine. We have compared these NPs to similar NPs coated with PEG-like 2-[2-(2-methoxyethoxy)ethoxy]acetic acid (MEEA) to investigate how surface chemistry affects the NP in vitro behavior. ZDS-coated NPs showed a very dense coating, that ensures high colloidal stability to the nanosystems in several aqueous media and negligible interaction with proteins. Treatment of HepG2 cells with increasing concentrations (from 2.5 up to 100 μg Fe/ml) of ZDS-NPs had no effect on cell viability and resulted in a low, dose-dependent NP uptake, lower than most reported data for the uptake of iron oxide NPs by HepG2 cells. Conversely, MEEA-coated NPs showed lower ligand density and formed micrometer-sized aggregates in deionized water. Such NPs had a cytotoxic effect for dose ≥ 50 μg Fe/ml, and were about 20-fold

more efficiently internalized than ZDS-coated NPs. We could conclude that the high-density ZDS layer prevented the biocorona formation and both aggregation and sedimentation of iron oxide NPs. Moreover, the very low internalization of ZDS-coated iron NPs inside HepG2 cells could be useful to achieve an active targeting upon specific functionalization. We have also explored the intracellular fate of ZDS-coated NPs, demonstrating that in HepG2 cells they are sent to the lysosomial pathway.

The second part of this Thesis concerned NPs coated with PEGylated ligands. Considering the well-known ability of the catechol (1,2-dihydroxyphenyl) group to bind iron ions with high affinity and give stable NP water dispersion, we chose this grafting group for our NP ligands based on a PEG 5000 polymer chain. We would also functionalize magnetic NPs with a large biomolecule, the Fab fragment of Trastuzumab (Herceptin®), that is a monoclonal antibody selectively binding the human epidermal growth factor receptor 2 (HER2), hoping in this way to endow the nanoparticles with active targeting functionality because the antibody fragment strongly binds to its antigen.

Therefore, we have designed different catechol molecules: (i) a bi-functional PEG ligand displaying a maleimide end-group able to react with the free thiol group of the Fab biomolecule; (ii) mono and bi-dentate OMe-terminated PEG ligands in order to employ them as co-surfactants to dilute the maleimide ligand, making the active molecule less sterically hindered while preserving water solubility and colloidal stability of the system. With poly-dentate structures, we wished to have an improvement in NP water stability by increasing the number of grafting groups per molecule and so decreasing the probability that a ligand is irreversibly lost from the NP surface. Such structures are based on ethylenediamine as a linker between the hydrophilic PEG chain and the catechol grafting groups. The PEG chain is linked to one of amine groups of the scaffold and the other amine group is linked to one or two 3,4-dihydroxybenzyl groups.

We chose to link the PEG chain to the central ethylenediamine scaffold as the last reaction step by coupling it to the mono- or di-catechol-diamine moiety since the isolation and characterization of the intermediate products are simplified. We have tested some protecting groups for catechol moieties such as tert-butyldimethylsilyl (TBDMS) ether or acetonide, but we have found that both these protecting groups might be – at least partially – deprotected in our reaction conditions. So we finally tried the benzyl ether protecting group, more stable in our reaction conditions since it is removed by hydrogenation. In addition to these synthetic studies, which are still in progress, I prepared and characterized two batches of iron oxide NPs coated with a mixture of the catechol-PEG-maleimide and catechol-PEG-OMe ligands. I synthesized one batch of NPs by solvothermal method, while the other batch was produced by alkaline co-precipitation from a stoichiometric

aqueous solution of $FeCl_3$ and $FeSO_4$. Solvothermal NPs are highly monodisperse and crystalline, whereas co-precipitated NPs can be produced in larger amount and in "green conditions", minimizing the use of toxic reagents, and are free from coating ligands. In both cases, the final yield in water soluble NPs was around 50%. Indeed, the two batches of NPs were coated by different amount of PEG ligands; the coating was more efficient for NPs produced by co-precipitation as evaluated by CHN analysis. Finally, having the aim to functionalize the nanosystems with the Fab fragment of Trastuzumab, I have quantified the reactivity of maleimide groups of the bi-functional linker present in the NP coating. In particular, I carried out such quantification with a commercially available fluorescent kit able to measure protein maleimide groups. By comparison with a shorter maleimido PEG (molecular weight ≈ 2000 Da), I concluded that this moiety was less reactive in the longer PEG5000 chain. However, a fraction of maleimide group exposed at the NP surface was actually reactive and sufficient to functionalize the NCs with the desired amount of anti-body fragment.

Therefore, both ZDS and PEGylated NPs could be considered promising in the development of theranostic nanosystems.

o Introduction

A possible definition of "nanomedicine" is "the application of nanotechnology (the engineering of materials with sizes in the nanometer range) in a healthcare environment, with the aim to prevent and treat diseases in the human body".

In general, a favorable prognosis is closely correlated to the detection and treatment of illness at an early stage of development. Therefore, huge efforts have been made by biomedical researchers in order to improve the sensitivity and accuracy of imaging techniques and the efficacy of medical cares. Recently, nanotechnologists have designed a variety of theranostic nanosystems, where the word "theranostic" was coined by Funkhouser[1] in 2002 to define a material that combines *thera*peutic and dia*gnostic* modalities within a single platform.

These nanosystems can be composed of either organic or inorganic materials.

Organic platforms comprise polymer-drug conjugates[2] such as poly(lactic-co-glycolic acid) (PLGA) nanoparticles[3], polymeric micelles[4], liposomes[5], high-density lipoproteins[6] and dendrimers and are mainly used for drug delivery and gene therapy. In these cases, the drug or the gene are entrapped, fixed, adsorbed, or enclosed into or onto the nano-matrices. Such systems increase drug efficacy and are less toxic with respect to traditional drugs, so several of them are being tested in clinical trials thanks to promising pre-clinical results such as those obtained using INGN-401, a liposomal formulation to deliver a cancer-suppressing gene against metastatic lung cancer. In some cases, organic nanosystems have already reached the market as Doxil®, a liposomal system to deliver doxorubicin for the treatment of patients with ovarian cancer, AIDS-related Kaposi's sarcoma, and multiple myeloma.

If we compare organic and inorganic nanoparticles (NPs), the latter are characterized by peculiar physical properties that often are different from those of the bulk materials, thanks to (quantum) size effects. For example, quantum dots (QDs)[7-8], dye-doped silica NPs[9], and upconverting NPs[10] are very useful NP fluorescent markers thanks to their advantageous features arising from quantum confinement effects at the nanometric scale. The ferrimagnetic iron oxides, *i.e.*, magnetite or maghemite, having diameter < 30 nm are in the so-called superparamagnetic regime, where their permanent magnetization changes orientation very rapidly, thus featuring appealing relaxation properties for use a MRI contrast agents..

In particular, we decided to focus our attention on magnetic NPs considering that, excluding humans whose body contains magnetizable material (such as medical devices with batteries or computer chips, vascular or intracranial metals), magnetic fields are not contraindicated for patients[11] and since, due to their special features, magnetic NPs appear as ideal platform materials for theranostics[12-13-14].

First, magnetic nanocrystals (NCs) can be synthesized with controlled size that normally is in the range from few nanometers up to tens of nanometers. They thus are smaller than cells (10-100 μm), larger than most organic molecules, and similar in size to viruses (20-450 nm) and biological macromolecules such as proteins (5-50 nm), and genes (2 nm wide and 10-100 nm long), as depicted in Fig 1[15]. For this reason, magnetic NPs can interact with biological objects, labeling them and potentially taking part in metabolic processes.

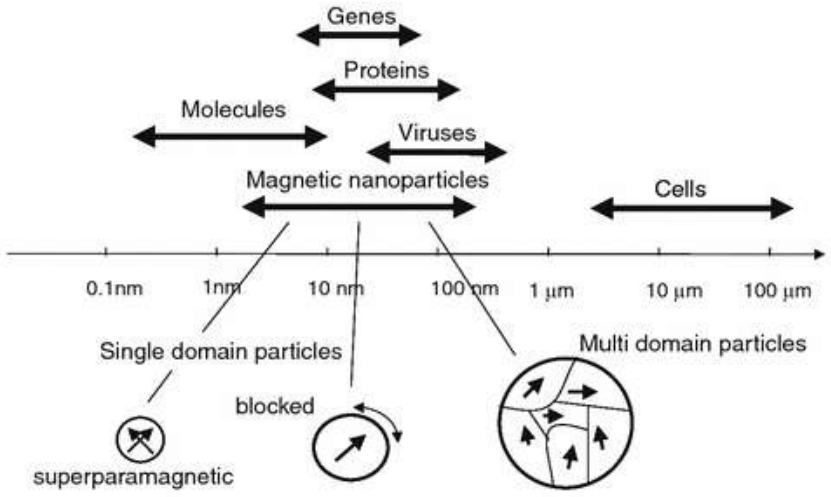

Fig 1. Comparison between the dimensions of magnetic nanoparticles and biological entities. Image from Ref 15.

Second, both the magnetic NP core and shell can be made of non-toxic material. For example, iron oxide NPs are usually employed in biomedical field for their biological compatibility. Moreover, in addition to biocompatibility, other functions can be inserted in their tailor-made surface coating, such as the ability to prevent the formation of the protein "corona", selectively bind to a specific biological entity or deliver compounds and drugs to defined sites.

Third, the permanent magnetic moment of magnetic NPs provides further functionalities. The above mentioned superparamagnetism makes magnetic NPs excellent MRI contrast agents because they strongly contribute to the relaxation of the hydrogen spins in water molecules. Furthemore the NP magnetic moment can be manipulated using an externally applied magnetic field. For instance, a magnetic field gradient can be used to separate NPs or localize them in particular regions of the body. Another example is based on the interaction of the magnetic NPs with an alternating magnetic

field (radiofrequency) which heats the NPs and can then be exploited in the field of hyperthermic therapy.

Magnetic NPs for separation devices

A magnetic field gradient can exert a force at a distance adequate to move magnetic NPs tagged, at their external coating, with molecules or biological entities which in this way could be separated from their native medium. Such magnetic separation can be obtained by passing the fluid mixture through a region where a magnetic field gradient immobilizes the magnetic NPs. In this simple device (Fig 2[12]) a magnet fixed to the container wall of a solution can collect the tagged particles, while the unwanted supernatant solution is removed.

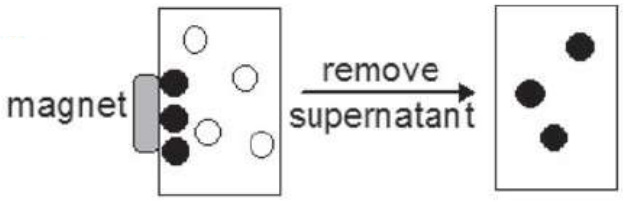

Fig 2. Standard method of magnetic separation of magnetically tagged (•) and unwanted (◦) biomaterials. Image from Ref 12.

The main limitation of this simple technique is the slow accumulation rates of the tagged NPs. Therefore other more complex magnetic separation devices are developed.

Magnetic NPs as colloidal mediators for hypertermia

In addition, an alternating magnetic field of sufficient strength and suitable frequency can permeate human target tissues and transfer energy to magnetic NPs, in order to heat them up. The environment close to the NPs is also heated by thermal conduction. This principle allows one to use NCs as agents for magnetic fluid hyperthermia, providing a promising therapeutic solution to the homogeneous treatment of deep or scattered cancers. In fact, hyperthermia is used to destroy malignant cells[11] in combination with other cancer therapy such as chemo- and/or radio-therapy since its local application can reduce side effects of treatment, such as systemic effects. The temperature is maintained in the range of 42-45 ˚C for 30 min or more, because it is known that tumor cells are more sensitive to temperature in this range than normal tissue cells. Magnetic NPs are appealing agents since they allow clinicians to heat only the target tissue (Fig 3) without damage of surrounding healthy cells.

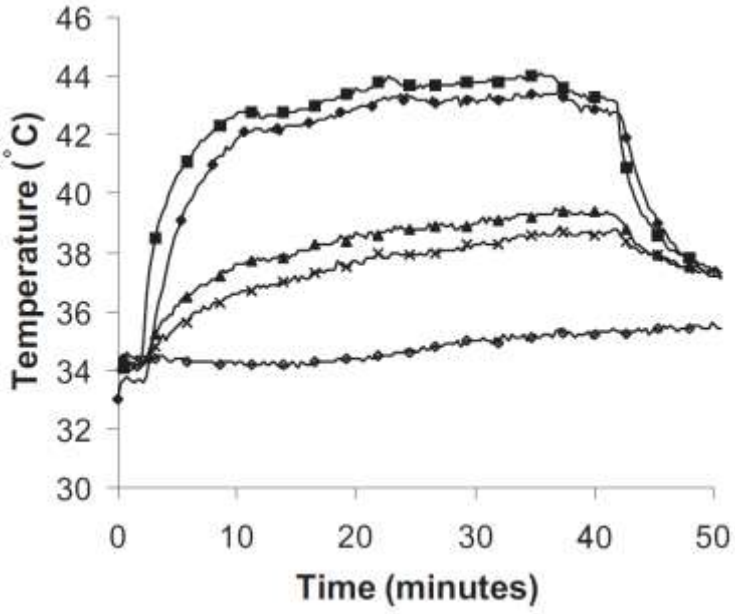

Fig 3. Animal trial data on hyperthermia treatments in rabbits,showing preferential heating of a tumour using intra-vascularly infused ferromagnetic microspheres; (■) tumour edge, (♦) tumour centre, (▲) normal liver 1–2 cm from tumour, (×) alternative lobe, and (◊) core body temperature. Image from Ref 12.

There are different types of hyperthermia depending on the size of the heated body part. In *local* hyperthermia heat is applied to a small area while in regional hyperthermia a large tissue portion (such as a body cavity or organ) is heated; whole-body hyperthermia is used to treat metastatic cancer that has spread throughout the body. The efficacy of hyperthermia therapy is connected to the temperature achieved during the treatment, as well as to the duration of treatment and cell and tissue features. To ensure that the desired temperature is reached without excess heating, the temperature of the tumor and surrounding tissue is monitored during the treatment by thermometers inserted inside small needles or tubes. Many clinical trials are being managed to evaluate the efficacy of hyperthermia. Magnetic hyperthermia is a promising type of hyperthermia which exploits the ability of small magnetic particles to strongly absorb electromagnetic radiation in the radiofrequency-microwave range and to transform it into heat. Magnetic hyperthermia is effective since radiofrequency-microwave easily penetrate tissue, well localizable (magnetic particles can be located in the region to be treated) and free from radiation-related side effects. Magnetic hyperthermia is currently in clinical use. MagForce is a company founded in 1997 that has launched in 2011 the first and only nanotechnology-based therapy (NanoTherm™) currently having the European regulatory approval (CE conformity marking) for the treatment of brain tumors. As

clearly described on their website, NanoTherm™ therapy employs magnetic NPs as elements able to absorb electromagnetic radiation, . in particular NPs with size of 15 nm, coated by aminosilane which endows them with water-solubility. These NPs, once introduced by injection into a solid tumor, remain in the cancerous tissue for some time and act as transducers, able to convert the energy coming from the alternating magnetic field applicator, the NanoActivator®, into heat. NanoActivator® devices (Fig 4) are installed in hospitals in Berlin, Münster, Kiel, Cologne and Frankfurt. can be used for tumors in all regions of the body. Indeed, NanoTherm® Therapy was already clinically tested on approximately 90 patients with brain tumors and about 80 patients with other tumors such as pancreatic, prostate or esophageal cancer.

Fig. 4. NanoActivator® (from http://www.magforce.de/en/produkte/nanothermr.html).

Magnetic NPs for drug delivery

In cancer therapy, magnetic NPs can be also coupled with targeting agents and therapeutic drugs, with the aim to enhance treatment specificity and to reduce general side effects of chemotherapies. Therefore, they are used as magnetic carriers to transport and release the active molecule at the desired tissue. For example, iron oxide NPs covalently conjugated with methotrexate (MTX), a chemotherapeutic drug able to cause apoptosis of malignant cells, can be addressed to tumor cells which over-expressed folate receptors such as human breast cancer cells (MCF-7), human cervical cancer cells (HeLa), 9L glioma cells[16-17]. Cancer cells internalized a higher level of functionalized NPs than healthy cells and the MTX release was obtained under low pH conditions through the action of intracellular enzymes within the lysosomal compartment (Fig 5).

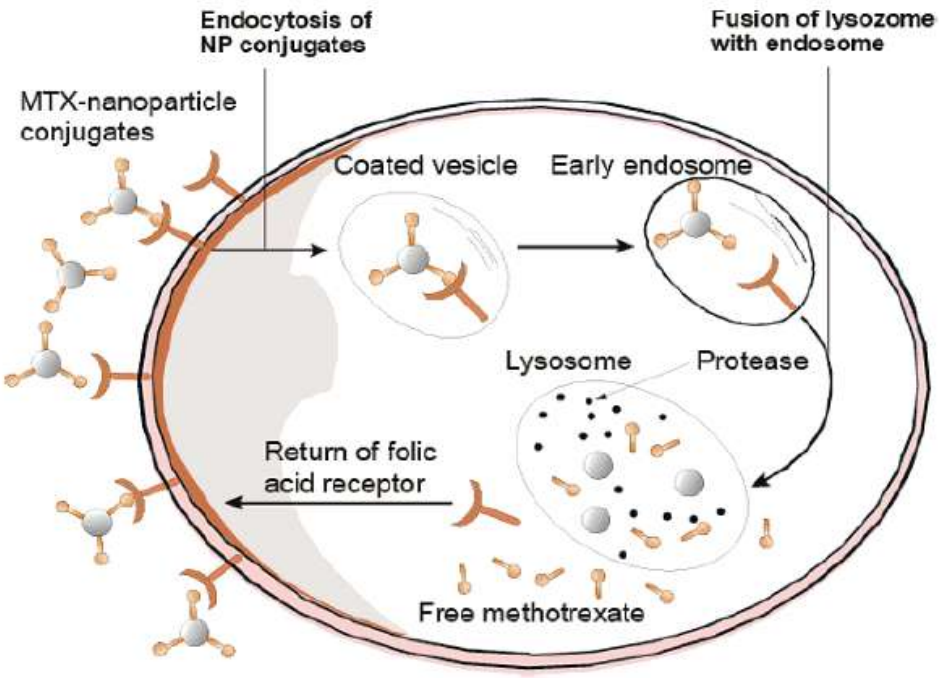

Fig 5. Schematic representation of the intracellular uptake of MTX modified NPs into breast cancer cells. After a receptor-mediated endocytosis, magnetic NPs are transported to early endosomes which then fuse with lysosomes containing proteases, which cleave the peptide bond between the NP and the drug, allowing its delivery into the target cell. Image from Ref 16.

Some interesting results have also been obtained using iron oxide NPs conjugated to the epidermal growth factor receptor (EGFR) inhibitor cetuximab against malignant gliomas, the most common and lethal primary brain tumor that frequently over-expresses EGFR receptor[18]. In this case, the treatment with -loaded NPs has an antitumor effect greater than with cetuximab alone.

Porous hollow NPs (PHNPs) of Fe_3O_4, produced by controlled oxidation of Fe NPs at 250 °C followed by acid etching, were filled with cisplatin by diffusion. They can release cisplatin at low pH condition. After coupling with Herceptin to the surface, the cisplatin-loaded hollow NPs provided efficient delivery of cis-platin to breast cancer SK-BR-3 cells with IC50 reaching micromolar concentration much lower than that needed for free cisplatin[19].

Magnetic NPs as contrast agents

Finally, magnetic NPs are employed as contrast agents for magnetic resonance imaging (MRI), a diagnostic technique usually used for three-dimensional non invasive scans of the human body. According to different relaxation pathways, MRI images can be classified as T_1- (longitudinal relaxation time)- or T_2- (transverse relaxation time)-weighted images. MRI contrast agents can

shorten both T_1 and T_2, helping to improve contrast in MRI images and to ease image interpretation by clinicians.

Magnetic NPs are T_2 contrast agents because they shorten T_2 when, under the application of a magnetic field, their magnetic moment quickens the magnetic relaxation processes of the water protons close to the NPs in the body tissue. Such changes result in darkening of the corresponding area in T_2-weighted MR images. The NP behavior *in vivo* is a significant challenge associated with their application as contrast agents. As better explained in the next section of the Introduction, all of these magnetic NPs are almost non-specifically taken up by the mononuclear phagocyte system (MPS) since they are recognized as not-self by the body, also in consideration of their size. NPs having diameters of ca 30 nm or more are rapidly collected by liver, spleen, and lymph nodes decreasing their effectiveness as MRI contrast agent, while particles with sizes of ca 10 nm or less are not so easily recognized by the MPS. The next generation of NP-based contrast agents should incorporate novel nanocrystal cores, coating materials, and functional ligands to improve their contrast effectiveness and specific delivery/targeting. In this way, they would also allow one to perform real-time monitoring of the pharmaceutical treatment. For example Herceptin®, that is an antibody specifically binding to the over-expressed HER2/neu marker on the surface of breast and ovarian tumors, was coupled to a series of metal-doped NPs having spinel structure MFe_2O_4 where M is a divalent cation such as Mn, Fe, Co or Ni[20]. As shown in Fig 6, $MnFe_2O_4$ NPs (MnMEIO) exhibited higher MRI sensitivity than Fe_3O_4 NPs (CLIO), consistent with the magnetization results.

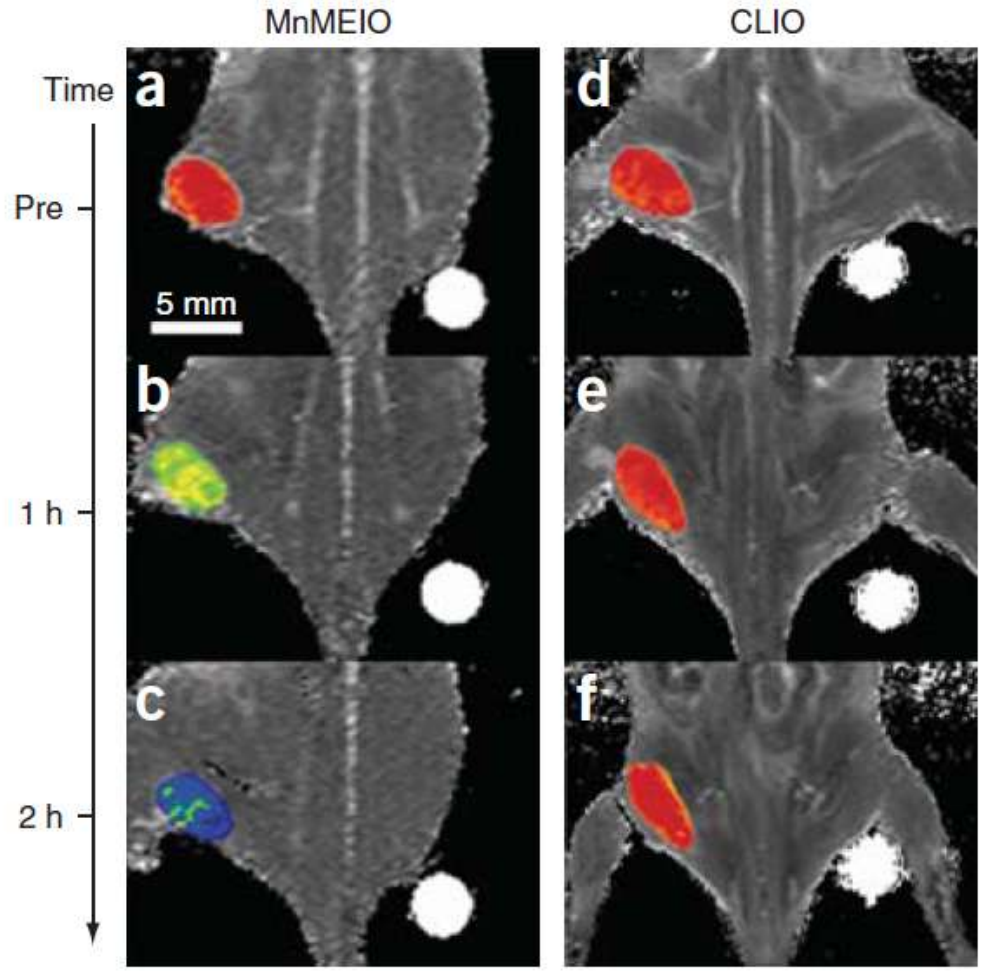

*Fig 6. In vivo MR detection of cancer using magnetic NP–Herceptin conjugates. Color maps of T_2-weighted MR images of a mouse implanted with the cancer cell line NIH3T6.7, at different time points after injection of 50 mg of MnMEIO-Herceptin conjugates or CLIO-Herceptin conjugates. In **a–c**, gradual color changes at the tumor site, from red to blue, indicate progressive targeting by MnMEIO-Herceptin conjugates. In contrast, almost no change was seen in the mouse treated with CLIO-Herceptin conjugate (**d–f**). Image from Ref 20.*

Magnetic NP plasma half-life and biodistribution

The use of magnetic NPs in nanomedicine requires a detailed knowledge of their interactions with the biological system.

In particular, one of the key aspects that influences the biodistribution and the biocompatibility of theranostic nanosystems throughout the body is protein binding[21]. Biologically active materials or NPs are often introduced into an organism via parenteral administration because all cells receive supplies thanks to the blood circulation. After the introduction into the physiological environment, the surface of the materials or NPs are bound by proteins, which form an adsorbed layer known as the protein "corona". The NP-protein complex is the dynamic outcome of multiple interplaying

factors. Several plasma proteins (immunoglobulins, apolipoproteins, clotting factors and complement proteins) have been identified bound to various NPs. In particular, it is known that the presence of certain plasma proteins, called opsonins, on the NP surface creates a "molecular signature" which is recognized by immune cells of the mononuclear phagocyte system (MPS), previously known as reticulo-endothelial system (RES). MPS comprises monocytes, which circulate in the blood, dendritic cells and macrophages present in tissues like the liver (Kupffer cells), spleen, lungs, and bone marrow[22]. Therefore, the opsonization process enhances the NP uptake from the bloodstream by MPS cells through endocytosis/phagocytosis and their concentration in organs with high phagocytic activity (Fig 7). Indeed the NP accumulation can induce tissue inflammation and release of toxic byproducts if the NPs decomposed.

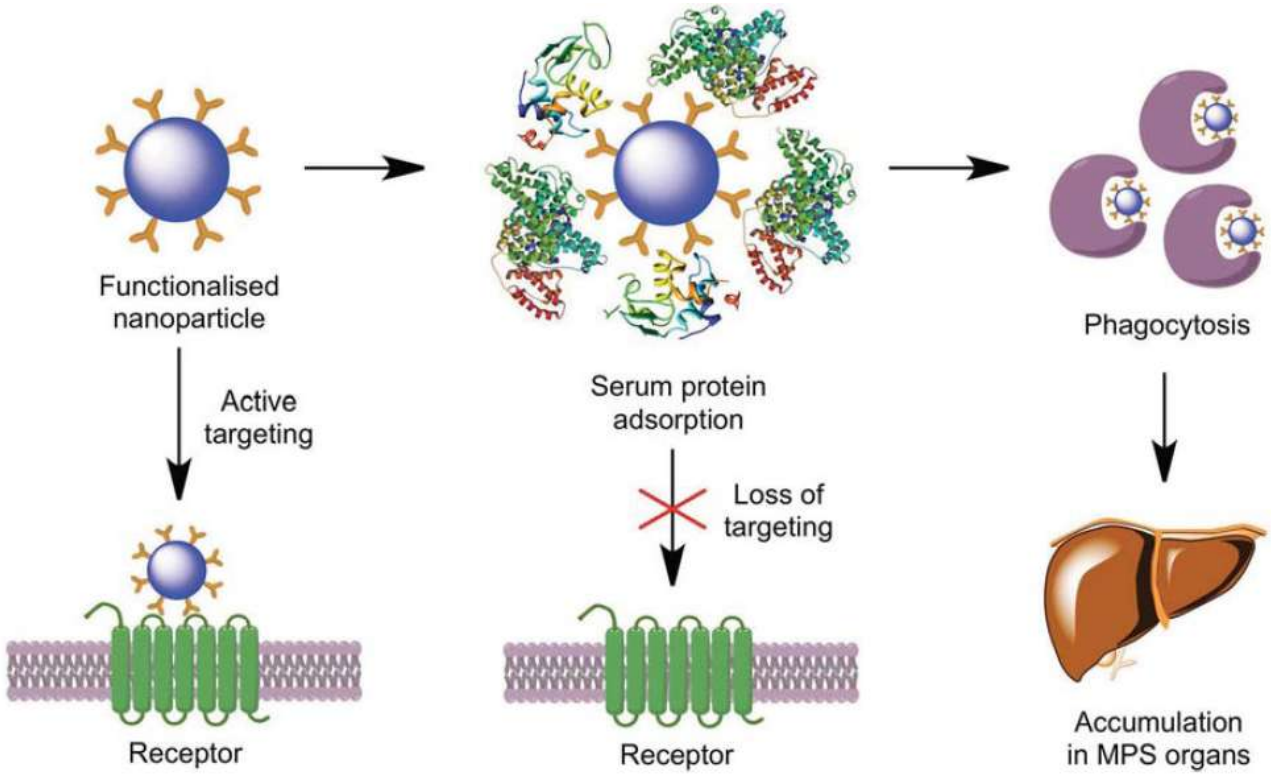

Fig 7. Schematic representation of biomolecular corona formation and its influence on active targeting. Under serum-free in vitro conditions, active targeting of functionalized NPs is achieved by interaction and recognition of cell membrane-located receptors with targeting moieties grafted onto the NP surface. In a biological milieu, a biomolecular corona is formed by non-specific adsorption of proteins and lipids to the NP surface. This process impairs active targeting and leads to NP accumulation in the tissues of the MPS. Image from Ref 22.

After i.v. injection, colloidal drug carriers are removed from the bloodstream within minutes and their typical final biodistribution is of 80–90% in the liver, 5–8% in the spleen and 1–2% in the bone marrow[23]. In fact Kupffer cells together with macrophages in the spleen rapidly uptake NPs with hydrodynamic diameters larger than approximately 100 nm[24]. Instead NPs with diameters of ≤ 5 nm are efficiently filtered by kidneys through their glomerulus pores (that have diameters around 10 nm) and are thus rapidly cleared from the blood[25-26] (Fig 7).

So, it is clear that the protein corona affects the further NP biological destiny inside the body, changing its rate and route of clearance from the bloodstream.

Other features that influence the biodistribution within the body, in particular of NPs with dimensions ranging from 5 to 100 nm, are size[27], shape[28], solubility, surface charge (as measured by zeta potential), coating functionalization, and route of administration. For NPs of the same composition, lower amounts of proteins are adsorbed onto smaller particles in comparison to larger particles, which are easily captured by MPS.

NPs having a sufficiently long half-life can accumulate inside the tissues in different ways depending on the morphology of the epithelium near their blood vessels. Such aspect could be effective in the cancer imaging and treatment since most solid tumors exhibit a “leaky” vasculature with structured fenestrations, due to the high metabolism rate of their cells. This feature, along with poor lymphatic drainage, endorses the passive accumulation and targeting of NPs with size between 30 and 200 nm within the tumor and it is called “enhanced permeability and retention (EPR) effect”. In addition to the passive targeting, most NPs are captured by cells via endocytosis that could be receptor mediated (the mechanism most efficient for NPs of 50 nm diameter), caveolae mediated or adsorptive (Fig. 8)[22].

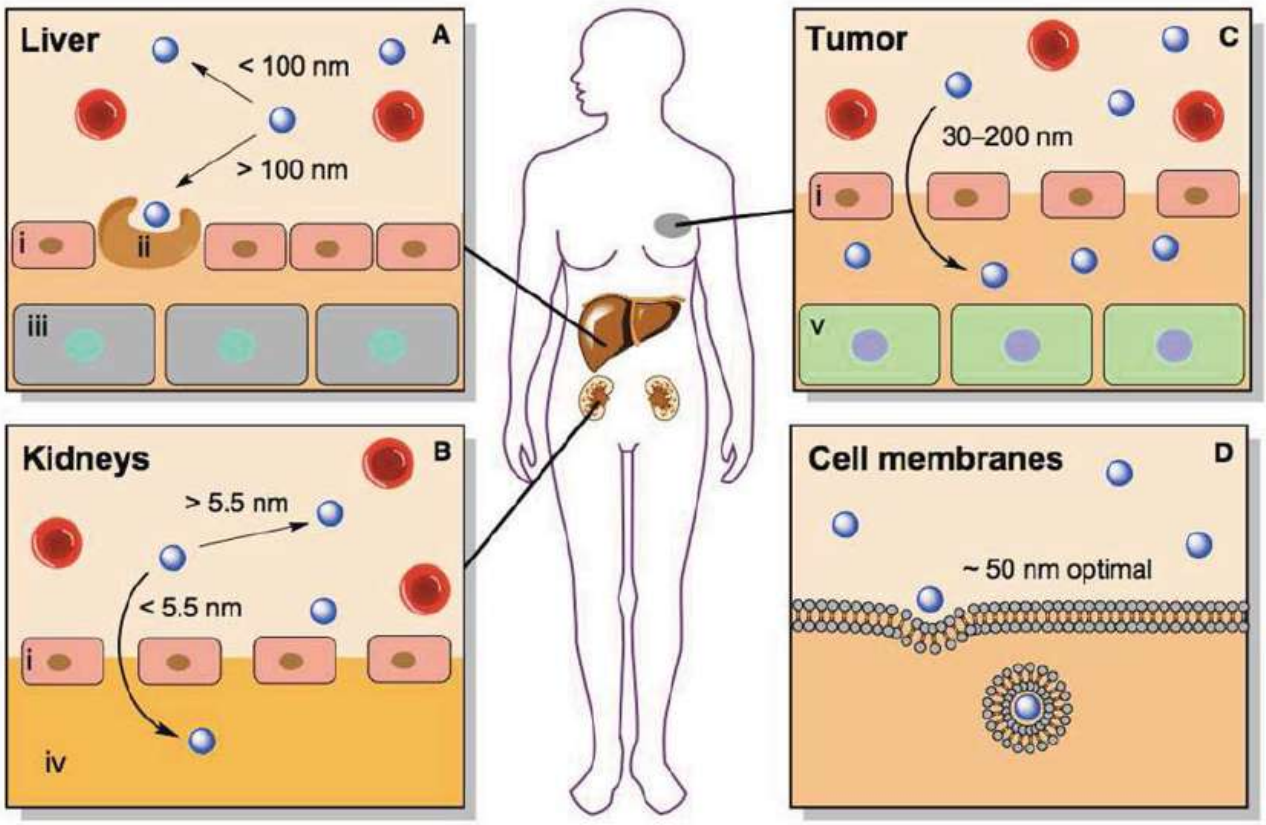

Fig 8. Graphical representation of the major size-dependent biological barriers that influence the biodistribution of blood-circulating NPs. (A): Phagocytosis of NPs with hydrodynamic diameters >100 nm by Kupffer cells in the liver. (B): Glomerular filtration and urine excretion of NPs smaller than 5.5 nm. (C): "Enhanced permeability and retention (EPR) effect"of NPs with hydrodynamic diameters between 30–200 nm in a large and well-vascularized tumor. (D): NP internalization mechanism by cells. Key: (i) endothelial cell; (ii) Kupffer cell; (iii) hepatocyte; (iv) glomerular basement membrane; (v) tumor cell. Image from Ref 22.

Therefore, researchers have to rationally design nanosystems in order to use them in the body, if they want to achieve active targeting. In particular, they have to minimize or delay the NP uptake by MPS cells in order to increase the NP plasma half-life as long as possible and consequently the probability of reaching the desired tissue. Such NPs could be named as "stealth NPs" .

With this aim, surface properties are more important than those of the core, because the coating is in direct contact with the blood and organs.

Anti-fouling and biocompatible coatings

Protein-repellent surfaces are characterized by electrical neutrality, hydrophylicity and the ability to play the role of hydrogen-bond acceptor, but not of hydrogen bond donor.

Until now, two types of NP surface modification have been mainly studied to prevent protein adsorption, the "traditional" polyethylene glycol (PEG) coating and zwitterionic molecules. Both of them are highly effective.

Protein adsorption can occur if the total free energy of the process is negative ($\Delta G_{ads} = \Delta H_{ads} - T\Delta S_{ads} < 0$)[29]. Since the enthalpic contribution is positive (the absorption of lysozyme[30] or bovine albumin, BSA, onto silica[31] were reported to be endothermic processes), the driving force of the process has to be entropic. For both PEG and zwitterion coatings the driving force has been attributed to the release of counterions, according to the mechanism reported for the complexation of proteins with charged polymers (see Fig 9). But for a neutral surface, such as a zwitterion or PEG group, the surface charge is internally balanced (zwitterion) or neutral (PEG) and formation of an ion pair with the adsorbate is improbable; therefore no ion is available for release from the surface and consequently no protein adsorption occurs.

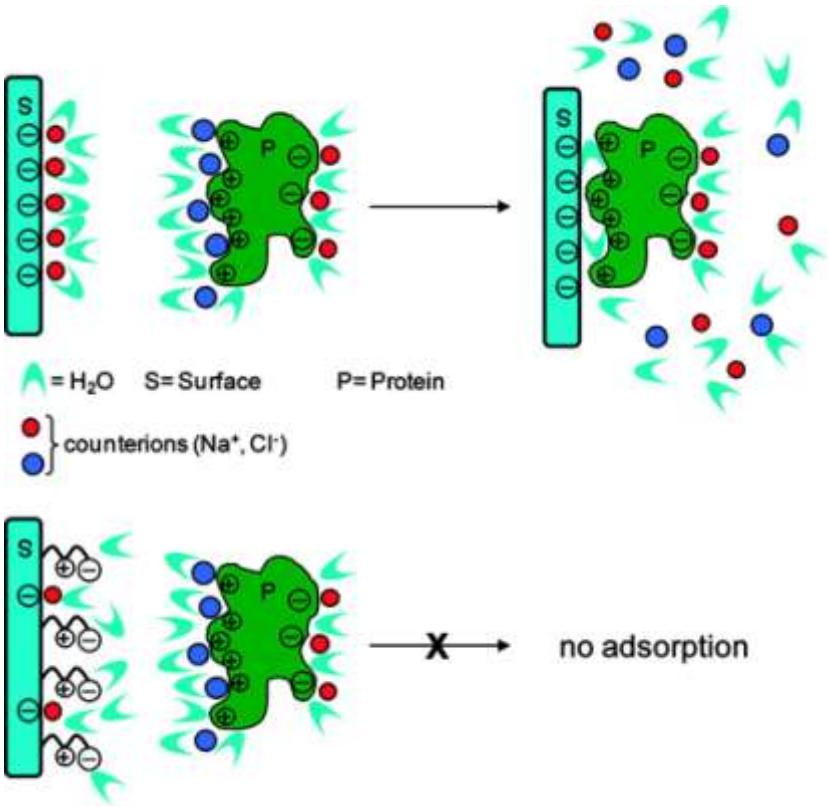

Fig 9. Cartoon for the ion-coupled adsorption mechanism of a protein with a net positive charge onto a negatively charged hydrophilic substrate. (Top) Adsorption of protein is facilitated by the release of counterions and formation of ion pairs between the sorbent and the adsorbate. (Bottom) Neutral surface (zwitterion or PEG) has no surface ions associated with it. The binding of protein to the surface will not result in a net increase in entropy due to counterion release, and thus, adsorption is not preferred. Note that some of the charge is still associated with the original surface but is inaccessible due to a steric barrier. Image from Ref 29.

Obviously, PEG and zwitterionic coatings show several differences mainly due to the largely different molecular size. For example, the zwitterions, due to their small size, produce a thin coating (a few nm thick) that does not much increase the size with respect to the uncoated NP, an important factor related to the NP stealthiness and feasibility of renal excretion. Long-chain PEG, with molecular weight > 1000 as normally used, forms a thick coating on the nanocore significantly increasing the NP size. This is particularly important when the hydrodynamic size is considered, since the PEG chain flexibility can lead to an increase of the NP hydrodynamic diameter by several tens of nm[32]. As we will describe in more detail in the following of this PhD thesis, we have analyzed both classes of PEG and zwitterion surfactants, starting from a literature overview.

References

[1] Funkhouser, J. Reintroducing pharma: Theranostic revolution, *Curr. Drug Discovery 2*, **2002**, 2, 17-19.

[2] Kamaly, N., Xiao, Z. Y., Valencia, P. M., Radovic-Moreno, A. F., Farokhzad, O. C. Targeted polymeric therapeutic nanoparticles: design, development and clinical translation, *Chem. Soc. Rev*., **2012**, 41, 2971−3010.

[3] Danhier, F., Ansorena, E., Silva, J. M., Coco, R., Le Breton, A., Preat, V. PLGA-based nanoparticles: An overview of biomedical applications, *J. Controlled Release*, **2012**, 161, 505−522.

[4] Gong, J., Chen, M., Zheng, Y., Wang, S., Wang, Y. Polymeric micelles drug delivery system in oncology, *J. Controlled Release* **2012**, 159, 312−23.

[5] Allen T. M., Cullis, P.R. Liposomal drug delivery systems: From concept to clinical applications, *Adv. Drug Delivery Rev.*, **2013**,65, 36−48.

[6] Kuai R., Li D., Chen Y. E., Moon J. J., Schwendeman A. High-Density Lipoproteins: Nature's Multifunctional Nanoparticles, *ACS Nano*, **2016**, 10, 3015−3041.

[7] Michalet, X., Pinaud, F. F. , Bentolila, L. A., Tsay, J. M., Doose, S., Li, J.J., Sundaresan, G., Wu, A. M., Gambhir, S.S., Weiss, S. Quantum Dots for Live Cells, in Vivo Imaging, and Diagnostics, *Science*, **2005**, 307, 538-544.

[8] Pinaud, F., Clarke, S., Sittner, A., Dahan, M. Probing cellular events, one quantum dot at a time, *Nat. Methods*, **2010**, 7, 275-285.

[9] Genovese, D., Rampazzo, E., Bonacchi, S., Montalti, M., Zaccheroni, N., Prodi, L. Energy transfer processes in dye-doped nanostructures yield cooperative and versatile fluorescent probes, *Nanoscale*, **2014**, 6, 3022-3036.

[10] Gnach. A., Bednarkiewicz, A. Lanthanide-doped up-converting nanoparticles: Merits and challenges, *Nano Today*, **2012** , 7 , 532- 563.

[11] Mornet, S., Vasseur, S., Grasset, F., Duguet, E., Magnetic nanoparticle design for medical diagnosis and therapy, *J. Mater. Chem.*, **2004**, 14, 2161-2175.

[12] Pankhurst, Q. A., Connolly, J., Jones, S. K., Dobson, J. Applications of magnetic nanoparticles in biomedicine, *J. Phys. D: Appl. Phys.*, **2003**, 36, 167–181.

[13] Lee, J.-H., Huh, Y.-M., Jun, Y.-w., Seo, J.-w., Jang, J.-t., Song, H.-T., Kim, S., Cho, E.-J., Yoon, H. G., Suh, J.-S., Cheon, J. Artificially engineered magnetic nanoparticles for ultra-sensitive molecular imaging, *Nat. Med.*, **2007**, 13, 95–99.

[14] Yoo, D., Lee, J.-H., Shin, T.-H., Cheon, J. Theranostic Magnetic Nanoparticles, *Acc. Chem. Res.*, **2011**, 44, 863-874.

[15] Trahms, L. Biomedical Applications of Magnetic Nanoparticles, in *Colloidal Magnetic Fluids*, **2009**, 763, 1-32, Springer, Berlin-Heidelberg.

[16] Kohler, N. , Sun, C., J. Wang, Zhang, M., Methotrexate-Modified Superparamagnetic Nanoparticles and Their Intracellular Uptake into Human Cancer Cells, *Langmuir*, **2005,** 21, 8858-8864.

[17] Kohler, N., Sun, C., Fichtenholtz, A., Gunn, J., Fang, C., Zhang, M., Methotrexate-Immobilized Poly(ethylene glycol) Magnetic Nanoparticles for MR Imaging and Drug Delivery, *Small*, **2006**, 2, 6, 785 – 792.

[18] Kaluzova, M., Bouras, A., Machaidze R., Hadjipanayis, C. G, Targeted therapy of glioblastoma stem-like cells and tumor non-stem cells using cetuximab-conjugated iron-oxide nanoparticles, *Oncotarget*, 2015, 6, 8788–8806.

[19] Cheng , K., Peng , S., Xu , C. J., Sun , S., Porous Hollow Fe3O4 Nanoparticles for Targeted Delivery and Controlled Release of Cisplatin, *J. Am. Chem. Soc.*, **2009** , 131 , 10637-10644.

[20] Lee , J. H., Huh , Y. M., Jun , Y., Seo , J., Jang , J., Song, H. T., Kim , S., Cho , E. J., Yoon , H. G., Suh , J. S., Cheon , Artificially engineered magnetic nanoparticles for ultra-sensitive molecular imaging, J., *Nat. Med*., **2007** , 13 , 95-99.

[21] Aggarwal, P., Hall, J. B., McLeland, C. B., Dobrovolskaia, M. A., McNeil, S. E., Nanoparticle interaction with plasma proteins as it relates to particle biodistribution, biocompatibility and therapeutic efficacy, *Adv. Drug. Delivery Rev.*, **2009**, 61, 428-437.

[22] Pombo García, K., Zarschler, K., Barbaro, L., Barreto, J. A., O'Malley, W, Spiccia, L., Stephan, H., Graham, B., Zwitterionic-Coated "Stealth" Nanoparticles for Biomedical Applications: Recent

Advances in Countering Biomolecular Corona Formation and Uptake by the Mononuclear Phagocyte System, *Small*, **2014**, 10, 2516–2529.

[23] Monfardini, C., Veronese, M. F., Stabilization of Substances in Circulation, *Bioconj. Chem.*, **1998,** *9*, 418-450.

[24] Moghimi, S. M., Hunter , A. C., Murray , J. C., Long-Circulating and Target-Specific Nanoparticles: Theory to Practice, *Pharmacol. Rev.*, **2001**, 53 , 283-318.

[25] Liu, W. H., Choi, H. S., Zimmer, J. P., Tanaka, E., Frangioni, J. V., Bawendi, M., Compact cysteine-coated CdSe(ZnCdS) Quantum Dots for In Vivo Applications, *J. Am. Chem. Soc.*, **2007**, 129, 14530−14531.

[26] Choi, H., Liu, W., Mirsa , P., Tanaka , E., Zimmer , J., Ipe , B., Bawendi , M., Frangioni. J., Renal clearance of quantum dots, *Nat. Biotechnol.*, **2007**, 25, 1165-1170.

[27] De Jong, W.H., Hagens, W.I., Krystek, P., Burger, M.C., Sips, A.J., Geertsma, R.E., Particle size-dependent organ distribution of gold nanoparticles after intravenous administration, *Biomater.*, **2008**, 29, 1912–1919.

[28] Chithrani B.D., Ghazani, A.A., Chan, W.C., Determining the size and shape dependence of gold nanoparticle uptake into mammalian cells, *Nano Lett.*, **2006**, 6, 662–668.

[29] Estephan, Z.G., Schlenoff, P.S., Schlenoff, J. B., Zwitterion as an alternative to PEGylation, *Langmuir*, **2011**, 27, 6794-6800.

[30] Jackler, G.; Steitz, R.; Czeslik, C., Effect of Temperature on the Adsorption of Lysozyme at the Silica/Water Interface Studied by Optical and Neutron Reflectometry, *Langmuir*, **2002**, 18, 6565–6570.

[31] Kulikova, G. A.; Ryabinina, I. V.; Guseynov, S. S.; Parfenyuk, E. V., Calorimetric study of adsorption of human serum albumin onto silica powders, *Thermochim. Acta*, **2010**, 503, 65–69.

[32] Mondini, S.; Drago, C.; Ferretti, A. M.; Puglisi, A.; Ponti, A. Colloidal stability of iron oxide nanocrystals coated with a PEG-based tetra-catechol surfactant, *Nanotechnology*, **2013**, 24, 105702.

Part I: Magnetic NPs coated with zwitterions

01. Introduction

Recently, zwitterionic ligands have been used as an alternative to PEGylated coatings, aiming at obtaining biocompatible nonfouling materials, able to prevent nonspecific protein adsorption to the NPs[1-2]. Some of the zwitterion functional groups more commonly employed in nanomedicine are aminoacid (e. g. cysteine), carboxybetaine, phosphorylcholine, and sulfobetaine (Fig 1).

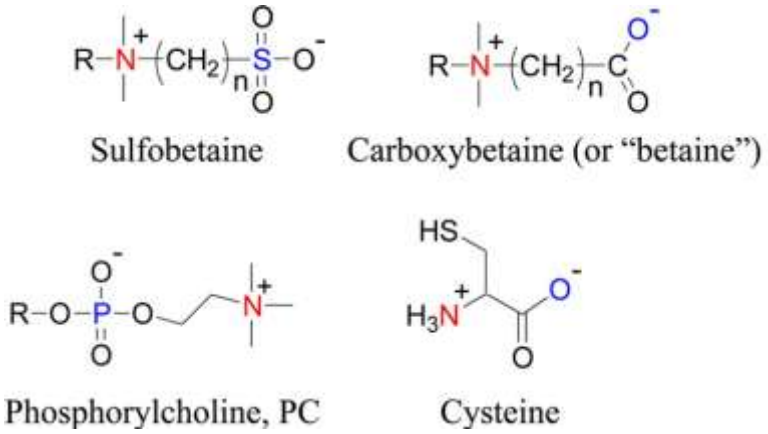

Fig 1. Zwitterionic functional groups. Image from Ref 1.

Cysteine is a zwitterionic amino acid and its thiol terminal group was used to stabilize NPs made from semiconductors, such as CdS[3], ZnS[4], and of noble metals Au[5] or Ag[6]. Cysteine is not able to prevent noble metal NP aggregation when the electrolyte concentration increases while it is efficient with semiconductor NPs[7] maybe thanks to a greater stability of the thiol-semiconductor over the thiol-gold bond. In this work, Bawendi and co-workers showed that quantum dots coated by cysteine and with a diameter less than 5.5 nm were collected in the bladder of rats since mainly excreted by kidneys. However, the cysteine inclination to spontaneous oxidation led to NP aggregation a few hours after preparation. A novel strongly-binding zwitterionic disulfide was used to prepare small (average diameter around 4 nm) water-soluble Au NPs by replacement of the pristine citrate ligand[8]. These NPs are stable in saline media with 3 M salt concentration and also when charged polyelectrolytes or biopolymers were added to the aqueous NP solution, witnessing the absence of nonspecific interactions. Afterwards, a siloxane sulfobetaine ligand was employed by Schlenoff and co-workers to coat and stabilize silica[9-10] and iron oxide[11] NPs by siloxane condensation chemistry, avoiding an appreciable increase of their hydrodynamic diameter. The

zwitterionic silica particles did not aggregate when exposed to aqueous 3 M NaCl and 50% FBS up to 24 h. The authors varied the zwitterionic siloxane concentration in order to produce iron oxide NPs small enough for renal clearance capability. They also demonstrated the NP stability in aqueous solution in the pH = 6–9 range, while the tendency of NPs to aggregate at lower pH was attributed to the presence of some pH-sensitive Fe-OH functionalities on the NP surface due to incomplete capping.

In the literature it was also proved that sulfobetaine polymers, in contrast to classic polyelectrolytes with a single type of ionized group, had a very small disturbing effect on the water hydrogen-bonded structure[12]. So their application was strongly advised in biomedical fields, e. g., iron oxide NPs coated with polymeric sulfobetaines have already been described[13-14].

Indeed, larger-size NPs coated with zwitterions have shown an extended circulatory lifetime which makes them ideal candidates as blood pool imaging agents. However, NPs with hydrodynamic diameter less than 5 nm are sufficiently small to be filtrated through kidneys and eliminated via the urine, a desirable feature for example if the NP is radioactively labeled[15]. In fact, a safe and successful NP application relies on a balance between a prolonged blood circulation (required to get the NPs to the desired target) and an effective clearing mechanism (enabling minimization of side effects due to a prolonged NP presence in the body, such as a deposition in non-targeted tissues and organs)[10]. To this purpose, an increase in NP size after the binding to the desired target, for example 20 h following the NP administration, can be useful for their elimination[10].

Considering the advantage which can arise from the small sizes of these zwitterionic ligands, we focus our attention on small zwitterionic molecules effective in coating nanocrystals while increasing their diameter only by a few nanometers.

The production, trough a nanoemulsion method, of a ultrathin coating layer of zwitterionic molecules adsorbed via hydrophobic and van der Waals interactions at the surface of oleic acid-NPs[16] has been reported (Fig 2). In this way, Lee et al obtained water-soluble NPs having high *in vivo* stability, as demonstrated by incubation in 1 M NaCl and 10% FBS solution. Moreover, the ultrathin coating layer led to a measured T_2 relaxivity much higher than that of commercial T_2 contrast agents.

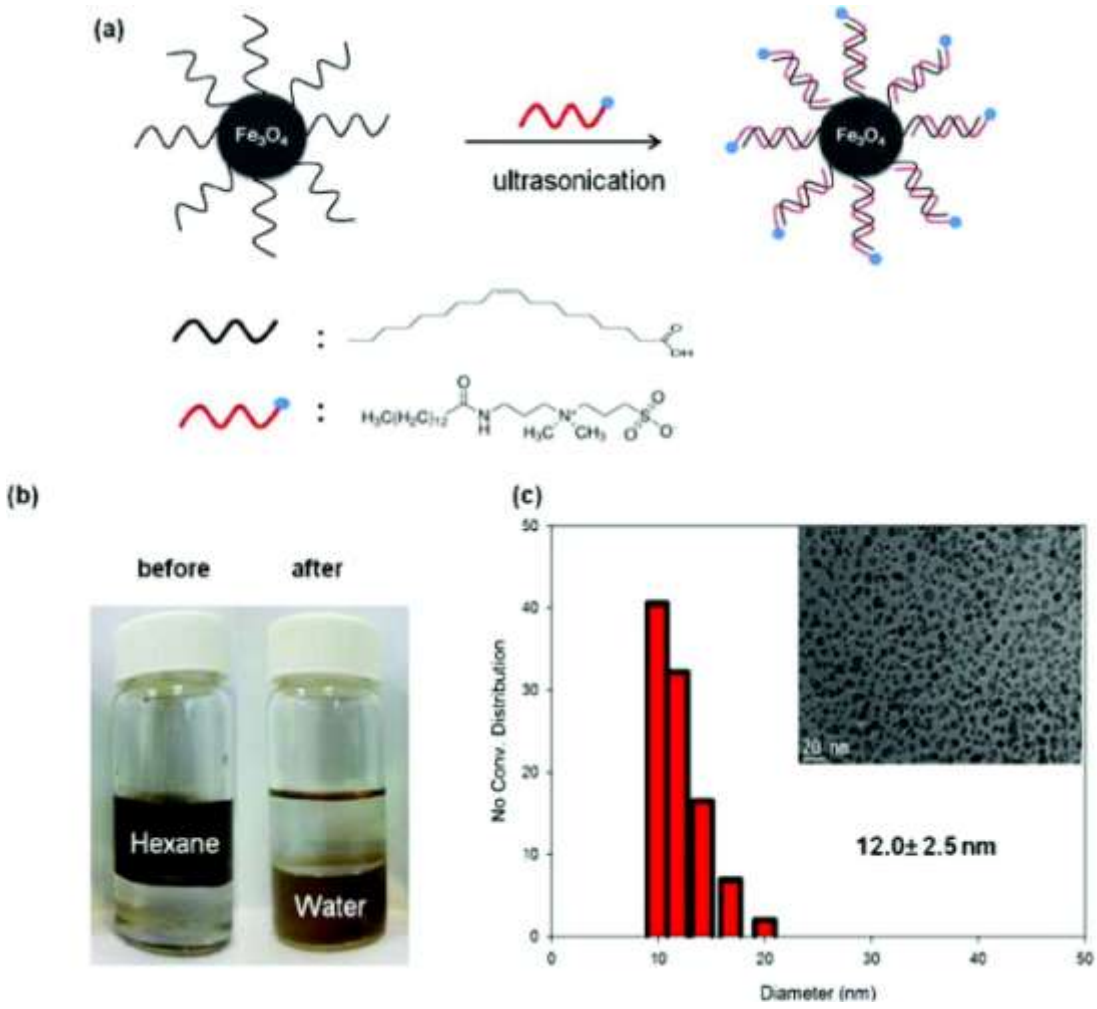

Fig 2. (a) Schematic of ZSPION synthesis and chemical structure of zwitterion surfactant. (b) Photograph of dispersion behavior of oleic acid stabilized SPIONs before and after the zwitterion surfactant coating in hexane/distilled water. (c) Hydrodynamic size distribution along with TEM image of ZSPIONs. The scale bar in the TEM images denotes 20 nm. Image from Ref 16 .

Furthermore, small sulfobetaines have been reported to graft to NP surfaces. Bawendi and co-workers synthesized and employed a novel dopamine sulfonate ligand to coat iron oxide NPs[17]. As the authors explained, the structure of the compound (see Fig 3) was designed considering that: (i) the catechol unit strongly binds the iron centers of NPs[18], (ii) the sulfonate moiety ensures high water solubility and (iii) in association with a quaternary amine group leads to a zwitterionic feature which provides pH stability to the nanosystem and reduces the nonspecific protein adsorption. Water-soluble ZDS-NPs, having a hydrodynamic diameter of 10 nm, were well dispersible in phosphate-buffered saline (PBS) and stable in the pH range between 6 and 8.5 and with respect to time and salinity. As expected from their zwitterionic nature, a reduced amount of serum protein bound these NPs in comparison to negatively-charged iron oxide NPs. Finally the authors

functionalized ZDS-NPs with streptavidin and fluorescent dyes for biotin-specific targeting and imaging (Fig 3).

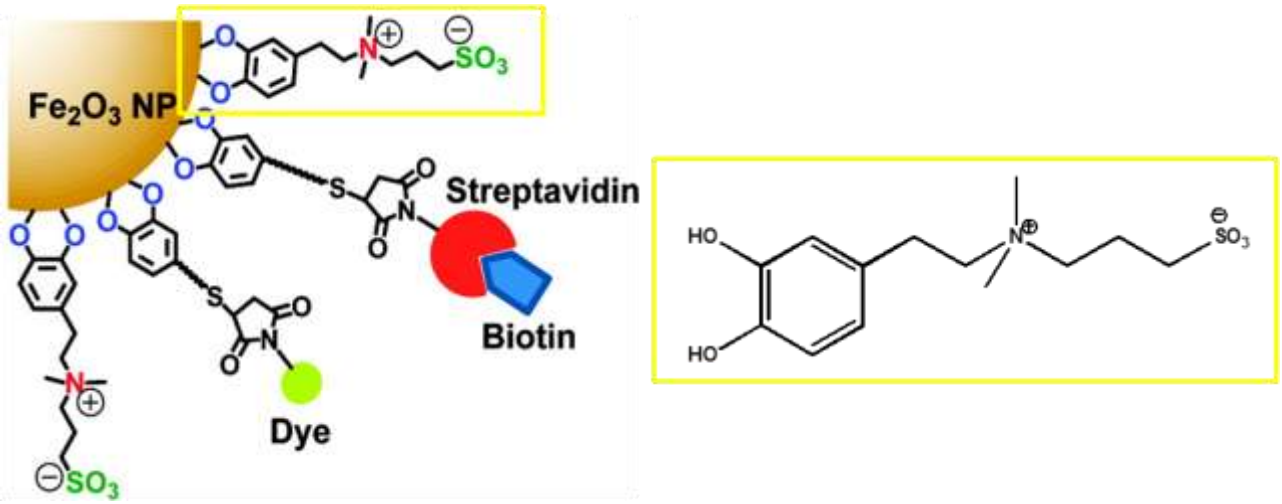

Fig 3. Functionalization of iron oxide NPs coated with dopamine zwitterion (ZDS) ligand whose chemical structure is reported in the yellow square. Image from Ref 18.

ZDS-coated NPs have a saturation magnetization (M_s) of 74 emu g^{-1} preserving the characteristics of pristine iron oxide NPs from which they were obtained by a ligand exchange process[19]. In the same report, the authors also tested *in vitro* NP uptake by HeLa cells and they observed a low aspecific cell internalization after 24 h incubation. In addition, they carried out an *in vivo* stability experiment by intravenous injection of ZDS-NPs in mouse. After 10 minutes, the hydrodynamic diameter showed only a small increase as observed by SEC.

Gao at al[20] employed ZDS to coat ultra-small iron oxide NPs, which they claim contain gadolinium species (e.g., Gd_2O_3 nanoclusters), that had a good performance as T_1 contrast agents. These novel NPs have a constant hydrodynamic diameter of approximately 5 nm measured in PBS buffer and FBS solution, again showing a low nonspecific protein interaction and a sufficiently long blood half-life (ca 50 min). Thanks to their size, such NPs are rapidly filtered by kidneys and can be passive targeted in tumors by the EPR effect, as tested in a human ovarian cancer as model.

Basing on these promising results about the potential application of ZDS-NPs in biomedical field, we have decided to use in this PhD thesis the ZDS molecule to produce water-soluble iron oxide NPs and we have compared them with a batch of NPs covered by the commercially available 2-[2-(2-methoxyethoxy)ethoxy]acetic acid (MEEA)[21], with structure $MeO(CH_2CH_2O)_2CH_2COOH$. The latter is about as large as ZDS, featuring a short PEG-like chain with a carboxylic acid group able to graft the NP surface as carboxylate anion[22]. Both coatings were characterized in detail by Fourier

Transform Infrared (FTIR) spectroscopy and Thermal Gravimetric Analysis (TGA) and their behavior towards protein adsorption was evaluated by Dynamic Light Scattering (DLS). Then, we have assessed the NP interaction with cells investigating their cytotoxicity, internalization, and intracellular destinyusing human liver carcinoma cells (HepG2) in view of their high phagocytic activity[23-24-25]. To study the NP localization inside the HepG2 cells, we prepared a new fluorescent catechol ligand.

Since ZDS and MEEA have similar molecular length, they form a coating of similar thickness. Using the same batch of monodisperse iron oxide NPs, we have obtained information about the nanosystem surface chemistry which is the main factor, as explained in the introduction, to produce "stealth NPs", essential for successful theranostic agents.

02. Preparation of iron oxide NPs coated with zwitterions

a. Synthesis of magnetic nanoparticles

Since NP properties are strongly size dependent, we planned to use NP comprising a crystalline iron oxide core with a very small size dispersion so that investigation of the surface chemistry is not hampered by size inhomogeneous NPs. The nanocrystal size and morphology can be controlled by various synthetic procedures as reported in literature[26-27]. A general way to produce monodisperse NCs is based on the high-temperature decomposition of metal complex in a high boiling solvent in the presence of a surfactant (solvothermal synthesis)[28]. In particular, two procedures are well known. In the *hot-injection* process, the metal complex is instantaneously decomposed by quickly injection inside a hot mixture of solvent and surfactant while in the *heating-up* process all reagents are dissolved in the solvent at moderate temperature and then the homogeneous reaction mixture is heat up to high temperature. The crystal growth control diversifies the two procedures. In both methods, reaction temperature and reactant concentrations determine the size distribution of the NPs. The most common surfactants employed in the solvothermal synthesis of NPs to stabilize them and modulate their dimension and shape are long-chain molecules such as oleic acid and oleylamine. Moreover, the most common metal precursor used in hot-injection are metal carbonyls (e.g. iron pentacarbonyl) while for heating-up procedures metal acetylacetonates or oleates are widely employed.

We obtained iron oxide NPs with diameter ca. 9 nm following a modification of a hot-injection procedure described in literature[29] (see Experimental Section). We modified another procedure to synthesize NPs[30] to produce larger NCs ($d \approx 12$ nm) by changing the molar ratio between metal

precursor and surfactant (from 1:4 to 1:3) in 1-octadecene (ODE). In both cases we produced monodisperse spherical iron oxide NPs coated with oleic acid (OlAc-NPs), as confirmed by TEM images (see Fig 4 and 5).

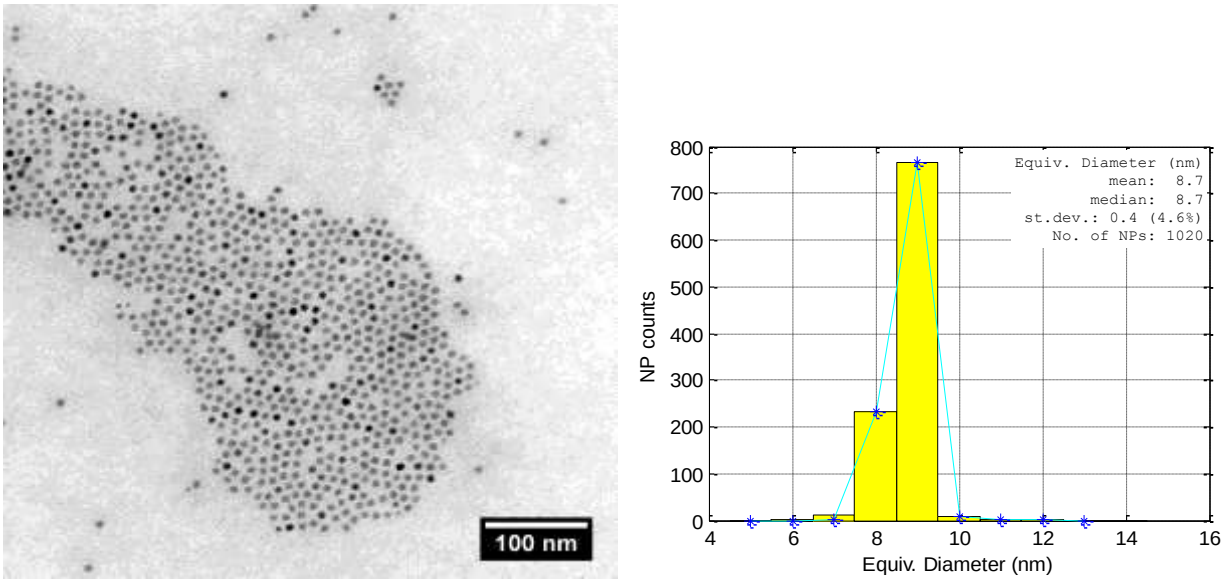

Fig 4. Smaller (8.7 nm) OlAc-coated NPs. Left) TEM image from Ref 21. Right) Histogram of the NP diameters measured by the software PEBBLES[31].

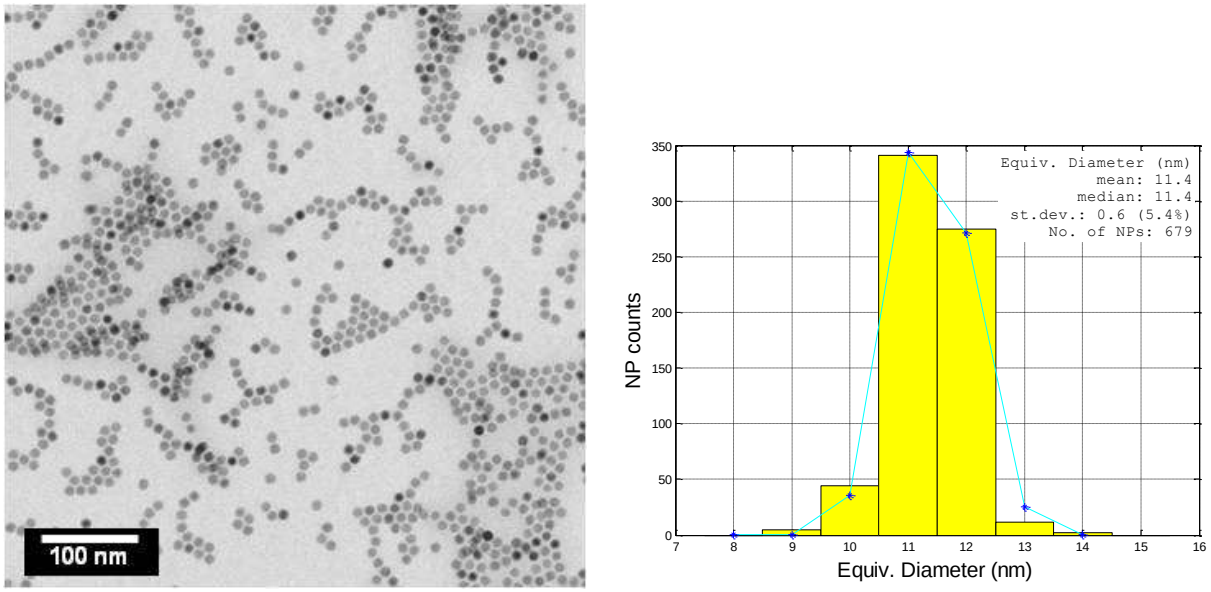

Fig 5. Larger (11.4 nm) OlAc-coated NPs. Left) TEM image. Right) Histogram of the NP diameters measured by the software PEBBLES[31].

For smaller iron oxide NPs the median diameter was $\langle d \rangle$ = 8.7 nm with a diameter standard deviation σ_d = 0.4 nm, witnessing a very low dispersion $\sigma_d/\langle d \rangle$ = 4.6%. For larger NPs the median diameter was $\langle d \rangle$ = 11.4 nm, with σ_d = 0.6 nm, showing again a very narrow dispersion $\sigma_d/\langle d \rangle$ = 5.4%.

Since the as-synthesized NPs have small size and magnetite (Fe_3O_4) and maghemite (γ-Fe_2O_3) have very similar electron diffraction pattern (Fig 6), we can at most conclude that our NPs are iron oxide NPs with cubic spinel structure and stoichiometry intermediate between magnetite and maghemite ($Fe_{3-x}O_{4-x}$, $0 < x < 1$).

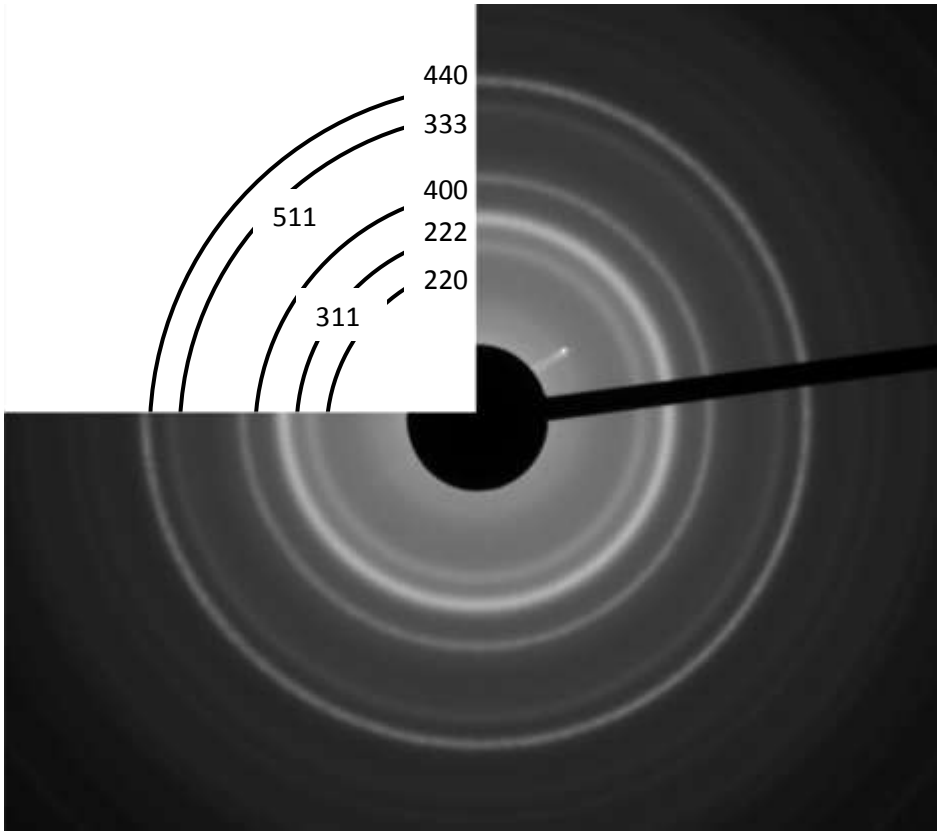

Fig 6 . Electron diffraction pattern of OlAc-NPs. All diffraction rings are indexed with reference to the magnetite structure. Image from Ref 21.

b. Catecholic ligands

The catecholic ligands used as iron oxide NP surfactants, were synthesized in collaboration with Dr. Carmelo Drago (CNR, Istituto di Chimica Biomolecolare, Catania).

The zwitterionic dopamine sulfonate (ZDS) (Fig 7) was obtained following a modified two-step pathway based on the previously reported procedure[17] and described in detail in the Experimental Section. Briefly, commercially available dopamine hydrochloride was deprotonated with aq. ammonia and reacted with propansultone to give the sulfonic acid DS, which was isolated and further reacted with a large excess of MeI in the presence of an inorganic base to obtain the desired zwitterion ZDS.

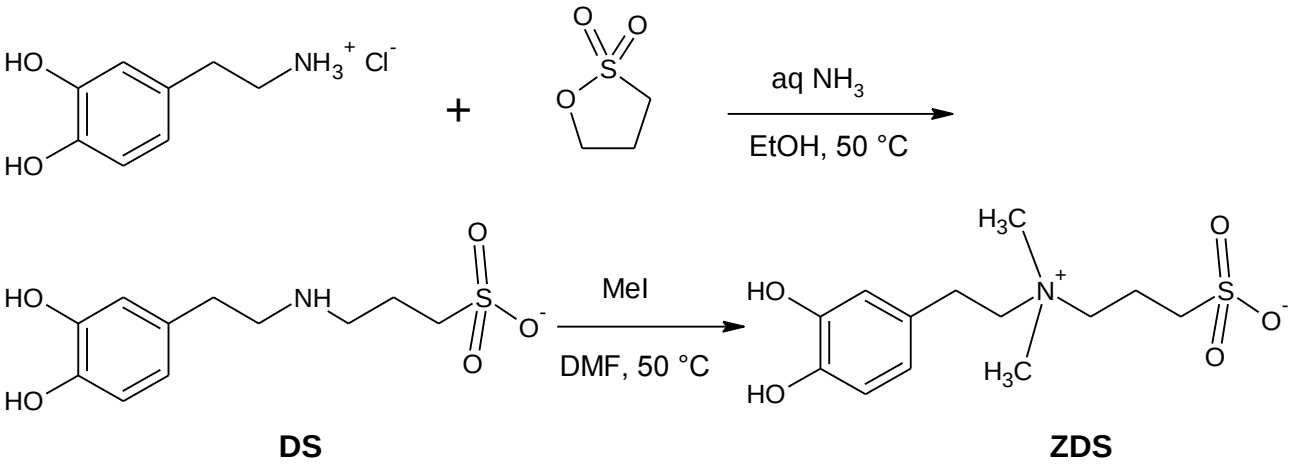

Fig 7. Synthesis of zwitterionic dopamine sulfonate ZDS [21].

Instead the fluorescent catecholic ligand (FCL), whose structure is depicted in Fig 8, was employed to study the intracellular fate of iron oxide NPs after their internalization into HepG2 cells. It was produced as reported in detail in the Experimental Section.

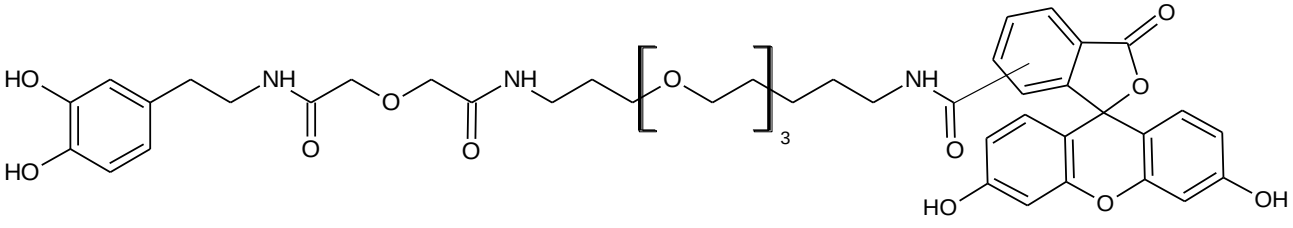

Fig 8. Chemical structure of fluorescent catecholic ligand (FCL). The position of the benzamido moiety is uncertain (5 or 6) because we used commercially available 5(6)-carboxyfluorescein.

c. Preparation of water-soluble NPs via ligand exchange procedure

To prepare water soluble iron oxide NPs, we employed the above described batches of monodisperse OlAc-coated NPs and we resorted to ligand exchange procedures in order to replace the pristine hydrophobic coating (oleic acid) with the desired hydrophilic one.

In particular, both MEEA- and ZDS-coated NPs were obtained following pathway modification of the literature procedure[17]. A similar process was used to produce the fluorescent NPs, which were coated with a mixture of FCL and ZDS. The presence of ZDS is required to endow the fluorescent NPs with good colloidal stability in water. The coating procedure is described in detail in the Experimental Section.

MEEA-, ZDS- and FCL-NPs were obtained from OlAc-NPs with <*d*> = 8.7 nm (see Fig 9), while ZDS-NPs were produced also from OlAc-NPs with <*d*> = 11.4 nm (see Fig 10). The latter were employed in DLS experiments. A summary of the NP morphological parameters before and after the exchange processes is reported in Table 1 and Table 2, respectively (see below).

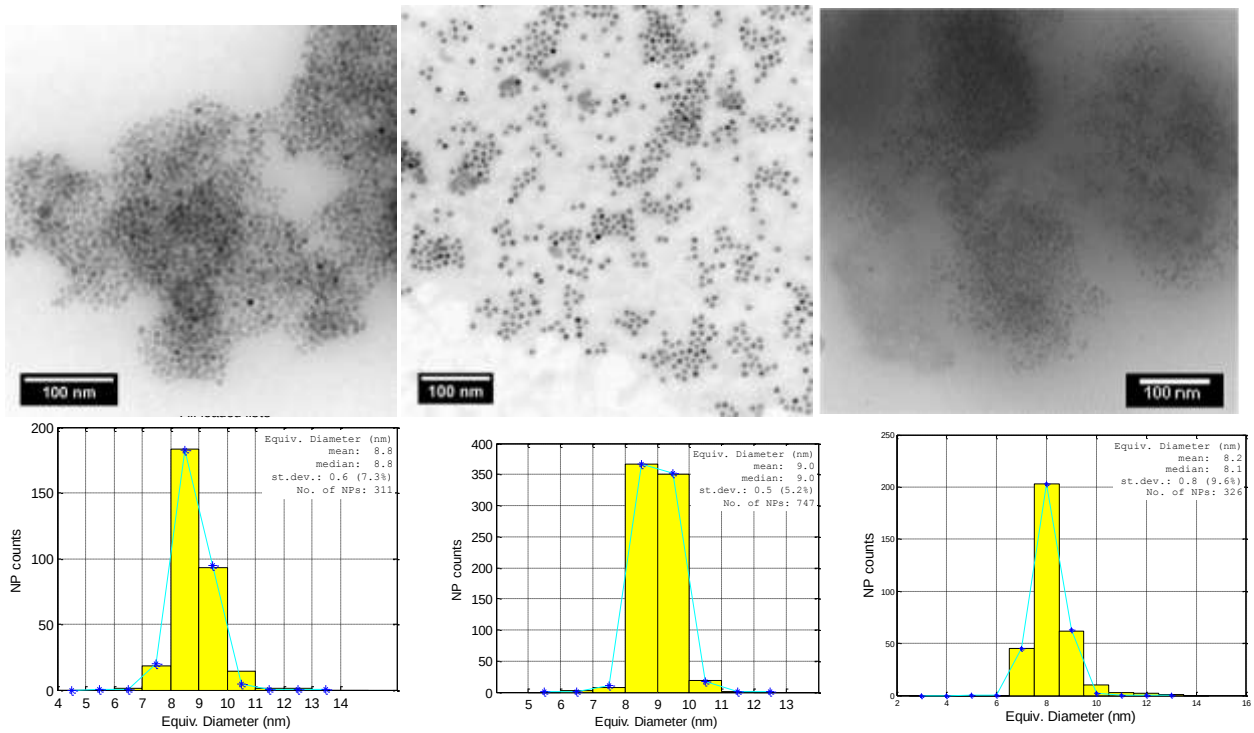

Fig 9. TEM images (top) and diameter histograms (bottom) of ligand-exchanged NPs prepared from 8.7 nm OlAc –NPs. Left) MEEA-NPS. Center) ZDS-NPs. Right) FCL-NPs.

	<d> (nm)	σ_d (nm)	σ_d/<d> (%)
OlAc-NPs	8.7	0.4	4.6
MEEA-NPs	8.8	0.6	7.3
ZDS-NPs	9.0	0.5	5.2
FCL-NPs	8.1	0.8	9.6

Table 1. Summary of the morphological parameters before and after the exchange process for NPs prepared from 8.7 nm OlAc –NPs.

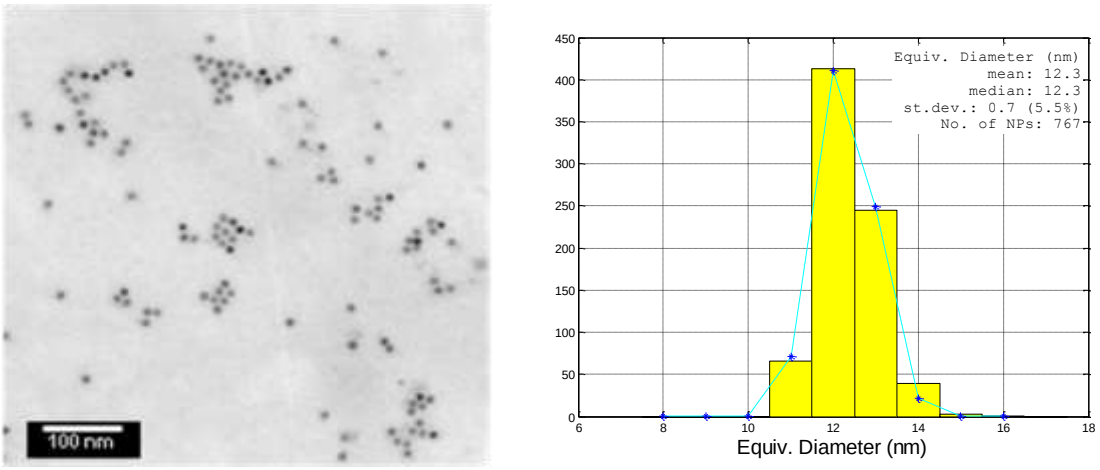

Fig 10. TEM image of ZDS-NPs coming from the batch of OlAc–NPs with diameter ca. 12 nm ("larger" OlAc-NPs). TEM image (left) and diameter histogram (right) of ZDS-NPs prepared from 11.4 nm OlAc –NPs.

Morphological parameters	<d> (nm)	σ_d (nm)	σ_d/<d> (%)
OlAc-NPs	11.4	0.6	5.4
ZDS-NPs	12.3	0.7	5.5

Table 2. Summary of the morphological parameters before and after the exchange process for ZDS-NPs prepared from 11.4 nm OlAc–NPs .

d. Characterization of NP coating

We studied the coating at the surface of the prepared NP types by Fourier-Transform Infrared (FTIR) spectroscopy and Thermogravimetric Analysis (TGA). UV-VIS spectroscopy was also used for fluorescent NPs.

d.01. FTIR spectra

The FTIR spectra of OlAc-, MEEA-, and ZDS-NPs are shown in Fig 11 (left) along with the corresponding FTIR spectra of pure ligands (right).

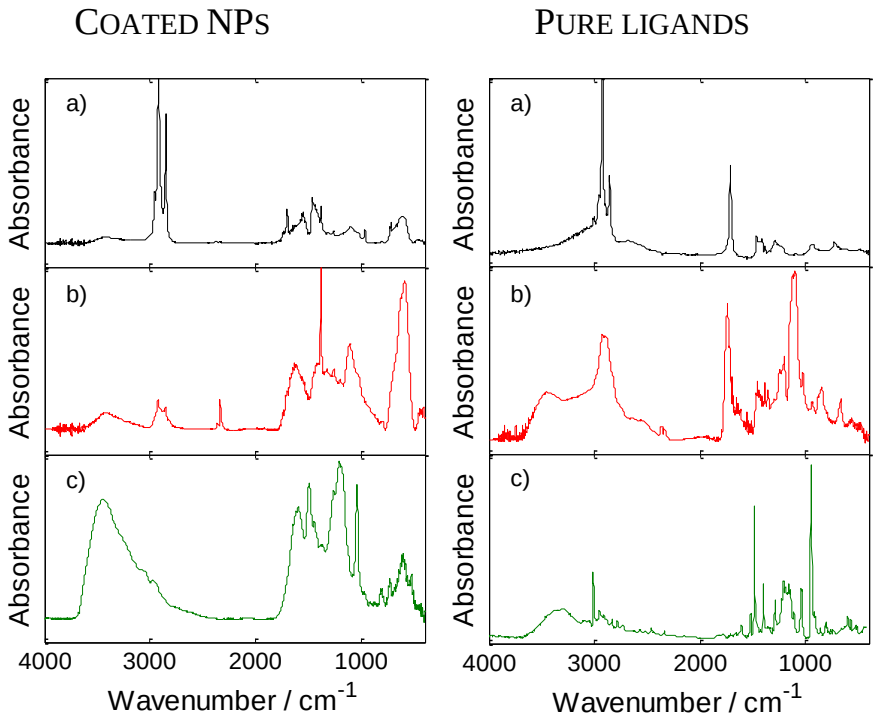

Fig 11. FTIR spectra of OlAc- (a), MEEA- (b), and ZDS-coated (c) iron oxide NPs (left). FTIR spectra of the pure ligands are shown in the right subpanels. Image from Ref 21.

In all NP spectra the peak at 590 cm^{-1} can be ascribed to the iron oxide core. In the spectrum of OlAc-NPs, strong C-H (2954, 2919, 2850 cm^{-1}) and carboxylate stretching peaks (1550 and 1463 cm^{-1}) are clearly recognizable. Instead, the spectrum of MEEA-NPs displays stretching bands related to C-H (weak; 2956, 2923, 2855 cm^{-1}), carboxylate (1634 and 1410 cm^{-1}) and C-O-C (1200 and 1100 cm^{-1})[22] typical of MEEA, as proof of evidence that the ligand exchange procedure was

effective. Finally, the FTIR spectrum of ZDS-NPs shows, in addition to the weak C-H stretching peaks (2850-2950 cm^{-1}), several diagnostic bands such as the S-O stretching peak (1209 cm^{-1}), the C-H deformation peaks of the dimethylammonium group (1496 and 1042 cm^{-1}), and the ring stretching (1596 cm^{-1}) and C-H deformation (914-732 cm^{-1}) peaks of 1,2,4-trisubstituted benzenes[21]. The ZDS-NPs spectrum is in agreement with that reported in literature for iron oxide NPs coated with a short siloxane sulfobetaine[32]. The intensity of the peaks in the C-H stretching region decreases passing from OlAc to MEEA and ZDS as a consequence of the efficient ligand exchange procedure.

d.02. TGA curves

MEEA- and ZDS-NPs were subjected to Thermogravimetric Analysis (TGA) by heating the NPs in air up to 950 °C. The TGA curves are shown in Fig 12.

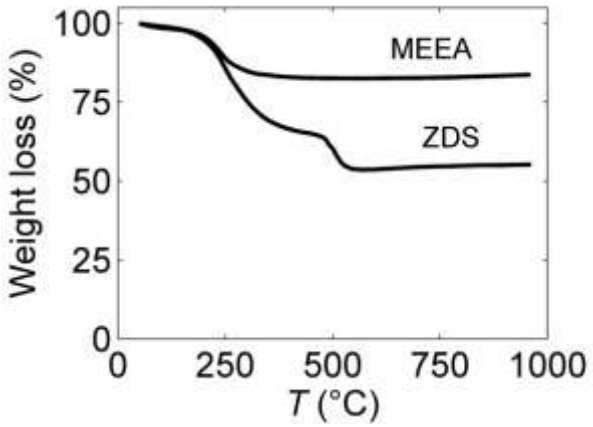

Fig 12. TGA curves of MEEA- and ZDS-coated iron oxide NPs.

In the case of MEEA-NPs the weight loss is 16.5%, in agreement with that already reported in literature[22]. Such percentage corresponds to a coating density of 6 molecule/nm^2 of MEEA in the coating, similar to the published data of 4.2-4.7 molecule/nm^2 evaluated for aliphatic carboxylic acids having comparable size[33]. Instead, TGA curves of ZDS-NPs show two percentage weight losses: 33% in the 100-440°C range and 12% in the 440-580°C range. We attributed the first weight loss to the decomposition of the aliphatic part of the ZDS and the second one to the combustion of the aromatic part, also considering that the aliphatic:aromatic weight ratio in ZDS is about 3:1. In

this case, the total weight loss (45%) corresponds to a very high coating density of 15 molecule/nm^2 that we have attributed to the presence of a ZDS *bilayer* at the NP surface, as already observed in the literature for zwitterionic molecules adsorbed onto the oleic acid coating of NPs [16] (i.e. with no ligand replacement).

d.03. UV-Vis spectra

The fluorescent coating of iron oxide NPs, comprising a mixture of ZDS and FCL was analyzed by UV-Visible spectroscopy (Fig 13). After purification by dialysis to remove the free ligands, we registered the absorption spectrum of ZDS/FLC NPs. As visualized in Fig 13, it was in agreement with that of the 5(6)-carboxyfluorescein chromophore of FLC, supporting the successful achievement of the desired fluorescent coating. Moreover, from the quantitative analysis of the UV-Vis spectrum we evaluated that the number of FCL molecules grafted to one iron oxide NP is around $4 \cdot 10^2$. This value can be compared with the ca. $3 \cdot 10^3$ anchored ZDS molecules per NP estimated from the above TGA results.

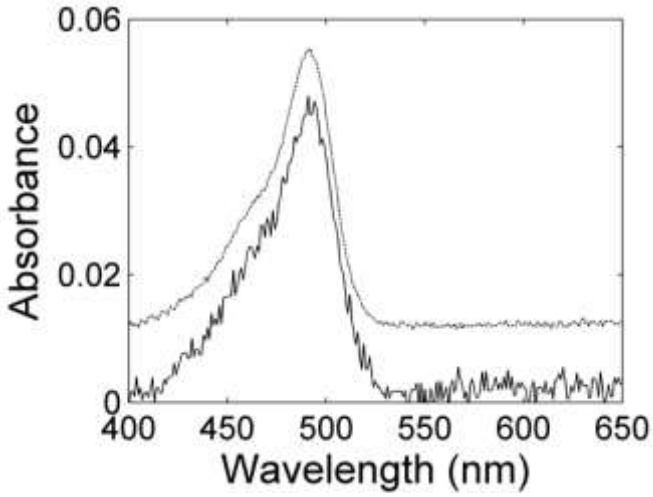

Fig 13. UV-Visible spectrum of fluorescent NPs coated with a mixture of ZDS and FLC in water (solid line) compared with that of 5(6)-carboxyfluorescein (dotted line, shifted upwards by 0.012 absorbance units for the sake of clarity). Image from Ref 21.

03. Study of NP colloidal stability

We decided to employ Dynamic Light Scattering (DLS) to study the colloidal stability of MEEA- and ZDS-NPs, first in deionized (DI) water and then in the complete culture medium of HepG2 cells. We have analyzed both the intensity weighted size distribution P_I and the volume-weighted size distribution P_V.

In deionized water, as shown in Fig 14, both P_I and P_V for MEEA-coated NPs display a single peak with mean diameter $D_I \cong D_V \cong 750$ nm. Therefore, these NPs were present in DI water as aggregates. Instead, ZDS-coated NPs were well dispersed in DI water, displaying a major (85%) peak in P_I at $D_I = 23$ nm and a minor (15%) peak at $D_I = 240$ nm. The size related to the major (99%) peak in the volume weighted distribution ($D_V = 12$ nm) is in agreement with values reported in literature[19] and confirms that the ZDS layer is less than 2 nm thick. Only a minor fraction of ZDS-NP mass is present as aggregates as evidenced by the peak area ratio of both P_I (85:15) and P_V (99:1).

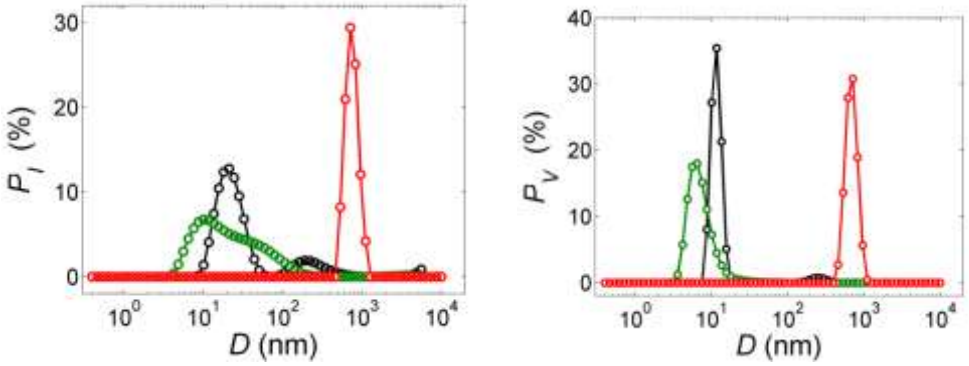

Fig 14. Intensity-weighted diameter distribution P_I (left) and volume-weighted diameter distribution P_v (right) of dispersions of MEEA- (red) and ZDS-coated (black) NPs in deionized water; P_I and P_v of the cell culture medium (green) is also shown. Images from Ref 21.

The ζ potential of ZDS-coated NPs in DI water was measured. Despite that ZDS is globally neutral molecule, the ζ potential of ZDS-NPs in DI was negative, ζ = −8.6 mV, in conformity with that previously measured for quantum dots coated with a polymer exhibiting sulfobetaine pendant moieties (−13.1 mV)[34] and Au NPs covered with sulfobetaine zwitterionic surfactants (−17.9/−14.8 mV)[2].

The DLS results provide an explanation of the very different visual appearance of water dispersion of MEEA- and ZDS-NPs having similar NP concentration (0.15 - 0.20 mg Fe/ml). Indeed, fresh

dispersions of MEEA-NPs appeared as turbid since they formed aggregates, while ZDS-NPs gave dark, clear, stable solutions (Fig 15).

Fig 15. Water dispersions of MEEA- (A) and ZDS-coated (B) iron oxide NPs. Image from Ref 21.

Since ZDS-NPs appeared as well dispersible in DI water, we decided to explore their stability in both the Roswell Park Memorial Institute (RPMI) cell culture medium (which is serum free) and the complete cell culture medium (RPMI supplemented with 2 mM L-glutamine, 100U/ml antibiotic, 1 mM sodium pyruvate and 10% FBS), which will be used to grow the HepG2 cells for the *in vitro* experiments described below. To this purpose, we analyzed the DLS intensity and size distribution of NP dispersions at the concentration and for the time interval used in the uptake experiments, starting from 9 nm ZDS-NPs.

The scattered intensity I_s is very sensitive to an increase of NP size due to protein adsorption or aggregation since I_s is proportional to the sixth power of the NP size (e.g., a 10% size increase causes a 2.5-fold increase of I_s). As shown in Fig 16, the scattered intensity I_s was constant for 24 h in the case of the complete cell culture medium while I_s displays a minor increase only at long times, especially in the 21−24 h range, for the dispersion of ZDS-NPs in the complete cell culture medium. These data witness the good colloidal stability of our dispersions and the absence of significant protein adsorption by ZDS-NPS. These results are confirmed considering that the volume-weighted size distribution P_V did not display significant variations over 24 h (Fig 16).

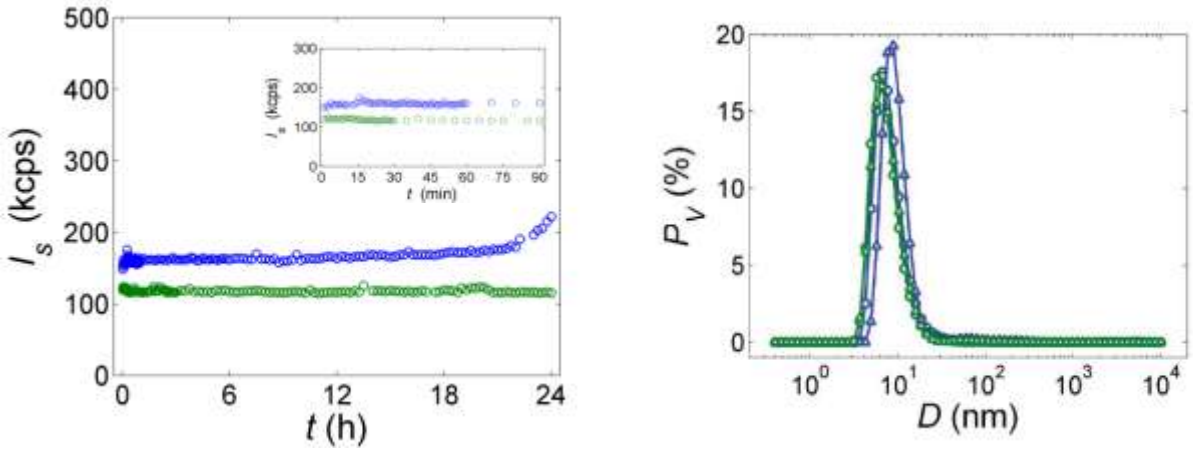

Fig 16. Comparison of DLS of complete cell culture medium with (blue) and without (green) ZDS-NPs. Left) intensity of the scattered light I_s as a function of time t (the inset shows the initial behavior). Right) Volume weighted distribution P_V of the hydrodynamic diameter. Circles: t = 0 h, triangles t = 24 h. Images from Ref 21.

The first order autocorrelogram $g_1(\tau)$ and intensity-weighted size distribution P_I (Fig. 17) indicate that P_I increased after 24 h. However, we have to consider that both I_s and P_I are very sensitive to size changes (I_s, $P_I \propto D^6$), so the size increase occurring after 24 h can be considered negligible. Indeed, this variation can be ascribed to changes occurring in the medium during time, since both $g_1(\tau)$ and P_I curves have similar behavior. For this reason, we could exclude that protein adsorption at the ZDS-NP surface occurred. Note that this process normally develops in a few minutes after contacting NPs and proteins and leads to a huge increase in I_s[35].

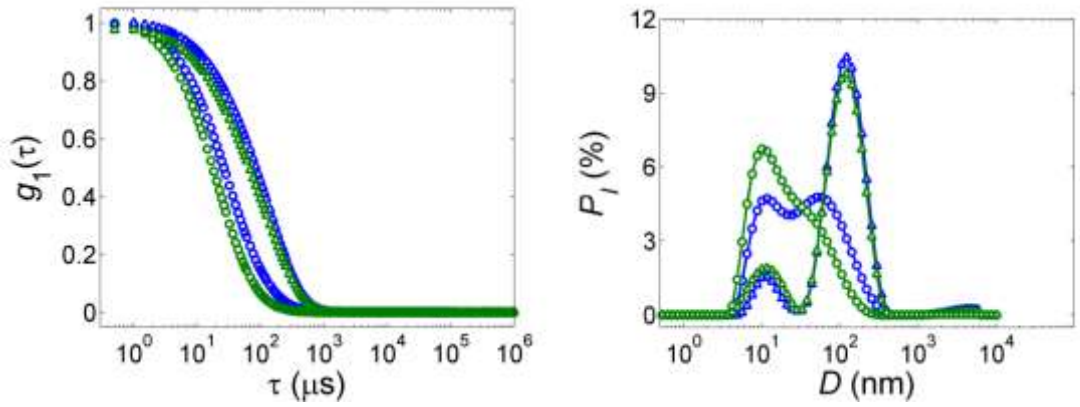

Fig 17. Normalized first-order autocorrelograms $g_1(\tau)$ (left) and intensity-weighted distribution P_I (right) of ZDS-NPs in complete cell culture medium (blue) and of the pure cell culture medium (green). Circles or triangles denote data at 0 h or at 24 h. Images from Ref 21.

To confirm the good stability of ZDS-coated NPs, we carried out the same DLS experiments employing ZDS-coated iron oxide NPs, having a diameter *ca*. 12 nm. Their D_V in deionized water was equal to 15 nm. After dispersing the NPs (0.05 mg/ml) in RPMI serum-free, we measured D_I = 19−23 nm and D_V = 15 nm. The NPs were colloidally stable for 24 h and a very minor aggregation was observed in P_I (Fig 18).

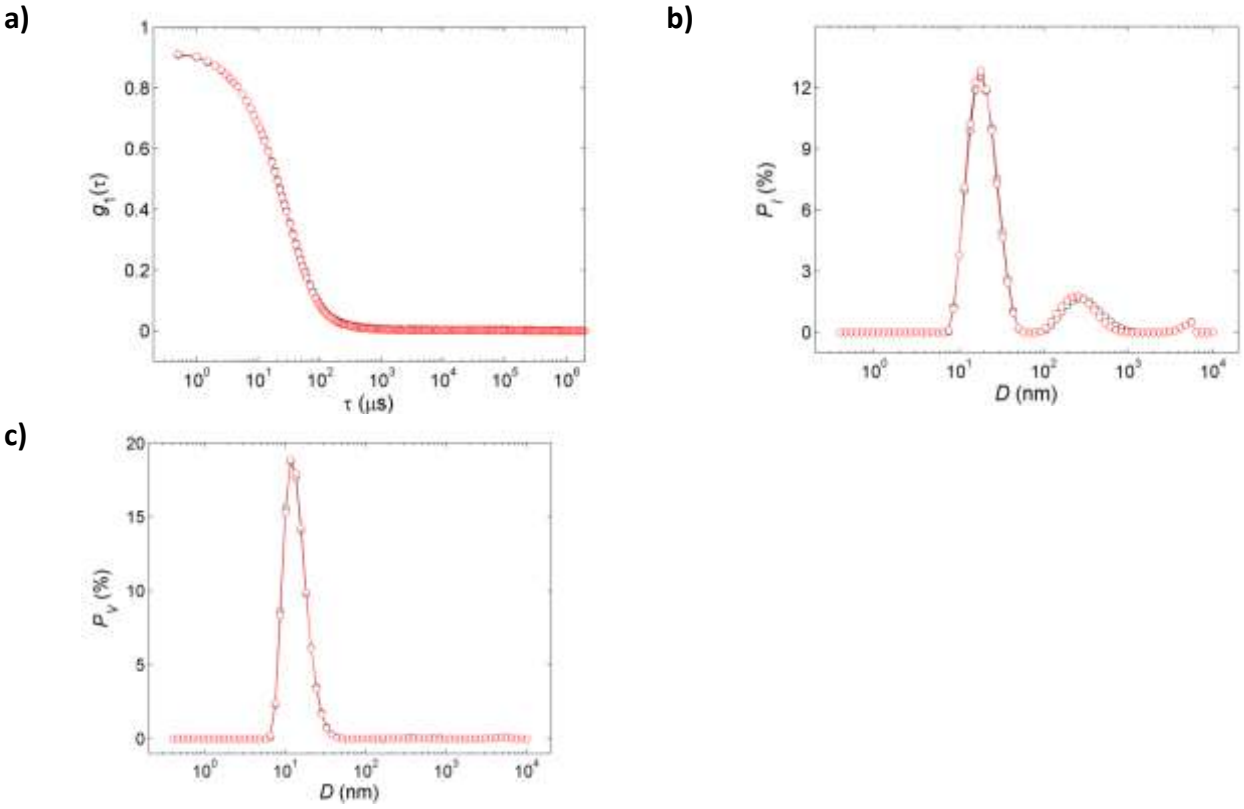

Fig 18. DLS of 12 nm ZDS-NPs in RPMI medium (serum free) at 0 (black) and 24 h (red). a) First-order autocorrelation function $g_1(\tau)$, b) intensity-weighted diameter distribution P_I, c) volume-weighted diameter distribution P_V. Image from Ref 21.

Next, DLS experiments were carried out on dispersions of 12 nm ZDS-coated NPs in the complete cell culture medium (Fig 19). Only very minor size changes (and hence protein adsorption) were observed.

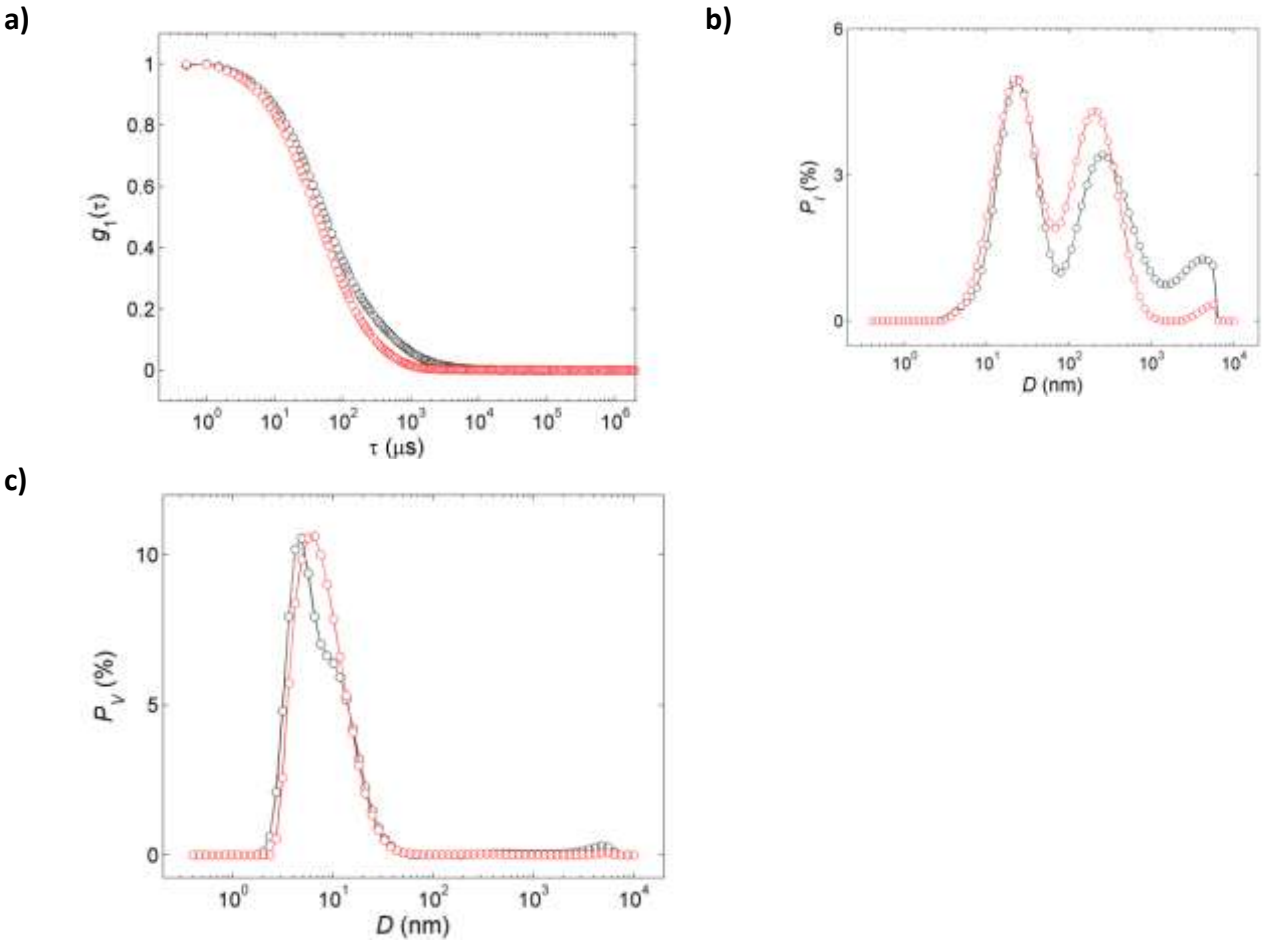

Fig 19. DLS of 12 nm ZDS-coated iron oxide NPs in cell culture medium (modified RPMI + 10% FBS) at 0 (black) and 24 h (red). a) Normalized first-order autocorrelation function $g_1(\tau)$, b) intensity-weighted diameter distribution P_I, c) volume-weighted diameter distribution P_V. Image from Ref 21.

Finally we studied the behavior of 12 nm ZDS-coated NPs in PBS 1× added with 10% FBS. All results confirmed the absence of protein adsorption and the substantial colloidal stability after 24 h for these nanosystems (Fig 20).

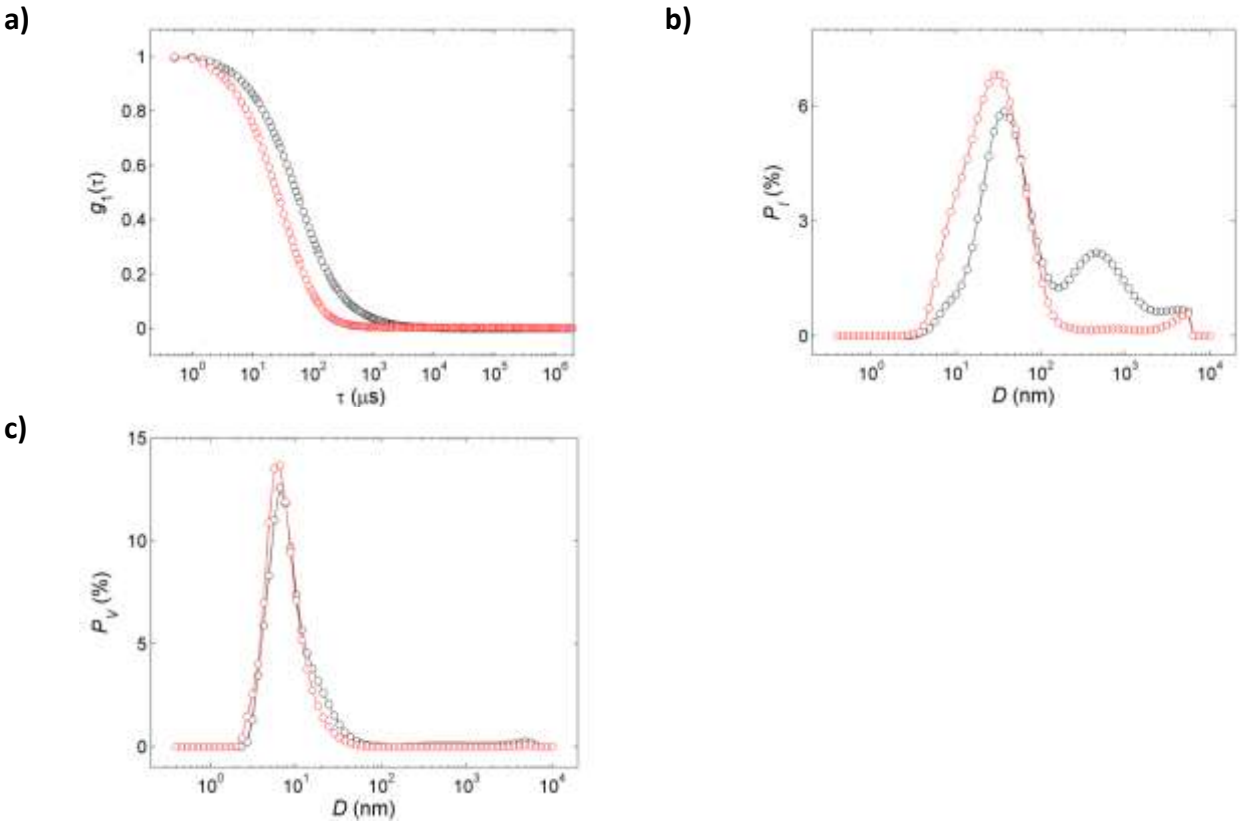

Fig 20. DLS of 12 nm ZDS-coated iron oxide NPs in PBS (1x) added with 10% FBS at 0 (black) and 24 h (red). a) Normalized first-order autocorrelation function $g_1(\tau)$, b) intensity-weighted diameter distribution P_I, c) volume-weighted diameter distribution P_V. Image from Ref 21.

04. NP Cytotoxicity

All biological experiments were made in collaboration with the group of Dr. Bice Chini (CNR, Istituto di Neuroscienze, Milano).

We tested the cytotoxicity of MEEA- and ZDS-coated iron oxide NPs by the MTS test, a colorimetric method that quantifies the metabolic activity of cells by evaluating the reduction of [3-(4,5-dimethylthiazol-2-yl)-5-(3-carboxymethoxyphenyl)-2-(4-sulfophenyl)-2H-tetrazolium] (MTS) (CellTiter 96® AQueous One Solution Cell Proliferation Assay, Promega). Viable cells reduce MTS molecule by NAD(P)H-dependent dehydrogenase enzymes to generate a colored formazan product that is soluble in the cell culture medium and whose absorbance can be measured at 490-500 nm. The applied procedure is described in detail in the Experimental Section.

We evaluated the toxic effect on HepG2 cells of iron oxide NPs (added to the cell medium to final concentrations of 2.5, 5, 10, 25, 50, and 100 μg Fe/ml) after 24 h exposure. The percentage

difference between treated and untreated cells was employed to express cell viability. In general, we observed that the addition of NPs to the cell culture medium did not significantly perturb its pH and osmolarity. In more detail, we found that the highest doses of MEEA-coated NPs (50 and 100 μg Fe/ml) induced a small cytotoxic effect whereas even the highest dose of ZDS-NPs did not induce a cytotoxic effect (Fig 21). Iron does not interfere with the MTS test even at the highest NP concentration employed in these experiments (100 μg/ml)[36].

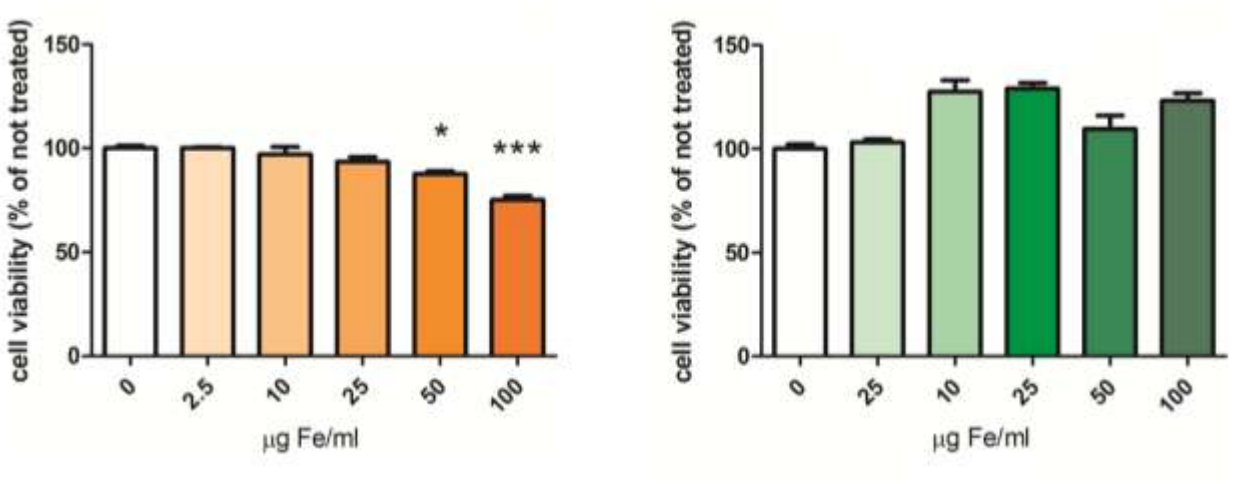

*Fig 21. Cell viability upon exposure to increasing concentrations of MEEA- (left) or ZDS- coated (right) NPs [MTS cell viability assay]. Obtained data are presented as mean ± SEM and compared to control values using ANOVA test. * $p<0.05$; *** $p<0.001$. Image from Ref 21.*

05. Uptake experiments by HepG2 cells

As already mentioned in the Introduction, we employed human liver carcinoma cells (HepG2) for the NP uptake experiments since these cells display a high phagocytic activity. We evaluated the NP internalization in two ways: qualitatively, by Prussian Blue staining and imaging, and quantitatively, by UV-Vis spectroscopy. In our assays, HepG2 cells were treated for 24 h with NPs added to the culture medium at final concentration of 0, 2.5, 10, 25, 50 or 100 μg Fe/ml.

e. Qualitative iron evaluation

To carry out a qualitative investigation of the NP internalization, HepG2 cells were exposed to increasing concentration of iron oxide NPs and then the internalization was observed by Prussian Blue staining of the washed cells. The complete procedure is described in detail in the Experimental Section. For both MEEA-NPs and ZDS-NPs the intracellular uptake increases with the NP dose.

Prussian Blue staining clearly revealed much larger intracellular MEEA-NPs than ZDS-NPs (Fig 22), probably because MEEA-NP aggregates were internalized.

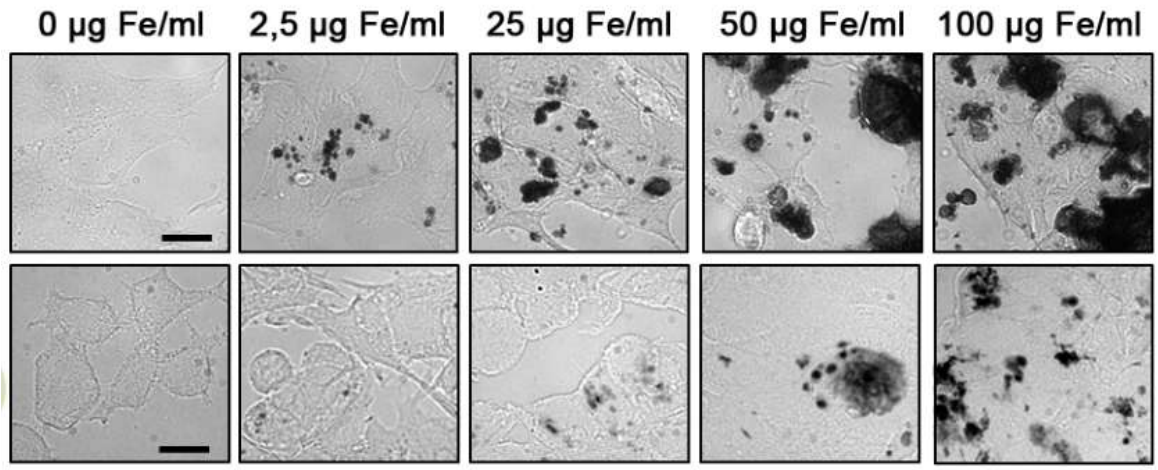

Fig 22. Prussian Blue staining of HepG2 cells after treatment with iron oxide NPs. HepG2 cells were exposed for 24 hours to different concentrations of MEEA- (top) or ZDS-coated (bottom) NPs, washed and processed for Prussian Blue staining and optical imaging. Black aggregates indicate the presence of iron. Scale bar = 10 µm. Image from Ref 21.

f. Quantitative iron quantification

HepG2 cells were treated for 24 h with NPs added to the culture medium at final concentration of 0, 2.5, 10, 25, 50 or 100 µg Fe/ml. To quantify the intracellular iron content we used a procedure described in detail in the Experimental Section. In brief, cellular pellets were digested with concentrated HCl/HNO_3 and the resulting aqueous solution was treated with tiron (disodium 4,5-dihydroxybenzene-1,3-disulfonate) at pH ≈ 7 to form the red complex $Fe(tiron)_3$. This complex is suitable for quantification by UV-Vis spectroscopy[37]. UV-Vis data were analyzed by fitting a broad spectral interval (400-800 nm), thus ensuring better accuracy with respect to previous methods[38,39]. The cell protein content was quantified by the BIORAD-Dc protein assay in order to express the NP internalization as mass(internalized iron)/mass(protein). The native iron content of HepG2 cells was $(m_{Fe}/m_{protein})_{control}$ = (0.4 ± 0.1) $\mu g_{Fe}/mg_{protein}$. The iron uptake was calculated as $U = (m_{Fe}/m_{protein})_{treated} - (m_{Fe}/m_{protein})_{control}$, where m_{Fe} and $m_{protein}$ are the cellular iron and protein mass, respectively, both evaluated after 24 h treatment and averaged over the replicates (Fig 23).

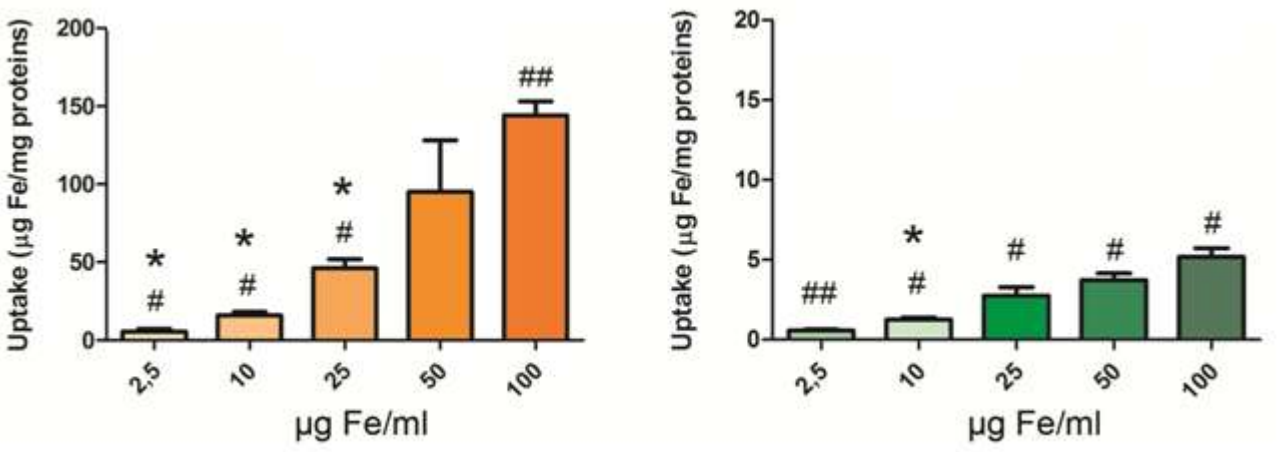

Fig 23. NP internalization in HepG2 cells after 24 h incubation with increasing concentrations of MEEA- (left) or ZDS-coated (right) NPs. Note the different vertical scales in the subpanels. Results are presented as mean ± SEM and their significance was assessed using Student's t-test, after testing for equal variance using the F-test. Student's t-test was applied to test for uptake differences between adjacent doses (*) and with respect to the control (#). p<0.05; # p<0.05, ## p<0.005. Image from Ref 21.*

The plots show that the NP internalization depends on the dose of NPs administered to HepG2 cells in the culture medium for both MEEA- and ZDS-coated iron oxide NPs. Experimental constraints, for instance an excessive volume of NP dispersion added to the culture medium, did not allow us to increase the NP final concentration to more than 100 µg Fe/ml. According with Prussian Blue staining observations, the amount of NPs taken up by HepG2 cells was closely related to the surfactant type: in particular the amount of internalized MEEA-NPs was 20-30 times higher than that of ZDS-NPs. Since these NPs have the same core and coating size, the surface chemistry is the only responsible for their different cell internalization. We could ascribe these results to the dissimilar surfactant charge (zwitterionic vs. neutral), which might influence the interaction of NPs with cell membranes. However, DLS results showed that such chemical differences primarily influenced NP colloidal stability in the culture medium, so that MEEA-coated NPs were internalized to a larger extent probably thanks to their presence as micrometer-sized aggregates[35], maybe involving a size-dependent uptake mechanism. On the other hand, DLS showed that ZDS-NPs did not vary their hydrodynamic size owing to protein adsorption or aggregation in the full cell culture medium, so they interacted as well-dispersed with cells affording low internalization.

We compared our uptake data with those reported in literature. First, we considered internalization of iron oxide NPs by HepG2 cells. In the case of MEEA-coated NPs our results are higher but comparable with the internalization observed for NPs forming aggregates. Some examples are the uptake of cationic and galactose-decorated magnetoliposomes[40], iron oxide NPs covered with

glucosamic acid[41] or aminopropylsiloxane groups[24] and commercially available "anionic" NPs[42]. Considering NPs well-dispersed to compare their behavior with ZDS-coated NPs, nanocrystals covered with PEG600 carboxylic acid[24] and anionic magnetoliposomes[40] were internalized in a larger amount with respect to our ZDS nanosystems. A slighty lower uptake than that of ZDS-NPs was reported for iron oxide NPs coated with dimercaptosuccinic acid[23]. Second, we considered two reports concerning the uptake of NPs coated with zwitterions, in particular with a polymeric coating functionalized with carboxybetaines. One report described the internalization by RAW 264.7 cells of well dispersed NPs (D = 19 nm) coated with polyacrylic acid bearing ammonium groups. The second report[14] described the exposure of RAW 264.7 and also HUVEC cells to NPs ($D \approx 130$ nm) coated with a polycarboxybetainemethacrylate polymer. Assuming that HepG2, RAW 264.7 and HUVEC cells have a comparable protein content, the internalizations of NPs coated with a zwitterionic polymer and with our small ZDS molecule were very similar. These comparisons suggest that the hydrodynamic diameter of zwitterionic NPs scarcely affects their uptake by cells.

06. Study of the intracellular NP fate

Finally, to explore the intracellular destiny of ZDS-NPs, we used fluorescent iron oxide NPs coated with a mixture of ZDS and FCL. TGA and UV-Vis data showed that the number of FCL molecules in the coating is about 10% of the number of ZDS molecules. HepG2 cells were exposed for 24 hours to different concentrations of the fluorescent NPs, then washed and processed for optical imaging according to the procedure described in detail in the Experimental Section. First, confocal microscopy images again witnessed a dose-dependent uptake by cells (Fig 24). Moreover, these NPs did not stain the plasma membrane, a remark supporting that the final washing of HepG2 with PBS solution was effective in removing non-internalized NPs.

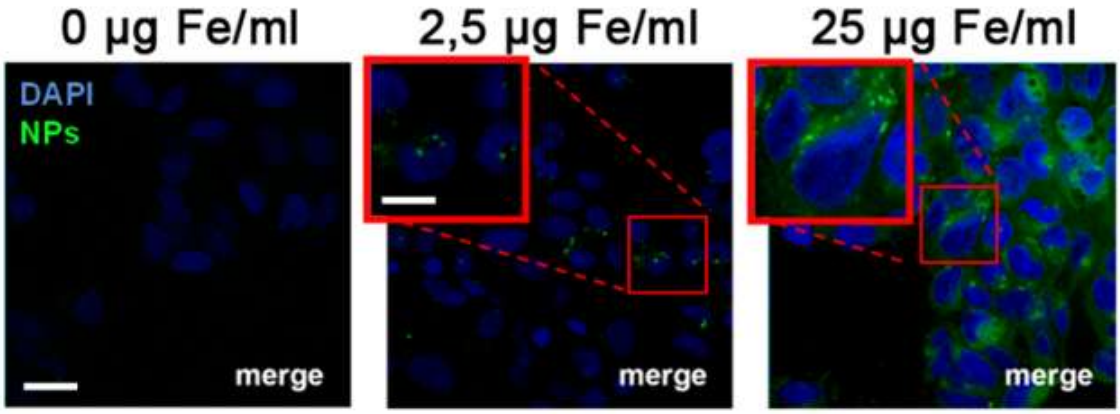

Fig 24. Confocal images of HepG2 cells treated with fluorescent NPs. The NPs are coated with a mixture of ZDS and FCL ca. 9:1 mol/mol. Scale bar = 20 µm. Inset scale bar = 10 µm. Image from Ref 21.

However, the most important information deriving from the study of the internalization of fluorescent NPs concerned the intracellular fate of the NPs (green) which was studied by labeling *in vivo* lysosomes with Lysotracker-Red (red) and cell nuclei with DAPI (blue). Co-localization of the green and red signals, 6 or 24 hours after the addition of NPs in the cell medium, proved that these NPs in HepG2 cells were localized in lysosomes (Fig 25).

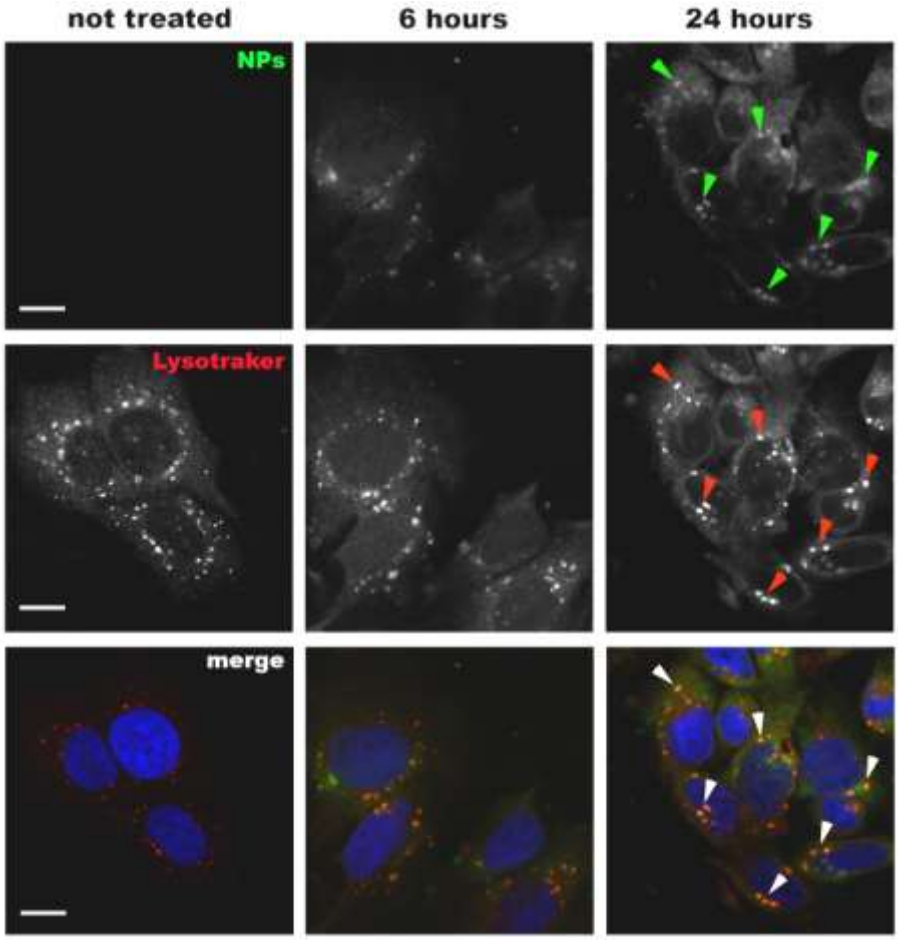

Fig 25. Lysosomal accumulation of fluorescent NPs, coated with a mixture of ZDS and FCL, in HepG2 cells. Cells were exposed to these NPs for 6 or 24 hours. Arrowheads indicates sites of colocalization between the green (NPs) and the red signal (Lysotracker). Scale bar: 5 μm. Image from Ref 21.

Such result could be interesting for the potential application of ZDs-coated NPs in cancer therapy because magnetic NPs with the same lysosomial destiny[39-43] have already been reported in the literature as efficient killers of tumor cells. Indeed, they induced cell death through the release of the lysosome content in the cytosol when exposed to an external magnetic field[43].

07. Conclusions

In this part of my PhD thesis, we prepared iron oxide NPs coated with a small zwitterionic molecule, ZDS, and we characterized them from the physico-chemical point of view, analyzing their coating structure and their colloidal stability in order to explore the protein adsorption on the NP surface. On the basis of such results, we also explored their cellular toxicity, uptake and intracellular destiny by HepG2 cells.

We compared the ZDS-coated NPS with MEEA-coated NPs obtained from the same batch of nanocrystals, with the aim of investigating the effects due to the different surface chemistry. ZDS-coated NPs have a high density of sulfobetaine ligands, which provides NPs with high colloidal stability even in the complete cell culture medium by avoiding NP aggregation or precipitation and the protein adsorption at their surface. Conversely, MEEA-coated NPs show low colloidal stability in deionized water and the fast formation of micrometer-sized aggregates.

Cellular toxicity and the efficiency of aspecific uptake are affected by such different behavior, which has a deep impact on the *in vitro* interaction between NPs and cells. Therefore, we have confirmed the centrality of NP surface chemistry in NP-cell interactions and why it is important to monitor the NP dispersion during biological *in vitro* assays.

ZDS-NPs were not toxic for HepG2 cells even at the highest administered concentration (100 µg Fe/ml), while MEEA-NPs caused cytotoxicity already at 50 µg Fe/ml. Both NP types are aspecifically internalized in HepG2 cells in a dose-dependent way, but to a very low extent for the zwitterionic NPs. One could benefit from this aspect when highly selective targeting through specific NP functionalization is desired.

Finally, ZDS-coated NPs showed a lysosomal intracellular destiny, which is desirable when we want to destroy targeted cells, such as in tumor treatment. Taken together, all the advantages underlined for ZDS-coated NPs, indicate that they could be considered as a good backbone for the development of theranostic nanosystems.

08. Experimental section

g. Materials

All chemicals [dopamine hydrochloride (98.5%), 1,3-propansultone, iodomethane, 4,7,10-trioxa-1,13-tridecanediamine, triethylamine, trityl chloride, diglycolic anhydride, pyridine (Pyr), N-hydroxybenzotriazole (HOBt), 1-ethyl-3-(3-dimethylaminopropyl)carbodiimide (EDC), N,N-diisopropylethylamine (DIPEA), triisopropylsilane (TIPS), trifluoroacetic acid (TFA), N-hydroxysuccinimide (NHS), N,N'-diisopropylcarbodiimide (DIC), iron pentacarbonyl ($Fe(CO)_5$), oleic acid (OlAc, 90%), octyl ether (99%) , 2-[2-(2-methoxyethoxy)ethoxy] acetic acid (MEEA, 90%)] and solvents [methanol, ethanol (98%), octadecene (ODE, 90%), aqueous ammonia, dimethylformamide (DMF), acetone (tech. grade), ethyl acetate, dichloromethane (DCM), diisopropylether] were acquired from Sigma-Aldrich and employed as received without further purification. To digest NPs we used concentrated acids (HNO_3 and HCl) that were Aldrich Trace Select reagents. Deionized (DI) water was obtained using a Milli-Q Plus water purification system (resistivity > 18.2 mΩ cm at 25 °C). The human liver carcinoma cells (HepG2) were obtained from the American Type Culture Collection.

h. Procedures

h.01. Acronyms used in the experimental section

OlAc = oleic acid
$Fe(CO)_5$ = iron pentacarbonyl
RT = room temperature
DMF = dimethylformamide
D_2O = deuterium oxide
TEA = triethylamine
$NaHCO_3$ = sodium hydrogen carbonate

Na_2SO_4 = sodium sulfate

$CDCl_3$ = deuterochloroform

TrCl = trityl chloride

DCM = dichloromethane

EDC = 1-ethyl-3-(3-dimethylaminopropyl)carbodiimide

Pyr = pyridine

HOBt = N-hydroxybenzotriazole

DIPEA = N,N-diisopropylethylamine

CH_3OH/ MeOH = methanol

iPrOH = isopropanol

CD_3OD = deuterated methanol

TIPS = triisopropylsilane

TFA = trifluoroacetic acid

i-Pr_2O = isopropyl ether

NHS = N-hydroxysuccinimide

DIC = N,N'-diisopropylcarbodiimide

CH_3CN = acetonitrile

DI water = deionized water

PBS = phosphate buffer saline

PFA = paraformaldehyde

HCl = hydrochloric acid

HNO_3 = nitric acid

DAPI = 4′,6-diamidine-2′-phenylindole dihydrochloride

tiron = disodium 4,5-dihydroxy-1,3-benzenedisulfonate

h.02. Preparation of 9 nm iron oxide NPs

9 nm iron oxide NPs were produced according to a modification of a published literature procedure[29]. Oleic acid (OlAc, 600 µl, 1.89 mmol) was dispersed in octyl ether (10 ml) and oxygen was repeatedly removed from the solution at RT by vacuum/nitrogen cycles. Afterwards, the solution was heated to 105 °C under nitrogen and, after another degassing cycle, $Fe(CO)_5$ (200 µl, 1.52 mmol) was injected into the reaction mixture ($Fe(CO)_5$:OlAc = 1:1.25 mol/mol). The mixture was heated to reflux (285 °C) with a rate of 3.3 °C/min and maintained at this temperature for 25

min. Around 260 °C the color of the reaction mixture changed from pale yellow to black. The reaction crude, cooled at RT, was treated with acetone and the precipitated NPs were collected by centrifugation (6000 rpm for 10 min). The NPs were washed several times with acetone or ethanol and recovered by centrifugation (6000 rpm for 10 min). Finally, the OlAc-coated NPs were dispersed in hexane (20 ml).

h.03. Preparation of 12 nm iron oxide NPs

12 nm iron oxide NPs were produced according to a modification of a published literature procedure[30]. $Fe(CO)_5$ was injected in a solution of 1-octadecene and oleic acid ($Fe(CO)_5$:OlAc = 1:3 mol/mol) at 120 °C and then heated to 320°C for 3 h under nitrogen. After cooling at RT, the NPs were precipitated by adding acetone and collected by centrifugation. Then, they were repeatedly washed with acetone and dispersed in toluene.

h.04. Synthesis of zwitterionic dopamine sulfonate (ZDS)

ZDS molecule was synthesized in two steps following the Scheme 1, a modification of an already reported procedure[17], which is detailed below.

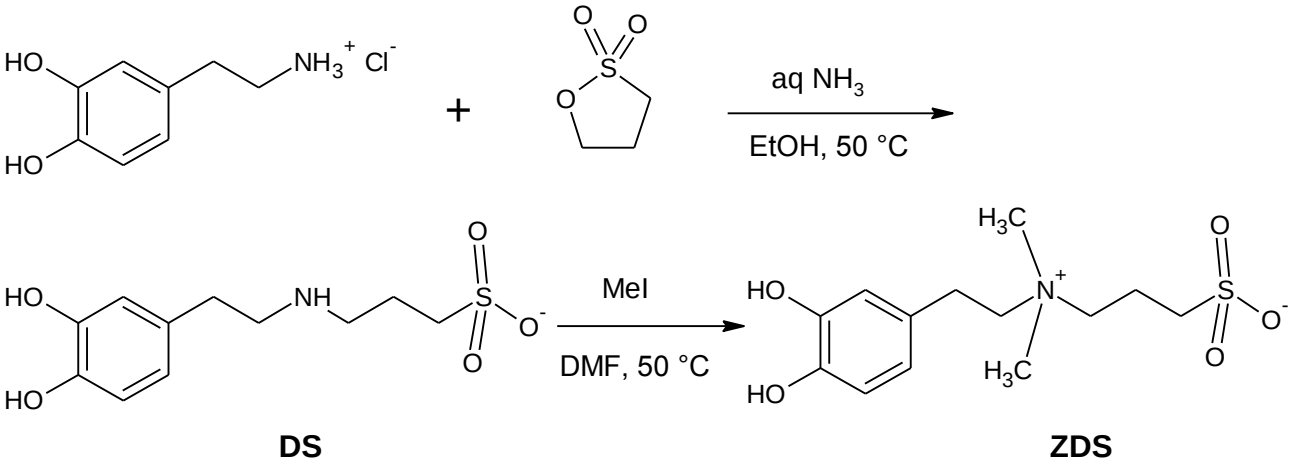

Scheme 1. Synthesis of ZDS molecule [21].

h.04. 1. Synthesis of dopamine sulfonate, DS

28% aq. ammonia (416 μL, 3.00 mmol) and 1,3-propanesultone (799 mg, 6.50 mmol) were slowly added to a solution of dopamine hydrochloride (1.14 g, 6.0 mmol) in ethanol (150 mL) under inert gas. The mixture was warmed up to 50 °C and stirred for 72 h, giving a white precipitate. The solid (DS) was recovered by centrifugation, washed with ethanol (3 x 10 mL) and finally dried under reduced pressure.

^{1}H-NMR (400 MHz, D_2O): δ (ppm) 2.00 (m, 2H), 2.78-2.82 (m, 2H), 2.86-2.91 (m, 2H), 3.06-3.12 (m, 2H), 3.16-3.18 (m, 2H), 6.72-6.74 (m, 1H), 6.78- 6.82 (m, 2H). ^{13}C-NMR (100 MHz, D_2O): δ (ppm) 21.1, 30.9, 46.1, 47.8, 48.6, 116.4, 121.1, 128.9, 143.0, 144.2.

h.04. 2. Synthesis of zwitterionic dopamine sulfonate, ZDS

Anhydrous sodium carbonate (0.254 g, 2.40 mmol) was added to a solution of DS (0.329 g, 1.00 mmol) in DMF (150 mL) and mixed under nitrogen for 2 h. After that, iodomethane (2.2 mL, 35 mmol) was added to the mixture, which was heated to 50 °C and continuously stirred overnight. After reaction completion, the solvent was evaporated under reduced pressure, obtaining an oil which was purified through several consecutive crystallization steps with DMF/ethyl acetate (1:10 v/v, 50 mL) finally leading to a white solid collected by centrifugation and dried under reduced pressure.

^{1}H-NMR (400 MHz, D_2O): δ (ppm) 2.21 (m, 2H), 2.92-2.95 (m, 4H), 3.13 (s, 6H), 3.47-3.51 (m, 4H), 6.74-6.76 (m, 1H), 6.83-6.88 (m, 2H). ^{13}C-NMR (400 MHz, D_2O): δ (ppm) 18.1, 27.7, 47.1, 50.7, 62.0, 64.6, 116.5, 121.2, 128.2, 143.0, 144.2.

h.05. Synthesis of fluorescent catecholic ligand (FCL)

The fluorescent catecholic ligand (FCL) was produced following the Scheme 2 reported below starting from the product commercially acquirable 4,7,10-trioxa-1,13-tridecanediamine (**1**).

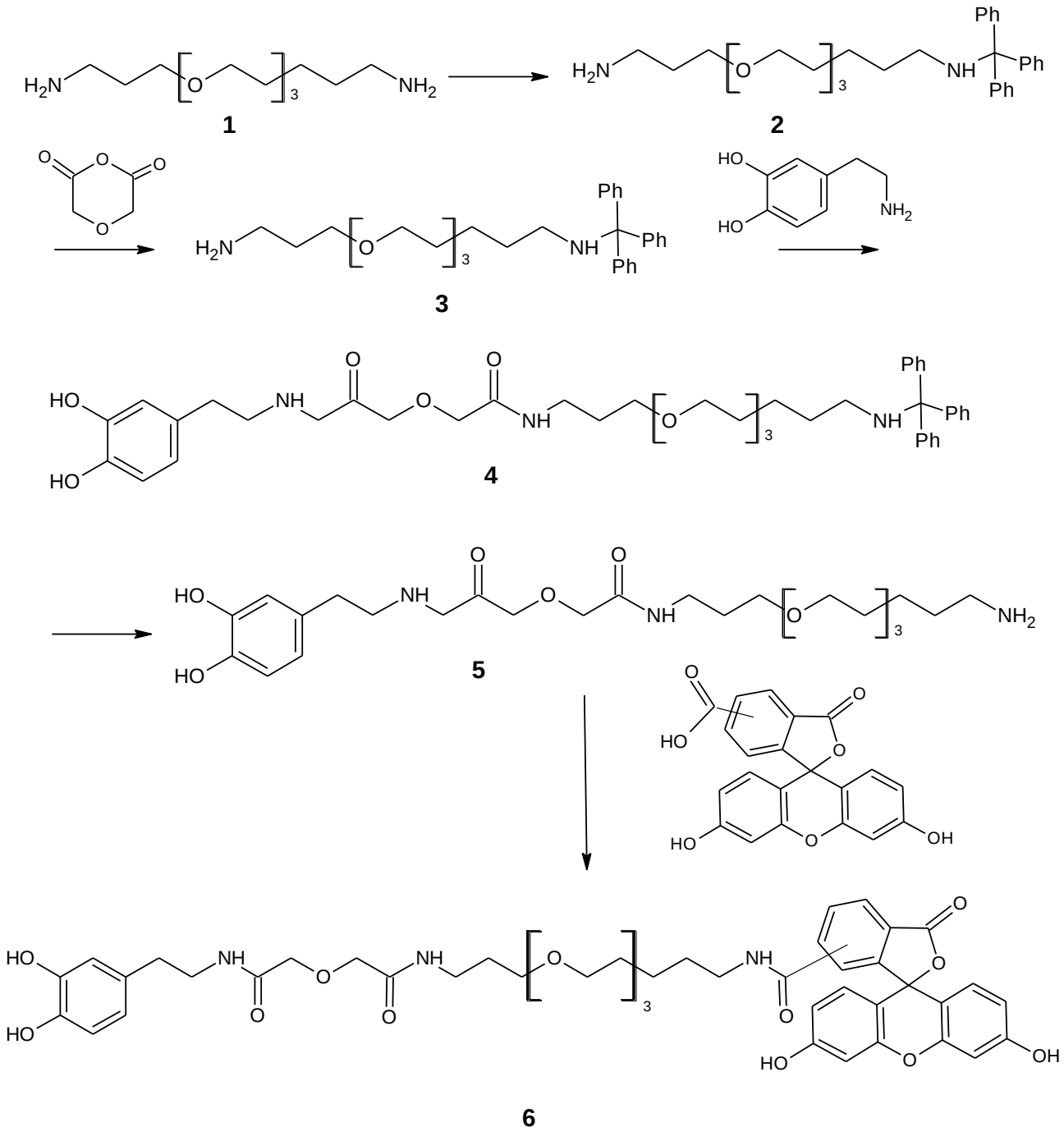

*Scheme 2. Synthetic pathway leading to the FCL (**6**)*[21].

h.05.1 Synthesis of compound 2

A solution of compound **1** (5 g, 22.70 mmol) in dichloromethane (250 ml) and TEA (0.475 mL, 3.41 mmol) was stirred for 30 min. After cooling to 0°C with an ice-bath, trityl chloride (TrCl, 632 mg, 2.27 mmol) was added to the crude in small portions. Then the ice-bath was removed and the reaction mixture was maintained overnight at RT. The DCM phase was washed twice with a $NaHCO_3$ saturated solution, dried with anhydrous Na_2SO_4, separated out and finally evaporated under reduced pressure to give product **2** (1.07 g, 2.27 mmol, quantitative yield).

^{1}H-NMR (400 MHz, $CDCl_3$, 25 °C): δ = 7.43-7.37 (m, 6 H, aromatic protons Tr), 7.23-7.17 (m, 6 H, aromatic protons Tr), 7.13-7.08 (m, 3 H, aromatic protons Tr), 3.58-3.41 (m, 12 H, $CH_2OCH_2CH_2OCH_2CH_2OCH_2$), 2.78 (t, 2 H, CH_2NH_2), 2.20-2.11 (m, 2 H, CH_2NH) 1.76-1.63 (m, 4 H, $CH_2CH_2NH_2$, CH_2CH_2NH). ESI-MS: m/z 463.5 [M+H]+.

h.05.2 Synthesis of compound 3

Compound **2** was dissolved in dry DMF (10 ml); then diglycolic anhydride (527 mg, 4.54 mmol) and pyridine (Pyr, 0.736 mL, 9.08 mmol) were added to the solution and were mixed for 16 h at RT. The crude was acidified to pH 5 with an aqueous solution of 5% citric acid. The desired and practically pure compound **3** was extracted from water with DCM, dried on anhydrous Na_2SO_4, filtered off and finally obtained by evaporation under reduced pressure.

^{1}H-NMR (400 MHz, CDCl3, 25 °C): δ = 7.63-7.51 (m, 5 H, aromatic protons Tr), 7.44-7.31(m, 10 H, aromatic protons Tr), 4.19 (s, 2H, CH_2COOH), 4.13(s, 2H, OCH_2CO), 3.55(m, 6 H), 3.52(t, 2 H,CH_2NHCO), 3.45-3.35(m, 6 H), 3.2(t, 2 H, CH_2NHCTr), 2.04(t, 2 H, CH_2CH_2NHCTr), 1.79(t, 2 H, CH_2CH_2NHCO). ^{13}C NMR (400 MHz, $CDCl_3$, 25 °C): δ = 138.8, 128.8, 128.7, 128.6, 71.3, 70.6, 70.5, 70.3, 70.1, 69.9, 69.4, 69.2, 45.4, 36.9, 36.3, 31.3, 28.7, 25.4 .ESI-MS: m/z 579.5 [M+H]+.

h.05.3 Synthesis of compound 4

EDC (154 mg, 0.801 mmol), HOBt (108 mg, 0.801 mmol) and DIPEA (0.458 mL, 2.676 mmol) were consecutively added at RT to a mixed solution of compound **3** (426 mg, 0.736 mmol) in DMF (5mL). After complete dissolution of the reagents, dopamine hydrochloride (127 mg, 0.669 mmol) was added and the reaction was stirred until completion, as assessed by HPLC-MS. Finally, the DMF was evaporated in vacuo and the crude product was recovered as pure **4** by BiotageTM C18

reverse phase chromatography. We applied the following BiotageTM eluant conditions: gradient from 90% H_2O-10% CH_3OH-iPrOH(6:4) to 100% CH_3OH-iPrOH (6:4). 286 mg, 0.399 mmol, 60% yield.

^{1}H-NMR (400 MHz, CD_3OD, 25 °C): δ = 7.46-7.40 (m, 6 H, aromatic protons Tr),7.29-7.21 (m, 6 H, aromatic protons Tr), 7.20-7.14 (m, 3 H, aromatic protons Tr), 6.68 (d, 1 H, catechol, Jortho= 8.3 Hz), 6.65 (d, 1 H, catechol, Jmeta= 1.7 Hz), 6.52 (dd, 1 H, catechol, Jortho= 8.3 Hz, Jmeta= 1.7 Hz), 4.00 (s, 2 H), 3.98 (s, 2 H), 3.61-3.51 (m, 8 H), 3.50-3.44 (m, 4 H), 3.41 (t, 2 H), 2.67 (t, 2 H), 2.25 (t, 2 H), 1.76 (qt, 4 H), 1.15 (d, 2 H). ^{13}C NMR (400 MHz, $CDCl_3$, 25 °C): δ = 129.7, 128.4, 127.0, 120.8, 116.6, 116.1, 71.3, 71.26, 71.22, 71.06, 70.99, 70.93, 68.6, 41.3, 40.5, 36.3, 34.5, 29.8, 29.0. ESI-MS: m/z 714.5 [M+H]+.

h.05.4 Synthesis of compound 5

A solution of compound **4** (120 mg, 0.168 mmol) solved in DCM (5 mL), TIPS (0.070 mL, 0.336 mmol) and TFA (0.250 mL) were stirred for 2 h at RT. Then, DCM was evaporated under reduced pressure. The crude residue was treated with water and extracted twice with i-Pr_2O. The organic phase was then dried on Na_2SO_4, removed in vacuo affording the product **5** (95 mg, yield 82%) which can be used without further purification. ^{1}H-NMR (400 MHz, D2O, 25 °C): δ 6.90 (d, 1 H, catechol, J_{ortho}= 7.6 Hz) 6.84 (d, 1 H, catechol, J_{meta}= 1.76 Hz), 6.75 (dd, 1 H, catechol, J_{ortho} = 7.6 Hz, J_{meta} = 1.76 Hz), 4.10 (s, 2 H), 4.03 (s, 2 H), 3.78-3.66 (m, 10 H), 3.62 (t, 2H), 3.53 (t, 2H), 3.30 (t, 2 H), 3.15 (t, 2 H), 2.78 (t, 2 H), 1.99 (qt, 2 H), 1.84 (qt, 2 H). ESI-MS: m/z 472.3 $[M+H]^+$.

h.05.5 Synthesis of compound 6 (FCL)

NHS (30 mg, 0.225 mmol) and DIC (90 µl, 0.56 mmol) were consequently added to a mixture of 5(6)-carboxyfluorescein (85 mg, 0.225 mmol) in dry DMF (4 ml) and then were stirred at RT for 18 h. After reaction completion, DMF was removed under reduced pressure and the residue was left under the high vacuum during the night. Then, it was diluted in dry DMF (3 ml) and then slowly added to a solution of compound **5** (0.225 mmol) and DIPEA (154 µl, 0.90 mmol) in dry DMF (2 ml), that was magnetically mixed over night at RT. Finally the organic solvent was evaporated and compound **6** was purified by HPLC using a C18 reverse column. We applied the following HPLC

eluant conditions: from 90% H_2O/ 10% CH_3CN to 100% CH_3CN with a flow rate 20 ml/min. Yield of pure FCL: 57% (106 mg, 0.128 mmol).

^{1}H-NMR (400 MHz, D_2O, 25 °C): δ = 8.40 [s, 1H, 5(6)-carboxyfluorescein], 8.14 [dd, 1H, 5(6)-carboxyfluorescein], 8.06 [dd, 1H, 5(6)-carboxyfluorescein], 7.61 [s, 1H, 5(6)-carboxyfluorescein], 7.26 [d, 1H, 5(6)-carboxyfluorescein], 6.72-6.43 (m, 10H, 5(6)-carboxyfluorescein and catechol), 3.94- 3.95 (2s, 4H), 3.57- 3.23 (m, 18H), 2.58-2.62(t, 2H), 1.89-1.60 (m, 4 H). ^{13}C NMR (400 MHz, D2O, 25 °C): δ = 133.75, 129.32, 129.18, 129.06, 119.67, 115.50, 115.03, 102.24, 70.11, 70.09, 70.05, 69.88, 69.79, 58.60, 48.48, 40.47, 34.45, 28.97. ESI-MS: m/z 830.7 [M]+; 852.7 [M+Na]+.

h.06. Ligand exchange procedures

h.06.1 Preparation of MEEA- or ZDS-coated NPs

The oleic acid coating of NPs was displaced with either MEEA or ZDS by a two-step ligand exchange procedure[17].

First as-synthesized OlAc-NPs (17 mg) were gently stirred at 70 °C for 5 h in the presence of a solution of MEEA (327 μl) in methanol (7.5 ml). NPs were collected by centrifugation after the addition of acetone and hexane in succession.

In the second step, in a mixture of DMF and water (7:1), the MEEA-coated NPS were treated with ZDS (250 mg, to obtain ZDS- NPS) or MEEA again (243 mg, to improve the coating density of MEEA- NPs) and heated up to 70°C for 12 h. The resulting NPs were precipitated with acetone and were solved in deionized water. Finally they were purified from the excess of surfactant by dialysis (MWCO 12500 Da) at different times: 48 h for ZDS-NPs, 3 hours for MEEA-NPs.

h.06.2 Preparation of FCL-coated NPs

Fluorescent iron oxide NPs was obtained by coating them with a mixture of ZDS and FLC. We followed again a two-step ligand exchange procedure. Initially, as-synthesized OlAc- NPs (0.804 mg) were treated with a solution of FCL (5 mg) in methanol (1 ml) and stirred at 45 °C for 6 days. Then, a solution of ZDS (5 mg) in DMF/water 8:5 (1.3 ml) was added to the NPs and the mixture

was mixed at 70 °C for 16 h. The NPs were precipitated with acetone, dispersed in DI water and afterwards purified by dialysis for 48 h against DI water (MWCO 12500 Da).

h.07. Evaluation of NP cytotoxicity

The assays to evaluate the NP cytotoxicity were performed in the log phase of growth after the HepG2 cells had been placed in 24-well plates (35,000 cells/cm^2) where they stayed for 24 hours. Aqueous solution of iron oxide NPs were added to the cell medium to final concentrations of 2.5, 5, 10, 25, 50, and 100 µg Fe/ml and left for 24 h. All experiments were performed in quintuplicate.

h.08. Evaluation of NP uptake by HepG2 cells

h.08.1 Qualitative determination of NP internalization

To carry out qualitative determination of NP internalization by Prussian Blue staining, HepG2 cells were placed on 24 mm glass coverslips (52,000/cm^2) for 24 h before the treatment with NPs, which were added at the desired concentration to a final volume of 2 ml of culture medium. The day after, all non-internalized NPs were washed away with large amount of PBS buffer and fixed for 30 min in a solution of paraformaldehyde (4% PFA). Then, coverslips were exposed for 30 min to freshly prepared Perls' reagent (4% potassium ferrocyanide / 12% HCl, 1:1 v/v), washed with PBS and then held onto slides for examination under an optical microscope (Axioplan, Zeiss) coupled to a CCD camera (AxioCam, Zeiss). Bright-field pictures were acquired at 63x magnification.

h.08.2 Quantitative iron evaluation

To perform quantitative determination of NP internalization, HepG2 cells were placed on 10 cm-plates, 45,000/cm^2 for 24 hours and then treated for 24 h with NPs at a final concentration, in the culture medium, of 0, 2.5, 10, 25, 50 or 100 µg Fe/ml. Afterwards, HepG2 cells were washed five times with PBS to remove the non-internalized NPs and separated from plates through trypsin treatment. Pellets were recovered after 5 minutes centrifugation at 800 *g* and suspended in DI water. Their protein content were quantified by the BIORAD-Dc protein assay. To carry out the quantitative determination of iron in the pellets, the cell pellets were digested with a mixture of

conc. HCl / conc. HNO_3 3:1 v/v able to oxidize the organic matter and transform the iron oxide NPs into soluble Fe^{3+} ions. We evaluated by UV-Vis spectroscopy[37] the formation of the stable red complex $Fe(tiron)_3$ (tiron = disodium 4,5-dihydroxy-1,3-benzenedisulfonate) at pH ≅ 7. We analyzed its absorbance considering the UV-Vis spectral profile between 400 and 800 nm[39].

In more detail, the cell pellet was dehydrated, treated with high-purity concentrated acids (150 µl HNO_3 and 450 µl HCl), heated in a gradual manner to boiling, added with 300 µl of HCl and again evaported to dryness. We repeated this procedure 3 times. The solid residue was left at RT during the night with acids (150 µl HNO_3 and 450 µl HCl). The day after, the digested residue was again heated to boiling, added with 300 µl of HCl and dried. Finally, the residue was recovered with 1 ml of 0.1 M HCl and dissolved in 10 ml of milliQ water. A sample (3 ml) of the aqueous solution was treated with powdered PBS until pH ≅ 7 and then treated with excess tiron (2 mg). One hour after the tiron addition, we recorded the UV-Vis spectrum of the sample. We had previously calibrate the procedure by measuring a series of diluted Fe^{3+}standard solutions at different concentrations in PBS buffer. In this way we had obtained the molar extinction coefficient ε(λ) of the $Fe(tiron)_3$ complex in the 400-800 nm range. The Levenberg-Marquard least-squares method was employed to fit the spectrum of the unknown sample to the ε(λ) curve.

h.09. Intracellular iron localization

Cells treated with fluorescent NPs were fixed for 30 min in a solution of paraformaldehyde (4% PFA) and then stained with DAPI (4′,6-Diamidine-2′-phenylindole dihydrochloride). Finally the coverslips were placed onto microscope slides for examination under a confocal microscope (LSM 510 Meta, Zeiss) at 63x magnification. Instead for Lysotracker labeling, the cell medium of HepG2 exposed for 6 or 24 hours to NP dispersions was removed and replaced with fresh medium containing 1 µM Lysotracker-Red (Molecular Probes). Then, cells were incubated for 30 minutes in the dark at 37 °C and washed with PBS before staining.

i. Characterization methods and instruments

^{1}H- and ^{13}C-NMR spectra were registered with a Bruker Avance spectrometer in (^{1}H: 400 MHz, ^{13}C: 100 MHz). Transmission electron microscopy (TEM) images were taken with a Zeiss LIBRA 200FE microscope (Carl Zeiss AG, Oberkochen, Germany). The TEM sample was obtained by evaporating in air a drop of diluted NP solution on a carbon covered copper grid. We measured the diameter distribution of the nanocrystal core using the software PEBBLES from TEM images [31].UV-Visible spectra were recorded on a Thermo Scientific Evolution 600 spectrophotometer. FTIR spectra were registered with a Thermo Nicolet NEXUS 670 FTIR spectrometer (Thermo Fisher Scientific, Waltham, MA, USA). The sample for FTIR was obtained by grinding and pelleting dry NPs with KBr (NP:KBr 1:100 w/w) or by evaporating a drop of NP solution on a thin silicon substrate. TGA curves were recorded employing a Perkin-Elmer 7HT instrument (Perkin Elmer Waltham, MA, USA). In particular the weight loss was monitored while heating up the sample in air from 50 °C to 900 or 1000 °C at a rate of 5°C/min. Hydrodynamic diameter and ζ potential of NPs were measured at 25 °C using a Zetasizer Nano ZS (Malvern Instruments Corp., Malvern, Worcestershire, UK) at a wavelength of 633 nm (solid state He-Ne laser) and at a scattering angle $\theta = 173°$; instead scattering intensity I_s was measured employing a BI 90 Plus (Brookhaven Instruments Corporation, Holtsville, NY, USA) at $\theta = 90°$. Moreover the NP dispersion had a final concentration of 50 µg Fe/ml medium, both in deionized water and in RPMI (serum-free and complete), since it was an usual value employed in the HepG2 internalization tests. We monitored the conditions at the start and at the end of the NP uptake experiments measuring DLS respectively after NP addition and after 24 h incubation in medium. A gentle shaking before the DLS analysis was made to ensure the sample homogenization and we took at least three measurements for each sample.

References

[1] Schlenoff, J. B., Zwitteration: Coating Surfaces with Zwitterionic Functionality to Reduce Nonspecific Adsorption. *Langmuir*, **2014**, 30, 9625–9636.

[2] Moyano, D. F., Saha, K., Prakash, G., Yan, B., Kong, H., Yazdani, M., Rotello, V. M., Fabrication of Corona-Free Nanoparticles with Tunable Hydrophobicity, *ACS Nano*, **2014**, 7, 6748–6755.

[3] Nosaka, Y., Ohta, N., Fukuyama, T., Fujii, N., Size Control of Ultrasmall Cds Particles in Aqueous-Solution by Using Various Thiols, *J. Colloid Interface Sci.*, **1993**, 155, 23−29.

[4] Bae, W., Mehra, R. K., Cysteine-capped ZnS Nanocrystallites: Preparation and Characterization. *J. Inorg. Biochem.*, **1998**, 70, 125−135.

[5] Aryal, S., Bahadur, K. C. R., Bhattarai, N., Kim, C. K., Kim, H.Y., Study of Electrolyte Induced Aggregation of Gold NanoparticlesCapped by Amino Acids, *J. Colloid Interface Sci.*, **2006**, 299, 191−197.

[6] Mandal, S., Gole, A., Lala, N., Gonnade, R., Ganvir, V., Sastry, M., Studies on the Reversible Aggregation of Cysteine-capped Colloidal Silver Particles Interconnected via Hydrogen Bonds, *Langmuir*, **2001**, 17, 6262−6268.

[7] Liu, W. H., Choi, H. S., Zimmer, J. P., Tanaka, E., Frangioni, J.V., Bawendi, M., Compact cysteine-coated CdSe (ZnCdS) Quantum Dots for In Vivo Applications, *J. Am. Chem. Soc.*, **2007**, 129, 14530−14531.

[8] Rouhana, L. L., Jaber, J. A.; Schlenoff, J. B., Aggregation-resistant Water-soluble Gold nanoparticles, *Langmuir*, **2007**, 23 (26), 12799−12801.

[9] Estephan, Z. G., Jaber, J. A., Schlenoff, J. B. , Zwitterion- Stabilized Silica Nanoparticles: Toward Nonstick Nano, *Langmuir*, **2010**, 26, 16884−16889.

[10] Estephan, Z. G., Schlenoff, P. S., Schlenoff, J. B., Zwitteration As an Alternative to PEGylation, *Langmuir*, **2011**, 27, 6794−6800.

[11] Rouhana, L. L., Schlenoff, J. B., Aggregation Resistant Zwitterated Superparamagnetic Nanoparticles, *J. Nanopart. Res.*, **2012**, 14, 835-846.

[12] Kitano, H., Imai, M., Sudo, K., Ide, M., Hydrogen-Bonded Network Structure of Water in Aqueous Solution of Sulfobetaine Polymers, *J. Phys. Chem. B*, **2002**, 106, 11391–11396.

[13] Xiao, W., Lin, J., Li, M., Ma, Y., Chen, Y., Zhang, C., Li, D., Gu, H., Prolonged in Vivo Circulation Time by Zwitterionic Modification of Magnetite Nanoparticles for Blood Pool Contrast Agents, *Contrast Media Mol. Imaging*, **2012**, 7, 320–327.

[14] Zhang, L., Xue, H., Gao, C., Carr, L., Wang, J., Chu, B., Jiang, S., Imaging and Cell Targeting Characteristics of Magnetic Nanoparticles Modified by a Functionalizable Zwitterionic Polymer with Adhesive 3,4-Dihydroxyphenyl-L-Alanine Linkages, *Biomaterials*, **2010**, 31, 6582–6588.

[15] Pombo García, K., Zarschler, K., Barbaro, L., Barreto, J. A., O'Malley, W, Spiccia, L., Stephan, H., Graham, B., Zwitterionic-Coated "Stealth" Nanoparticles for Biomedical Applications: Recent Advances in Countering Biomolecular Corona Formation and Uptake by the Mononuclear Phagocyte System, *Small*, **2014**, 10, 2516–2529.

[16] Kim, D., Chae, M. K., Joo, H. J., Jeong, I. L., Cho, J. H., Lee, C., Facile Preparation of Zwitterion-Stabilized Superparamagnetic Iron Oxide Nanoparticles (ZSPIONs) as an MR Contrast Agent for in Vivo Applications, *Langmuir*, **2012**, 28, 9634-9639.

[17] Wei , H., Insin , N., Lee , J., Han , H., Cordero , J., Liu , W., Bawendi , M., Compact Zwitterion-Coated Iron Oxide Nanoparticles for Biological Applications, *Nano Lett*, **2012** , 12 , 22-25 .

[18] Mazur , M., Barras , A., Kuncser , V. Galatanu , A., Zaitzev , V., Turcheniuk , K.V., Woisel , P., Lyskawa , J., Laure , W., Siriwardena , A., Boukherroub , R., Szunerits , S.; Iron oxide magnetic nanoparticles with versatile surface functions based on dopamine anchors, *Nanoscale*, **2013** , 5 , 2692-2702 .

[19] Wei, H., Bruns, O. T., Chen, O., Bawendi, M. G., Compact zwitterions-coated iron oxide nanoparticles for in vitro and in vivo imaging, *Integr. Biol.*, **2013**, 5, 108-114.

[20] Zhou, Z., Wang, L., Chi, X., Bao, J., yang, L., Zhao, W., Chen, Z., Wang, X., Chen, X., Gao, J., Engineered iron-Oxide-Based Nanoparticles as Enhanced T1 Contrast Agents for Efficient Tumor Imaging, *ACS Nano*, **2013**, 3287-3296.

[21] Mondini, S., Leonzino, M., Drago, C., Ferretti, A. M., Usseglio, S., Maggioni, D., Tornese, P., Chini, B., Ponti, A., Zwitterion-coated iron oxide nanoparticles: surface chemistry and intracellular uptake by hepatocarcinoma (HepG2) cells, *Langmuir*, **2015**, 31, 7381-7390.

[22] Déry, J.-P., Borra, E. F., Ritcey, A. M., Ethylene Glycol Based Ferrofluid for the Fabrication of Magnetically Deformable Liquid Mirrors, *Chem. Mater.*, **2008**, 20, 6420−6426.

[23] Liu, Y., Chen, Z., Wang, J., Systematic Evaluation of Biocompatibility of Magnetic Fe_3O_4 Nanoparticles with Six Different Mammalian Cell Lines., *J. Nanoparticle Res.*, **2010**, 13, 199–212.

[24] Yathindranath, V., Sun, Z., Worden, M., Donald, L. J., Thliveris, J. A, Miller, D. W., Hegmann, T., One-Pot Synthesis of Iron Oxide Nanoparticles with Functional Silane Shells: A Versatile General Precursor for Conjugations and Biomedical Applications., *Langmuir*, **2013**, 29, 10850–10858.

[25] Li, Y., Chen, Z., Li, F., Wang, J., Zhang, Z., Preparation and in Vitro Studies of MRI-Specific Superparamagnetic Iron Oxide antiGPC3 Probe for Hepatocellular Carcinoma., *Int. J. Nanomedicine*, **2012**, 7, 4593–4611.

[26] Peng, X., An Essay on Synthetic Chemistry of Colloidal Nanocrystals, *Nano Res* , 2009, 2, 425-447.

[27] Kim, B. H., Hackett, M. J., Park, J., Hyeon, T., Synthesis, Characterization, and Application of Ultrasmall Nanoparticles, *Chem. Mater.*, **2014**, 26, 59–71.

[28] Hao, R., Xing, R., Xu, Z., Hou, Y., Gao, S., Sun, S., Synthesis, Functionalization, and Biomedical Applications of Multifunctional Magnetic Nanoparticles, *Adv. Mater.*, **2010**, 22, 2729-2742.

[29] Hyeon, T., Lee, S. S., Park, J., Chung, Y., Na, H. B., Synthesis of Highly Crystalline and Monodisperse Maghemite Nanocrystallites without a Size-Selection Process., *J. Am. Chem. Soc.*, **2001**, 123, 12798–12801.

[30] Calcagnile, P., Fragouli, D., Bayer, I. S., Anyfantis, G. C., Martiradonna, L., Cozzoli, P. D., Cingolani, R., Athanassiou, A., Magnetically Driven Floating Foams for the Removal of Oil Contaminants from Water, *ACS Nano*, **2012**, 6, 5413–5419.

[31] Mondini, S., Ferretti, A. M., Puglisi, A., Ponti, A., Pebbles and PebbleJuggler: Software for Accurate, Unbiased, and Fast Measurement and Analysis of Nanoparticle Morphology from Transmission Electron Microscopy (TEM) Micrographs, *Nanoscale*, **2012**, 4 , 5356–5372. PEBBLES is freely available from the authors, http://pebbles.istm.cnr.it.

[32] Rouhana, L. L., Schlenoff, J. B., Aggregation Resistant Zwitterated Superparamagnetic Nanoparticles, *J. Nanoparticle Res.*, **2012**, 14, 835-846.

[33] Shen, L., Laibinis, P. E., Hatton, T. A., Bilayer Surfactant Stabilized Magnetic Fluids: Synthesis and Interactions at Interfaces, *Langmuir* , **1999**, 15, 447–453.

[34] Han, H.-S., Martin, J. D., Lee, J., Harris, D. K., Fukumura, D., Jain, R. K., Bawendi, M., Spatial Charge Configuration Regulates Nanoparticle Transport and Binding Behavior in Vivo, *Angew. Chem. Int. Ed. Engl.*, **2013**, 52, 1414–1419.

[35] Safi, M., Courtois, J., Seigneuret, M., Conjeaud, H., Berret, J. F., The Effects of Aggregation and Protein Corona on the Cellular Internalization of Iron Oxide Nanoparticles, *Biomaterials*, **2011**, 32, 9353–9363.

[36] Soenen, S. J. H., De Cuyper, M., Assessing Cytotoxicity of (iron Oxide-Based) Nanoparticles: An Overview of Different Methods Exemplified with Cationic Magnetoliposomes, *Contrast Media and Molecular Imaging*, **2009**, 4, 207–219.

[37] Yoe, J. H., Jones, A. L., Colorimetric Determination of Iron with Disodium-1,2-Dihydroxybenzene-3,5-Disulfonate, *Ind. Eng. Chem. Anal. Ed.*, **1944**, 16, 111–115.

[38] Yuan, Y., Rende, D., Altan, C. L., Bucak, S., Ozisik, R., Borca-Tasciuc, D.-A, Effect of Surface Modification on Magnetization of Iron Oxide Nanoparticle Colloids, *Langmuir*, **2012**, 28, 13051–13059.

[39] Galimard, A., Safi, M., Ould-Moussa, N., Montero, D., Conjeaud, H., Berret, J. F., Thirty-Femtogram Detection of Iron in Mammalian Cells, *Small*, **2012**, 8, 2036–2044.

[40] Soenen, S. J. H., Brisson, A. R., Jonckheere, E., Nuytten, N., Tan, S., Himmelreich, U., De Cuyper, M., The Labeling of Cationic Iron Oxide Nanoparticle-Resistant Hepatocellular Carcinoma Cells Using Targeted Magnetoliposomes, *Biomaterials*, **2011**, 32, 1748–1758.

[41] Jiang, W., Lai, K., Wu, Y., Gu, Z., Protein Corona on Magnetite Nanoparticles and Internalization of Nanoparticle-Protein Complexes into Healthy and Cancer Cells, *Arch. Pharm. Res.*, **2014**, 37, 129–141.

[42] Huang, C.-Y., Ger, T.-R., Wei, Z.-H., Lai, M.-F., Compare Analysis for the Nanotoxicity Effects of Different Amounts of Endocytic Iron Oxide Nanoparticles at Single Cell Level, PLoS One, 2014, 9 , e96550.

[43] Domenech, M., Marrero-Berrios, I., Torres-Lugo, M., Rinaldi, C., Lysosomal Membrane Permeabilization by Targeted Magnetic Nanoparticles in Alternating Magnetic Fields, *ACS Nano*, **2013**, 7, 5091–5101.

○ Part II: Magnetic NPs coated with functionalized polyethylene glycol (PEG)

01. Introduction

Until now, the protection and/or modification of the NC surface with polymers such as polysaccharides, polyacrilamide, poly(vinyl alcohol) and poly(ethylene glycol) (PEG) is the most common method used to ensure to the NPs the appropriate pharmacokinetic features for a specific application *in vivo* (such as good colloidal stability, reduced biomolecular corona formation, and increase of the NP half life)[1].

In particular, NP functionalization with biocompatible PEG chains, a method known as "PEGylation", is currently applied to improve the "stealth" properties of nanosystems which are known as the "enhanced permeation and retention" (EPR) effect of PEGylated surfaces. Chemically, PEG is a polymer of the ethylene glycol monomer ($HO\text{-}CH_2\text{-}CH_2\text{-}OH$). It is commercially available in a range of different molecular weights from several hundreds to a few thousands of Dalton.

PEG has some well-known favorable features: (i) excellent solvating properties, (ii) good stability against oxidation, reduction, and decomposition and (iii) the possibility to modify it with different terminal groups useful to attach large biomolecules such as antibodies, drugs, fluorescent TAGs (for example by the selectively oxidation of the PEG terminal OH moiety[1]). Moreover, a PEGylated coating shields the surface charge of nanosystems, enhances water solubility and provides flexibility to the NPs. These features, together with PEG high surface density, determine the ability of PEGylated NPs to avoid non-specific opsonin absorption and the subsequent internalization by the reticuloendothelial system (RES), also known as mononuclear phagocyte system (MPS). PEG chains, both covalently and electrostatically bound to the NP surface, can show effective protein rejection tendency[2]. Nevertheless, the higher stability of covalent bonding can ensure that the PEG coating maintain its properties *in vivo*, during blood circulation, or when the NPs are stored in ionic media. The use of PEG as surfactant increased also thanks to its non-immunogenicity and the knowledge of full toxicity profiles of some PEG compounds. In the literature the most appropriate molecular weight for PEG to achieve the EPR effect has been reported to be in the 1500–5000 Da range[3]. However, such large molecular weight increases considerably the NP hydrodynamic diameter[4], thus being a limitation in the use of PEG since even NPs based on very small core nanocrystals could not be excreted by kidneys and would accumulate in the body. In addition, long

PEG chains may also entrap biomolecules potentially present on the NP surface and interfere with their presentation to the environment.

As depicted in Fig 1, NPs can be PEGylated by 1) direct PEGylation (PEG molecules are adsorbed at the NP surface via physical bonding during the synthesis of NPs using PEG as solvent or other thermal/hydrothermal methods), 2) covalent attachment by anchoring groups. The latter strategy includes (i) monofunctional PEG (this way is very effective for inorganic materials characterized by high and selective binding affinity towards a specific group, such as gold NPs for thiol –SH groups), and (ii) bifunctional PEG molecules (which, besides a grafting group, have a moiety useful to achieve functionalization of the NP with selected ligands for theranostic features)[1]. Inorganic NPs such as metal and metal oxide NPs are usually PEGylated in these ways.

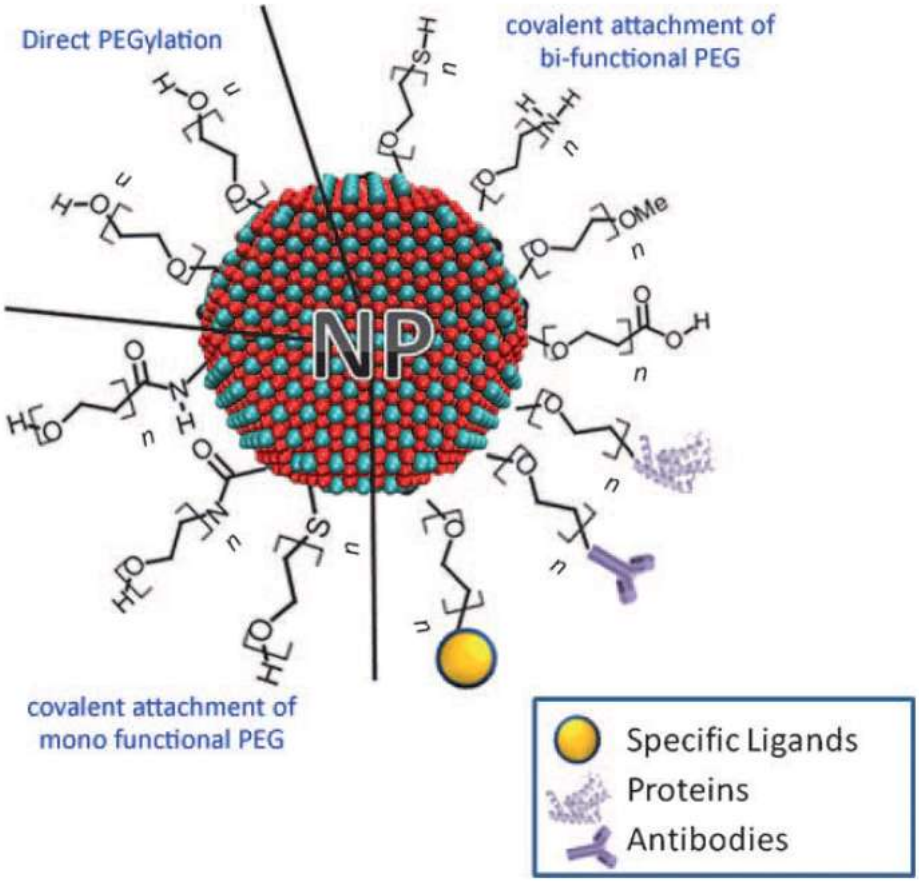

Fig 1. Various strategies for the PEGylation of NPs. All the strategies result in NPs that are water soluble and can repel opsonin proteins. Direct PEGylation (by physical or electrostatic adsorption) has the advantage of a simple synthesis. Monofunctional PEGs can be used to achieve covalent bonding between the PEG molecules and the NPs providing long-term stability and high dispersion stability. The vectorization of NPs can be achieved by using bifunctional PEG molecules wherein the free terminal functional groups of PEG can be covalently grafted to other polymers, fluorescent tags, and targeting antibodies or proteins. Image from Ref 1.

As mentioned before, thiol (–SH) terminated PEGs are used to coat gold NPs because of the very strong binding affinity between Au and SH moieties (S-Au bond energy = 47 kcal mol^{-1}). PEG molecules with molecular weight below 5000 Daltons are often preferred over higher molecular weights. Another important parameter is the spacer length of the PEG, for example when fluorescent tags are also present in the NP coating, because of the spacer length-related change of fluorescence intensity. As Ti and coauthors reported, PEG5000 chains could be covalently linked to Au NPs through thioctic acid (TA), a compound containing a cyclic disulfide[5]. The presence of TA increased the NP stability in phosphate buffer saline, stability which was also controlled by NP size (20 and 40 nm Au NPs showed a lower tendency toward aggregation than 80 nm NPs and a delayed clearance from the blood). These results were ascribed to a lowest surface PEG density of 80 nm Au NPs. Nanosystem instability might come from oxidation of thiolated species and from exchange reactions with other thiol compounds present inside the body.

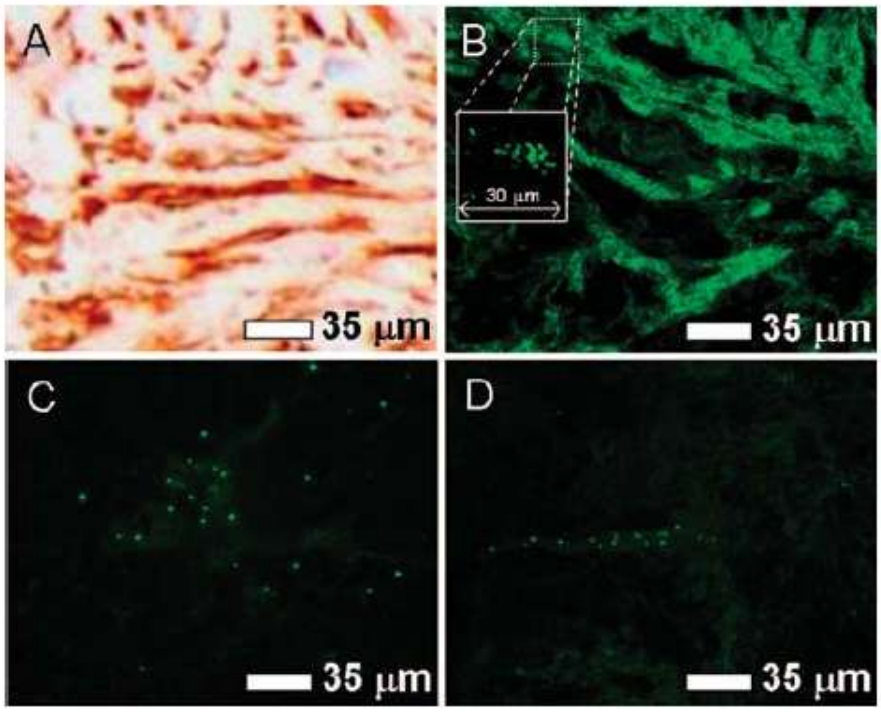

Fig 2. (A) Representative pancreatic cancer tissue thin sections labeled using secondary antibody staining (red regions). (B) Dark field transmission scattering images of GNP-F19-labeled pancreatic cancer tissue, (C) GNP-F19-labeled healthy tissue, and (D) GNP-mIgG-labeled pancreatic cancer tissue. The expanded section in B has been contrast enhanced to emphasize the presence of individual GNP-F19.Image from Ref 6.

Homo and hetero bifunctional PEG can be employed to covalently bind a specific functionality. For example Mason et al[6] synthesized ≈ 15 nm spherical Au NCs coated with PEG ligands having a dithiol group for grafting to the NC surface and a terminal carboxy moiety for binding F19 monoclonal antibodies. The NP dispersions did not aggregate for a long time as demonstrated by DLS, size exclusion chromatography, and TEM analysis. Finally the authors demonstrated the NP ability to selectively stain a human pancreatic cancerous tissue (Fig 2).

Focusing now on magnetic iron oxide NPs, those produced by aqueous routes can be directly PEGylated. For example, Reimhult et al. stabilized NPs obtained by aqueous precipitation using methoxy-PEG(550)-gallol, methoxy-PEG(5000)-6-hydroxy-dopamine, biotin-PEG(3400)-6-hydroxy-dopamine or their mixtures[7] (Fig 3). The NPs can be freeze dried thanks to the high binding affinity of the trihydroxy-benzene groups toward iron oxide surface, stored for at least 20 months and easily redispersed in water as individual particles when necessary. To produce MRI contrast agents, the authors functionalized their NPs with anti-human vascular cell adhesion molecule 1 (VCAM-1) antibodies binding them to the biotinylated PEG-gallol units through neutravidin. VCAM-1 was chosen since it is over expressed at the endothelial cell periphery of atherosclerotic sites, aging as early marker of this disease.

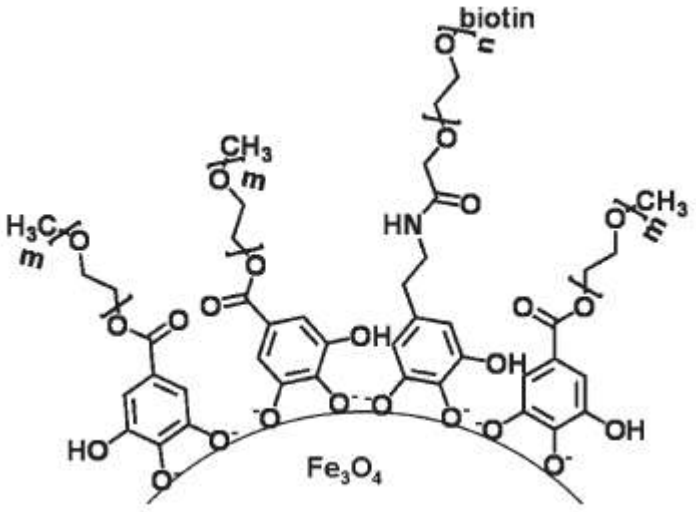

Fig 3. Schematic image of PEG-gallol stabilized iron oxide nanoparticles where m ≈10 and n ≈73. Approximately 9 mol% of the adsorbed PEG-gallol was biotinylated. Image from Ref 7.

In another article Reimhult and coauthors have extensively analyzed the capacity of eight different PEG5000-based mono-catechols to act as anchors for iron oxide NPs[8]. Stability tests in 4-(2-hydroxyethyl)-1-piperazineethanesulfonic acid (HEPES) buffer (pH 7.2) containing 150 mM NaCl

showed that electron-attractive groups, such as nitro-group, present on the catechol ring, were effective in enhancing the NP stabilization.

Going back to the NP PEGylation strategies, the direct PEGylation, in addition to small and uniform NC size, was obtained in the literature also by a non-hydrolytical synthesis. In particular, $Fe(acac)_3$ was thermally decomposed in 2-pyrrolidone and in the presence of monocarboxyl-terminated poly(ethylene glycol) (MPEG-COOH)[9], which results as covalently bound to the NP surface by COOH moieties. NPs displayed excellent water solubility and biocompatibility and so they were tested as magnetic resonance imaging (MRI) contrast agents.

Instead, NPs produced by non-hydrolytically routes are typically coated with hydrophobic molecules such as oleic acid or oleylamine[10]. Therefore, in order to PEGylate these systems it is necessary to follow different exchange procedures in which the new surfactant is typically formed by two parts, a region grafting the NP surface and the PEG chain as hydrophilic part exposed to the aqueous medium (named as "bifunctional ligand" in Fig 4).

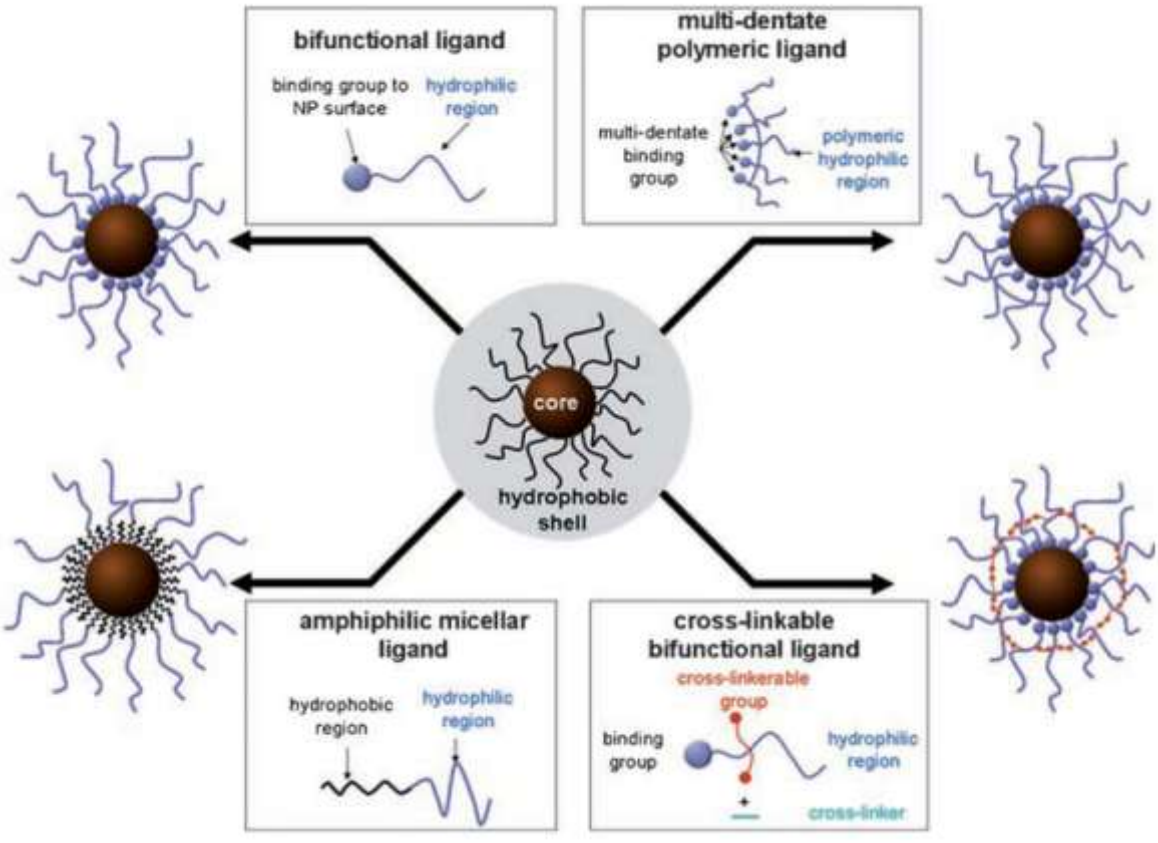

Fig 4. Surface modification strategies for designing MNP probes with high colloidal stability. Image from Ref 4.

For example Sun et al[11] synthesized monodisperse Fe NPs through thermal decomposition of $Fe(CO)_5$ in the presence of oleylamine in octadecene at 180°C. Then the NP dispersion in hexane

was exposed to air in order to oxidize the iron surface producing a crystalline Fe_3O_4 shell. The oleylamine exchange with PEG-dopamine leads to a stable aqueous NP dispersion in PBS, useful for biomedical application (Fig 5).

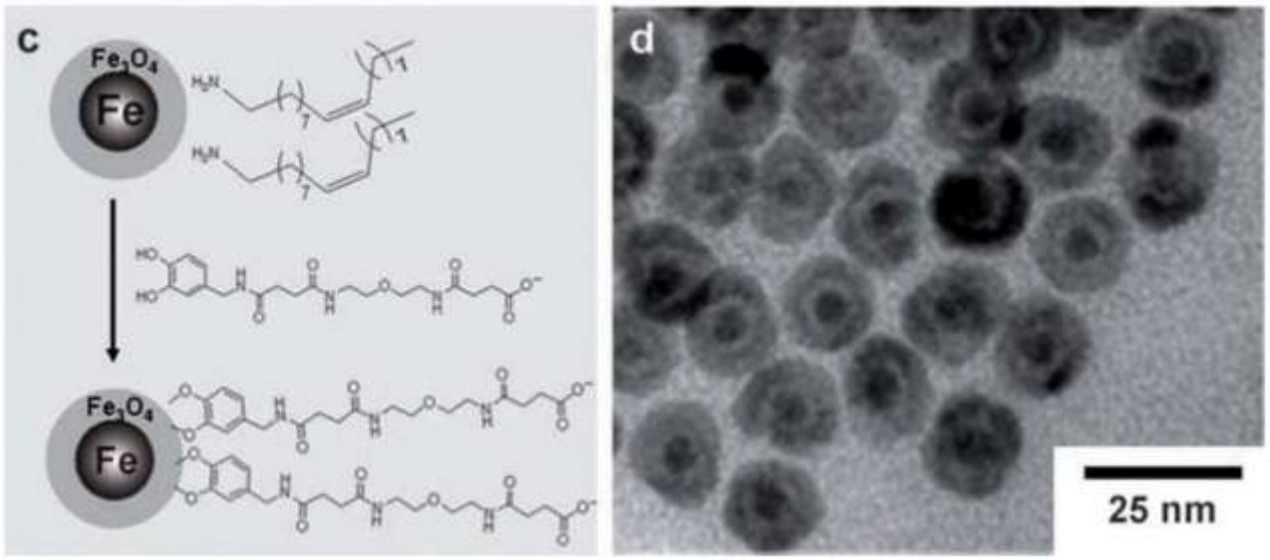

Fig 5. c) Exchange of ligands on $Fe@Fe_3O_4$ nanoparticles for PEG–dopamine. d) TEM image of water-soluble $Fe@Fe_3O_4$ nanoparticles. Images from Ref 11.

The colloidal stability of NP solution was further increased thanks to employment of multidentate polymeric ligands, since the approach of increasing the number of grafting groups in a NP surfactant allows to minimize its loss. For instance Matoussi et al[12] have developed some oligomers named as OligoPEG-Dopa, since they were formed by several catechol groups binding NC surface, a short poly(acrylic acid) backbone and polyethylene glycol chains. In addition, PEG allowed further coupling with different biomolecules, for example by azide-alkyne cycloaddition when the PEG had an azide end-group. These oligomers gave quick exchange process and exhibited a better colloidal stability varying the pH range and in the presence of electrolytes, compared to other olygomers having several carboxyl groups or to monodentate ligands having a catechol or a carboxyl moiety. The authors verified also the ability of magnetite NPs coated with OligoPEG-Dopa to act as T_2 contrast agents and tested their cytotoxicity in live cells which resulted low significant. Bawendi and coauthors showed another example of multidentate ligand, a PEG-polymeric phosphine oxide ligand which was used to transfer various NPs (Au, γ-Fe_2O_3, Pd, and QD) from organic solvents to water maintaining their physical properties and reactivities[13].

Considering the well-known ability of the catechol group and its derivatives to bind with high affinity iron ions and give stable NP water dispersion[14-15], in this PhD thesis we have decided to

choose this grafting group for our NP dispersion. Moreover about PEG chain molecular weight, we resorted to PEG 5000.

We would also functionalize magnetic NPs with the Fab fragment of Trastuzumab (Herceptin®), which is a monoclonal antibody specifically binding the human epidermal growth factor receptor 2 (HER2). Such receptor is up-regulated in 20-30% of breast cancer cells and also in some classes of adenocarcinoma cells of the gastro-esophageal junction and of stomach. In this case the large biomolecule provides the NPs with (i) an active targeting since the antibody strongly binds to its antigen and (ii) therapeutic features since Trastuzumab affects the cellular proliferation mechanism in different ways. In a future application in cancer therapy, the functionalization of the iron NPs with Fab Trastuzumab will improve treatment specificity and reduce toxicity and side effects typical of a traditional chemotherapy. The Fab fragment was produced by Bioker srl; it has a molecular weight around 5.6 kDa and a dimension of 5 nm. Therefore we have designed and tested different catechol molecules: (i) a bi-functional PEG displaying besides to the catechol anchor moiety, a maleimide terminal group in order to react with the free thiol group of the Fab biomolecule; (ii) mono and bi-dentate polymeric ligands in order to employ them as co-surfactants to dilute the bi-functional linker described before at the NP surface. Their chemical structures will be presented in detail in the next Chapter, together with the description of the procedures used to obtain PEGylated NPs and their characterization.

02. Preparation of iron oxide NPs coated with functionalized polyethylene glycol

a. Synthesis of magnetic nanoparticles

Two synthetic strategies were followed in order to prepare magnetic iron oxide NPs, hot-injection of metal precursor and co-precipitation of iron salts.

a. 01. Synthesis of magnetic NPs by hot-injection

We prepared monodisperse spherical iron oxide NPs coated with oleic acid (diameter 9.6 nm) following a hot-injection method in 1-octadecene (ODE) described in the literature (see Experimental Section) with a molar ratio between metal precursor and oleic acid equal to 1:3[16].

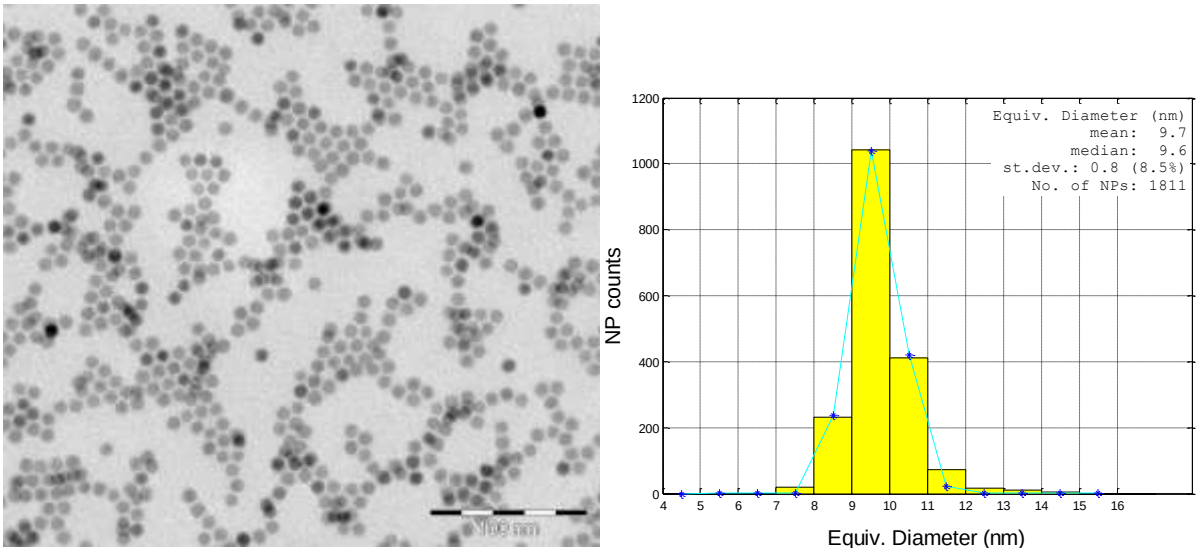

Fig 6. OlAc-coated NPs synthesized by hot-injection. Left) TEM image. Right) Diameter histogram (as measured by the software PEBBLES[17]). The median diameter is 9.6 nm.

As shown in Fig 6, the median diameter measured from the TEM images was $\langle d \rangle$ = 9.6 nm with a diameter standard deviation σ_d = 0.9 nm, corresponding to a dispersion $\sigma_d/\langle d \rangle$ = 8.5 %.

These iron oxide NPs had a spinel structure (Fig 7) and stoichiometry intermediate between magnetite (Fe_3O_4) and maghemite (Fe_2O_3).

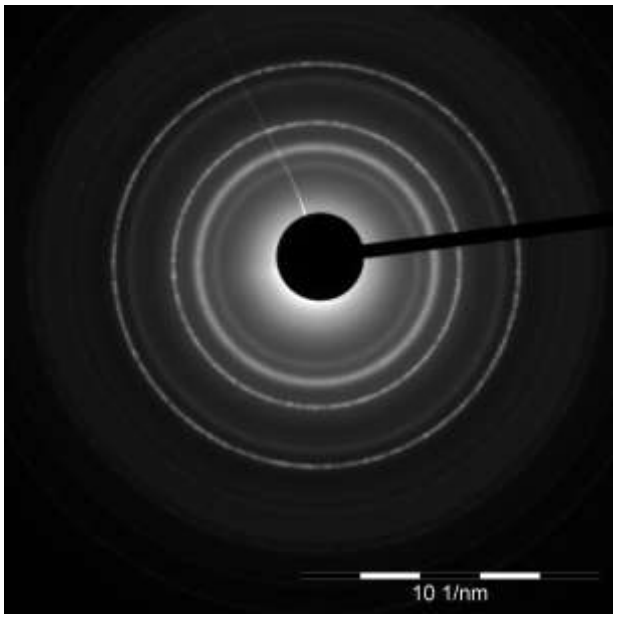

Fig 7 . Electron diffraction pattern of OlAc-coated NPs synthesized by hot-injection.

a. 02. Synthesis of magnetic NPs by co-precipitation

Iron oxide NPs are typically obtained on a large scale by co-precipitation from a stoichiometric mixture of Fe^{3+} and Fe^{2+} salts in alkaline aqueous media. This method for the synthesis of magnetite NPs by precipitation of $FeCl_3$ and $FeCl_2$ with alkali was introduced by Massart[18]. The possibility of a large-scale preparation along with the use of "green chemistry" methods, that avoid the employment of toxic reagents, are appealing prerequisites for a scalable synthesis of magnetic NPs to industrial applications for medical use[19]. In this case, the resulting NPs are free from surfactants, so in principle more suitable to being directly dispersed in water after coating by hydrophilic molecules such as PEG ligands. Precursor, reaction temperature, and pH are the experimental parameters to control NP morphology and dimension but it is however difficult to synthesize NPs with a narrow size distribution[20]. Other drawbacks of these magnetite NPs are their instability and poor crystallinity, with a loss in magnetic susceptibility[19]. We used as metal precursor $FeCl_3.6H_2O$ and $FeSO_4.7H_2O$. The followed synthetic procedure was described in detail in the Experimental Section. As clearly visualized in TEM image (Fig 8), our NPs are polydisperse according with those produced in the literature. The measured NP size was 2.9 nm with a diameter standard deviation σ_d = 0.8 nm.

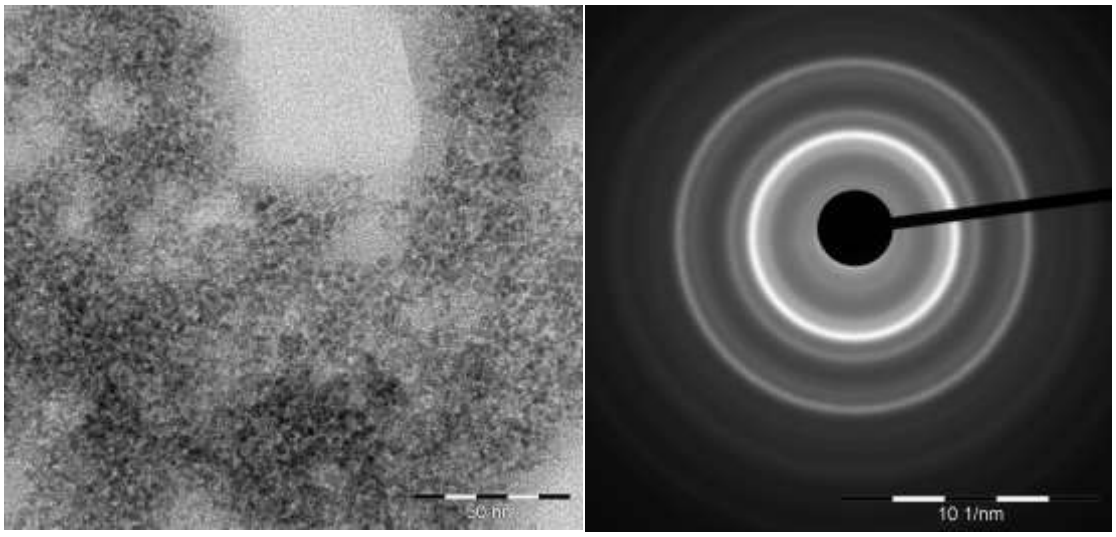

Fig 8. TEM image (left) and electron diffraction pattern (right) of "naked" iron oxide NPs obtained by co-precipitation.

b. Synthesis of catecholic PEG ligands

We have designed the organic preparation of different types of PEG 5000 catecholic ligands whose structures are shown below (Fig 9). In our strategy, we attributed to them different roles as surfactants: in particular, structure (a) refers to the bi-functional linker which we are going to bind to the Fab fragment of Trastuzumab thanks to its maleimide end group; structures (b) and (c) display possible co-surfactants of the bi-functional linker. In this case, we want to employ ligands chemically similar to the bi-functional linker and in addition, with compounds (c), to explore the effect, if present, of a bidentate grafting group on the NP colloidal stability. Indeed, we could potentially improve the NP water stability by increasing the number of grafting groups per ligand and so decreasing the chance that a surfactant molecule is irreversibly lost from the NP coating.

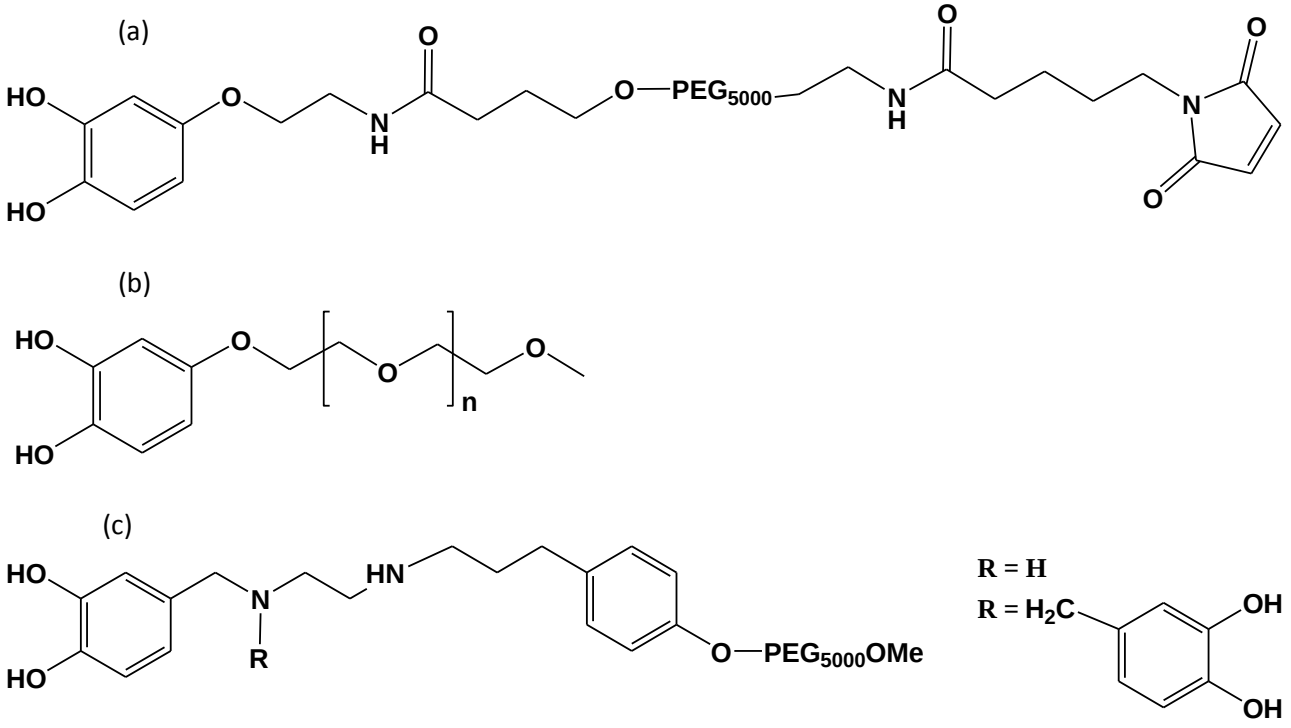

Fig 9. Chemical structures of the desired PEG_{5000} catecholic ligands displaying different functions: the bi-functional linker (a) to bind biomolecules; co-surfactants (b) and (c).

b. 01. Synthesis of catechol (a) and (b) compounds

The synthesis of compounds (a) and (b), named as SS33 and SS20_A respectively, were made in collaboration with the laboratory of CISI scrl inside the RSPPTECH project ("Ricerca e sviluppo di

prodotti e piattaforme tecnologiche per la competitività dell'industria Lombardia) of Regione Lombardia that financially supported us (see the detail in the Experimental Section).

b. 02. Synthesis of catechol (c) compounds

We designed the linker structures of (c) starting from the ethylenediamine scaffold. One of the nitrogen atoms of ethylenediamine is linked to the PEG 5000 chain while the other nitrogen atom is bound to one or two (3,4-dihydroxyphenyl)methyl moieties. We could bind the PEG chain to the central amine scaffold (I) before the introduction of the 3,4-dihydroxyphenyl groups or (II) as the final reaction step, by coupling it to mono- or di-catechol-diamine fragment. In both these approaches, we planned that the PEG chain is going to react with one of the nitrogen atoms of ethylenediamine as the brominated PEG derivative **12** (see *Scheme 3* in the Experimental Section). We obtained the compound **12** following the procedure reported in literature by Cozzi et al[21] in order to achieve, from the starting material **9**, whose hydroxyl group is not reactive enough because of steric hindrance, substrate **11** that is more reactive in S_N2 reactions, thanks to the introduction of the 3-(4-hydroxyphenyl)propanol spacer. Considering that in the general type-(I) strategy, the isolation and characterization of the intermediate substances could be more difficult due to the high molecular weight of the PEG chain, we decided to follow the type-(II) procedure visualized in *Scheme 4* in the Experimental Section in order to produce the desired mono-catechol **16**.

Since many protecting groups for the 3,4-dihydroxyphenyl moiety were in principle appropriate, we have synthesized different examples of hydroxyl-protected derivative **13**, first exploring the R = *tert*-butyldimethylsilyl (TBDMS) ether. The derivative **13_TBDMS** was synthesized starting from 3,4-dihydroxybenzaldehyde **17** following the *Scheme 5* depicted in the Experimental Section.

However, when compound **14_TBDMS** was treated with **12**, according to the general synthetic pathway (*Scheme 4)* proposed to achieve the mono-catechol surfactant, the reaction did not proceed and we did not obtain **16**. Therefore, we tried to investigate in detail this step to clarify if the reason was again a poor reactivity of a high molecular weight PEG derivative. With this purpose we designed the reaction reported in the *Scheme 6* of the Experimental Section, where the compound **14_TBDMS** was treated with compound **21** directly derived from the 3-(4-hydroxyphenyl)propanol spacer. Also in this case, although in absence of the long PEG chain, ^{1}H-NMR and HPLC-mass analysis confirmed that the reaction did not proceed to the desired product **22** and gave a mixture of byproducts.

For this reason, we modified the chosen protecting group R focusing on the acetonide functionality. The protected derivative **13_Acetonide** was prepared from 3,4-dihydroxybenzoic acid **23** (see

Scheme 7 in the Experimental Section). Unfortunately, we could not proceed beyond molecule **14-Acetonide** because it did not react with **12** as also occurred with the derivative **14_TBDMS**. We have correlated these negative results to the - at least partial - deprotection of both tert-butyldimethylsilyl ether and acetonide protecting groups in our reaction conditions. So, we finally resorted to the benzyl ether protecting group, which we have already employed in our previous work[22] to obtain a PEG-based tetra-catechol surfactant, hoping that it can be more stable in our reaction conditions. As shown in the *Scheme 7* of the Experimental Section, with this protecting group, in addition to **13_BnO bromide,** we want also to consider the **13_BnO chloride** and **13_BnO mesylate**, trusting that their dissimilar S_N2 reactivities could allow us to achieve, in a controlled way, both the mono- or bi- cathecol linkers (c) by nucleophilic substitution on the ethylendiamine scaffold. These experiments are in progress.

c. Preparation of water-soluble PEG-ylated NPs

To prepare PEG-ylated NPs, we employed the previous batches of magnetic iron oxide NPs synthesized by hot-injection and co-precipitation.

In the first case, we followed a ligand exchange procedure in order to displace the pristine oleic acid with the desired PEG molecules whereas in the second case the "naked" NPs were directly treated with PEG surfactants (see Experimental part). Here I reported TEM image (Fig. 10) of iron oxide NPs produced by co-precipitation and coated with a mixture of bi-functional linker (**a**) and co-surfactant (**b**). The measured NP size was 2.6 nm with a diameter standard deviation σ_d = 0.7 nm.

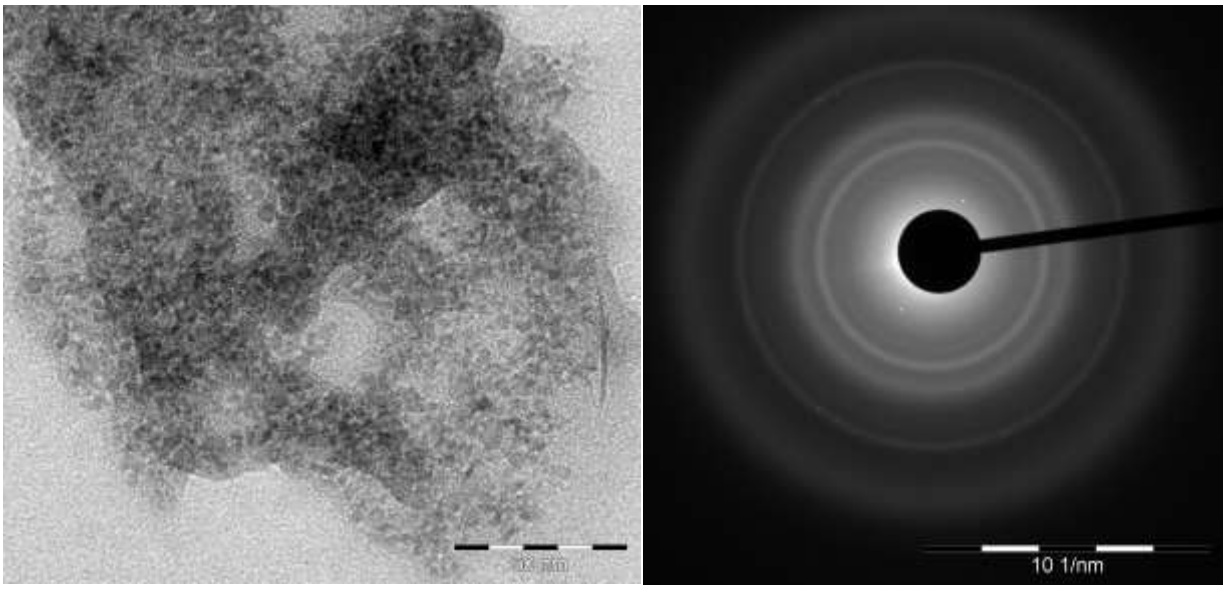

*Fig 10. TEM image (left) and electron diffraction pattern (right) of iron oxide NPs produced by co-precipitation and coated with a mixture of bi-functional linker (**a**) and co-surfactant (**b**).*

d. Characterization of PEG-ylated NPs

We have characterized PEG-ylated NPs by different techniques. First, we carried out Fourier-Transform Infrared (FTIR) spectra of PEG molecules SS33 and SS20_A alone. As expected, the FTIR spectra are similar spectra since they are dominated by the presence of the high molecular weight PEG chain (*Fig 11*).

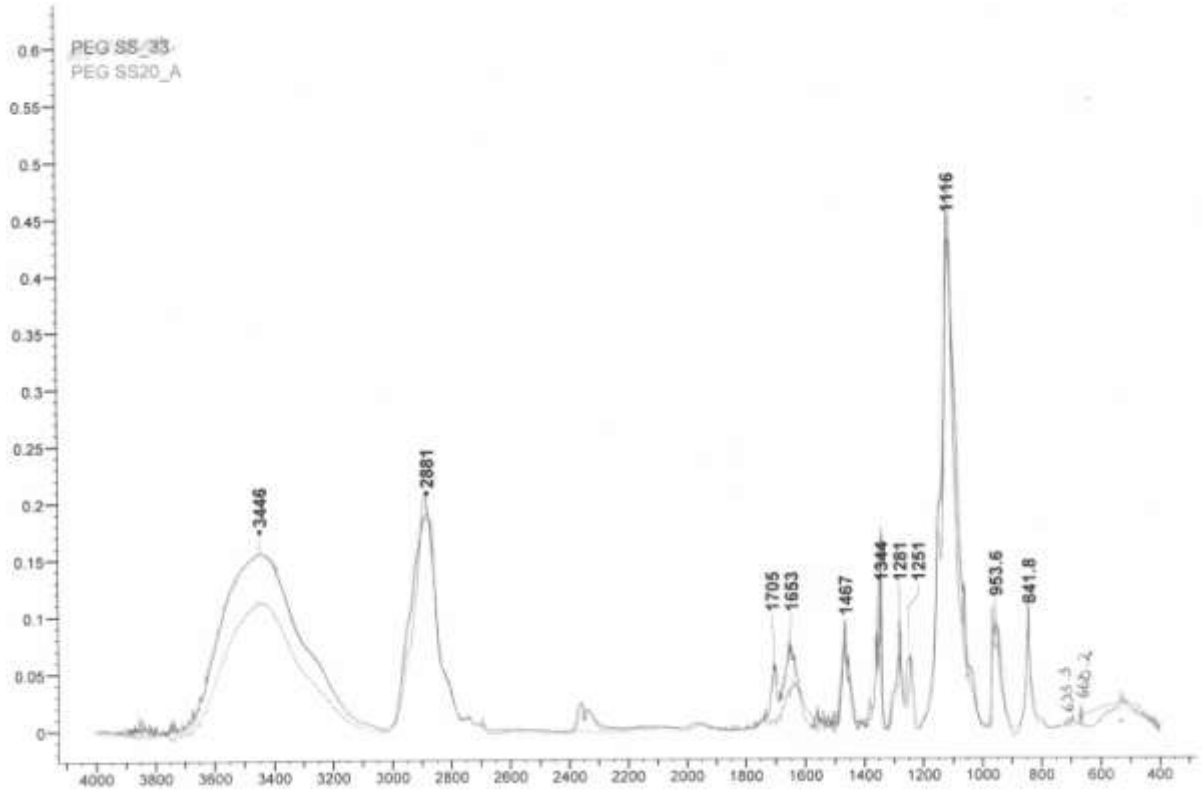

Fig 11. Comparison between IR Spectra of SS33 and SS20_A PEG molecules.

In particular, we could observe the vibrations of the PEG which comprise CH_2 bending (1467 cm^{-1}), CH_2 wagging (1344 cm^{-1}), CH_2 twisting (1281, 1251 cm^{-1}), C–O and C–C stretching (1116 cm^{-1}), and CH_2 rocking (953.6, 841.8 cm^{-1})[22]. In the spectrum of PEG molecule SS33 we can appreciate also the presence of a strong band of at 1705 cm^{-1} arising from the out-of-phase stretching of C=O of maleimide moiety.

In addition IR spectra allow us to confirm that the exchange process was effective since iron oxide NPs appeared coated with PEG derivative (*Fig 12, 13, 14*), without bands coming from the pristine oleic acid surfactant.

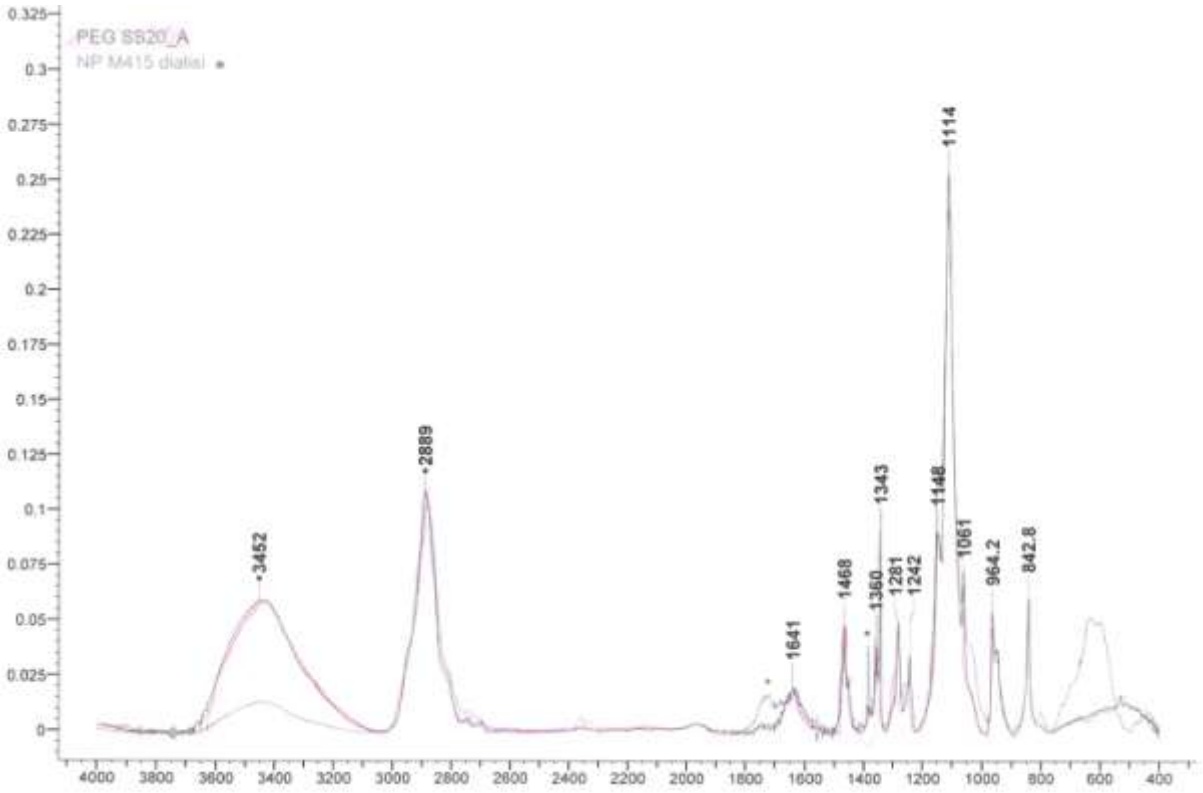

Fig 12. Comparison of IR spectra of PEG derivative SS20_A and iron oxide NPs coated with it, after the exchange process.

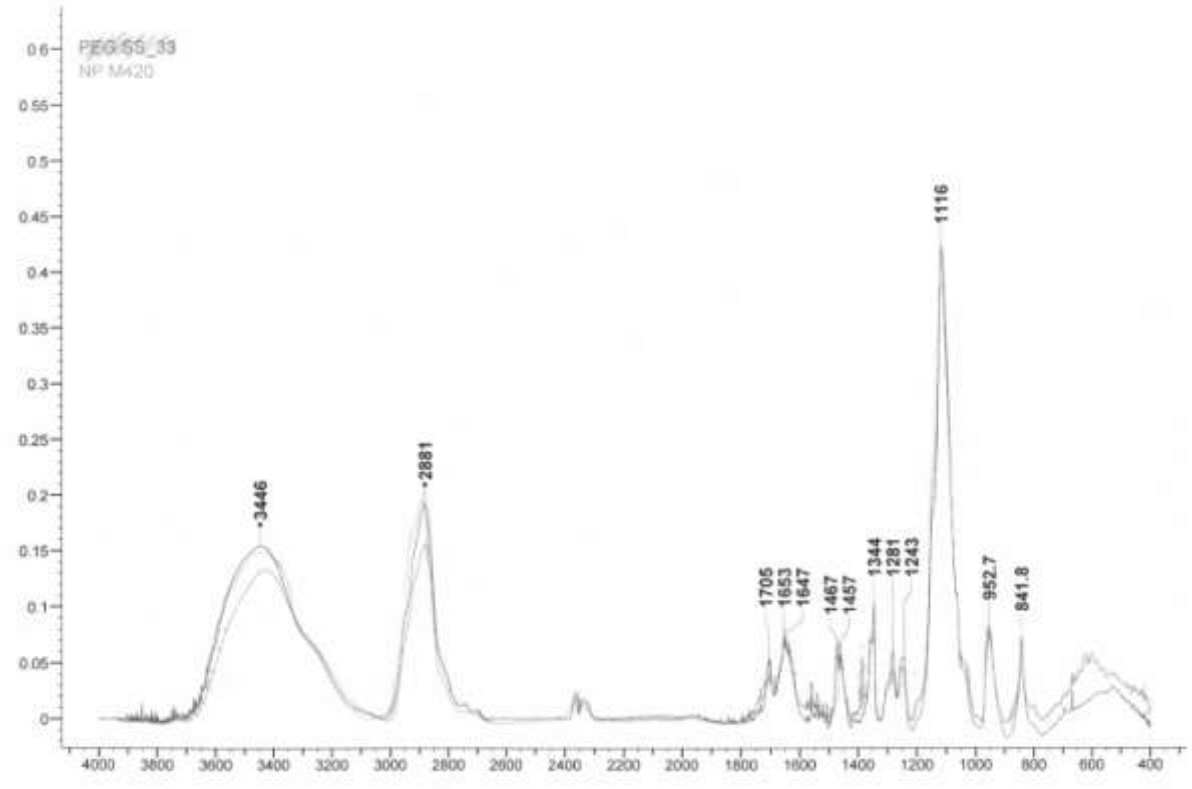

Fig 13. Comparison of IR spectra of PEG derivative SS33 and iron oxide NPs coated with it, after the exchange process.

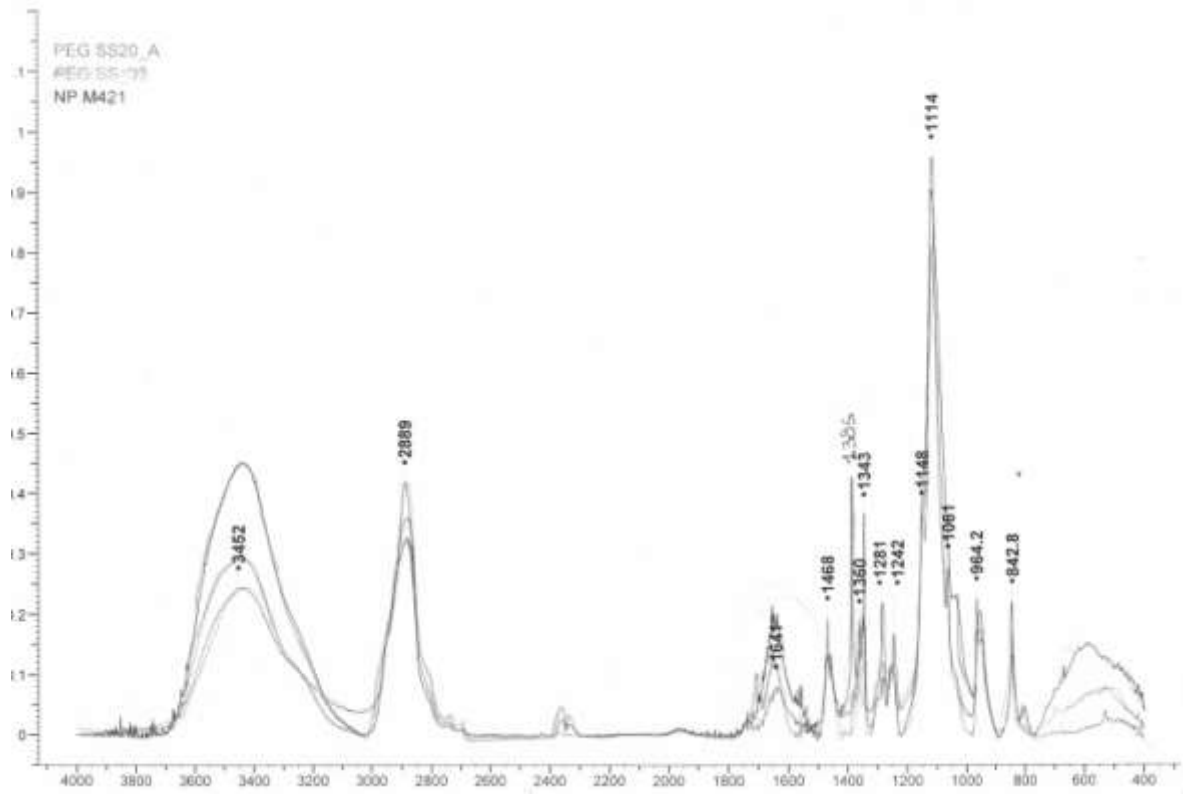

Fig 14. Comparison of IR spectra of PEG derivative SS20_A, PEG SS33 and iron oxide NPs coated with a mixture of them, after the exchange process.

We have also measured by DLS the (intensity weighted) hydrodinamic diameter of the PEGylated NPs, after dialysis and filtration, that resulted around 240 nm for co-precipitated NPs and 120 nm for solvothermal NPs (see Experimental Section).

By measuring the iron content of our NP solution with UV-Vis method described in the Part I, we have evaluated that the yield in water soluble NPs is approximately the same, around 50%.

Instead by calculation of the percentage of organic portion present at the NP surface from CHN analysis data, we deduced that this value is higher for NPs obtained by co-precipitation (around 90%) than that of solvothermal NPs (around 70%) (See Experimental Section).

Finally, having the idea of functionalizing the nanosystems with the Fab fragment of Trastuzumab, we need to investigate and potentially quantify the reactivity of maleimide groups of the bi-functional linker (compound (a) or PEGSS 33) present in the NP coating.

In particular, we carried out such quantification with a commercially available fluorescent kit (Amplite^{TM} fluorimetric maleimide quantitation kit) able to measure protein maleimide groups.

As the producers specified, this kit employs a dye that has enhanced fluorescence after reaction with a maleimide. It is able to detect as little as 100 nM in concentration of maleimide, performing the analysis directly in a 96-well-plate and choosing Ex/Em = 490 nm/520 nm. By comparison with

a shorter maleimido PEG (molecular weight ≈ 2000 Da), we have concluded that maleimide moiety was less reactive in the longer PEG5000 chain. However, a fraction of maleimide group exposed at the NP surface was actually reactive and sufficient to functionalize the NCs with the desired amount of anti-body fragment.

03. Conclusions

In the second part of my PhD thesis, we have explored examples of PEGylated molecules in order to ensure colloidal stability to our nanosystems, as indicated in the literature.

In particular, we have also designed a compound, the bi-functional linker, potentially able to react with large biomolecule, such the Fab fragment of the monoclonal antibody Trastuzumab.

In this way we are trying to achieve iron oxide NPs provided with an active targeting.

From a synthetic point of view our efforts are focused on producing water-soluble PEG-ylated linkers with one or two catechol grafting group(s) that we want to use as co-surfactants for the bi-functional linker, having the same chemical nature and preserving the good water solubility and stability of our nanosystems. Although several protecting groups for the catechol moiety are in principle usable, we have proved that in our experimental conditions, some of them (tert-butyldimethylsilyl ether and acetonide) are at least partially deprotected. Therefore, we have selected the benzyl group as a promising protecting group for catechol moieties.

In addition to these synthetic studies, we have produced and characterized two batches of iron oxide NPs coated with a mixture of the bi-functional linker and a catechol-PEG5000-OMe acting as co-surfactant. One batch of NPs was produced by hot-injection of $Fe(CO)_5$ in 1-octadecene and in the presence of oleic acid, while the other by co-precipitation of iron salts in water. Solvothermal NPs showed a good size dispersion and crystallinity, whereas co-precipitated NPs can be produced in large amount and in "green chemistry" conditions. In both cases, the yield in "water soluble NPs" was estimated around 50%. Indeed, evaluating by CHN analysis the amount of PEG molecules present in their coating, this was higher for NPs produced by co-precipitation.

Finally, thanks to a commercially fluorescent kit, we have deduced that the maleimide moiety was less available for reaction in the longer PEG chain than in the shorter one (molecular weight around 2000 Da). However, a fraction of the maleimide groups present at the NP surface was reactive, enough to functionalize the NCs with the desired antibody fragment avoiding problem arising from steric hindrance.

Therefore, as already deduced for zwitterionic iron oxide NPs, also PEGylated NPs could be considered promising in the development of theranostic nanosystems.

04. Experimental section

e. Materials

All chemical and solvents were acquired from Sigma-Aldrich and used without further purification. Aldrich Trace Select concentrated acids (HNO_3 and HCl) were employed to digest NPs.

f. Procedures

f.01. Acronyms used in the experimental section

$Fe(CO)_5$ = iron pentacarbonyl

RT = room temperature

NaOH = sodium hydroxide

$FeCl_3.6H_2O$ = iron (III) chloride hexahydrate

$FeSO_4.7H_2O$ = iron (II) sulfate heptahydrate

HCl = hydrochloric acid

PEG 5000 = polyethylene glycol with molecular weight around 5000 D

PPTS = pyridinium *p*-toluenesulfonate

EtOAc / AcOEt = ethyl acetate

$LiAlH_4$ = lithium aluminium hydride

THF = tetrahydrofuran

Na_2SO_4 = sodium sulfate

CH_3OH/ MeOH = methanol

NH_3 = ammonia solution

DCM = dichloromethane

CD_3OD/ MeOD = deuterated methanol

$CDCl_3$ = deuterochloroform

K_2CO_3 = potassium carbonate

PBr_3 = phosphorous tribromide

H_2O = water

CH_3CN = acetonitrile

TEA = triethylamine

TBDMS-chloride = *tert*-butyldimethylsilyl chloride

$NaBH_4$ = sodium borohydride

Et_2O = diethyl ether

HBr = hydrogen bromide

H_2SO_4 = sulfuric acid

EtOH = ethanol

$NaHCO_3$ = sodium hydrogen carbonate

DMP = 2,2-dimethoxypropane

$SOCl_2$ = thionyl chloride

$CHCl_3$ = chloroform

f. 02. Synthesis of magnetic NPs by hot-injection

We obtained 9.6 nm iron oxide NPs according to a published literature procedure[16]. In particular $Fe(CO)_5$ (12 ml) was injected in a mixture of 1-octadecene (45.96 g) and oleic acid (7.68 g, molar ratio metal precursor: surfactant 1: 3) at 120°C which was then heated up to 320°C for 3h under nitrogen. After cooling at RT, the NPs were collected by precipitation with acetone and centrifugation, repeatedly washed with acetone and finally solved in toluene.

f. 03. Synthesis of magnetic NPs by co-precipitation

We prepared iron oxide NPs following a method reported in the literature[23] using sodium hydroxide instead of the ammonium base to co-precipitate ferrous and ferric ion water solutions in stoichiometric molar ratio (1:2). 4.17 ml of NaOH 10M was injected inside a solution of $FeCl_3.6H_2O$ (0.65 g , 2.4 mmol) and $FeSO_4.7H_2O$ (0.333 g, 1.2 mmol) in water (25 ml) and concentrated HCl (130 μl) under mechanical stirring. Immediately a black precipitate formed and was stirred for 1 hour. Then iron oxide NPs were collected by centrifugation, washed with deionized water until the pH became neutral and dispersed in 26 ml of water (concentration ≈ 10 mg of Fe_3O_4 /ml water as used by Reimulth and coauthors in following exchange process with mono-functional catechol PEG 5000[8]).

f. 04. Synthesis of the bi-functional linker (SS33)

The bi-functional linker (SS33) was produced inside the laboratory of CISI scrl following the *Scheme 1* reported below and starting from the product commercially acquirable (**1)**.

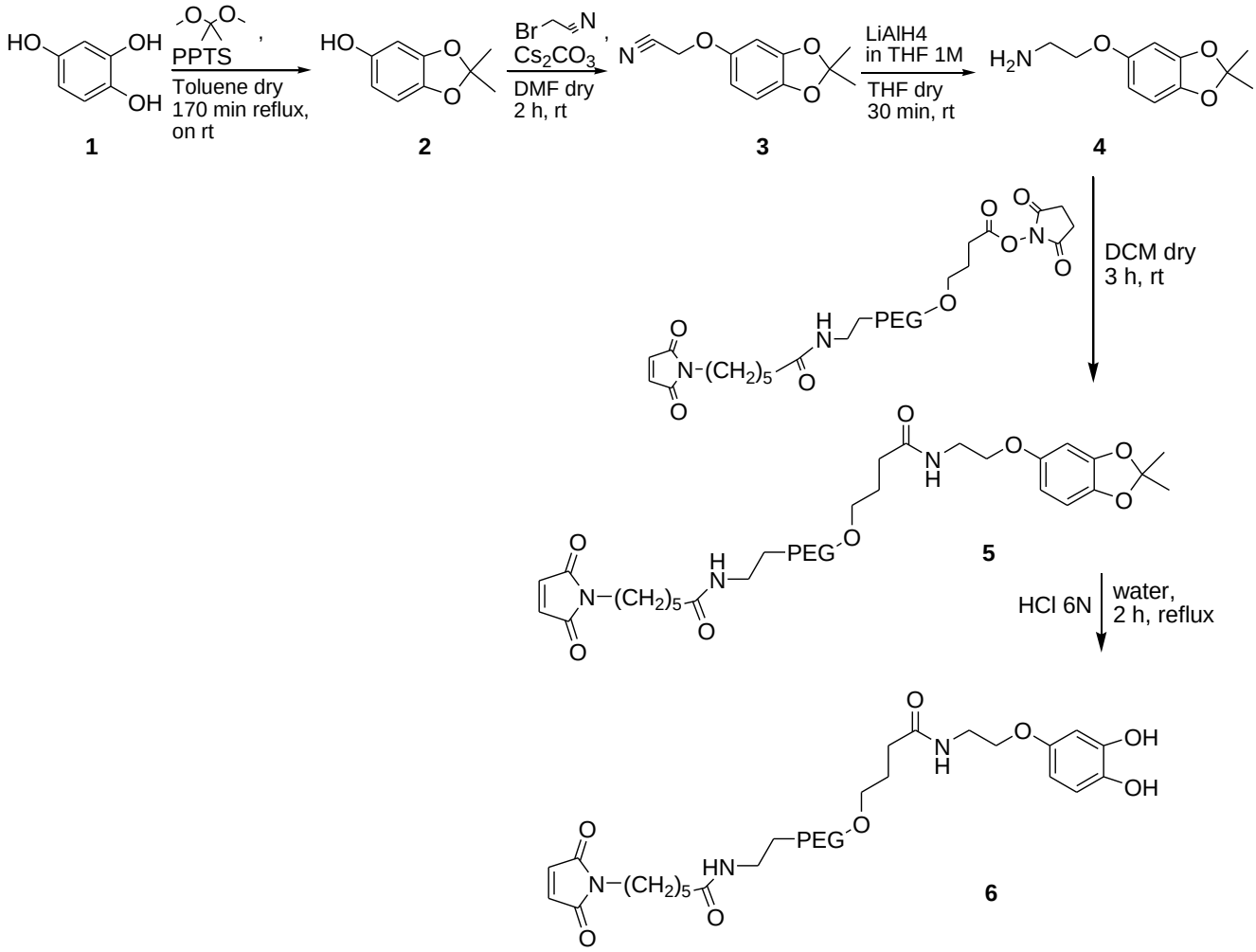

*Scheme 1. Synthetic pathway leading to the SS33 (**6**).*

f. 04. 1 Synthesis of compound 2

The product **2** was produced according with a method reported in literature[24] and employing a two-necked flask, furnished with a distillation apparatus in one neck and a stopcock in the other. A mixture of benzene-1,2,4- triol (0.4g, 3.17 mmol), pyridinium *p*-toluenesulfonate (0.64 mg, $2.54x10^{-3}$ mmol), and dry toluene (32 mL) was stirred and heated to reflux with distillation of the solvent. During the reaction 2,2-dimethoxypropane in portion (0.096 mL x 4; 0.064 mL x 4; 4.63 mmol) and dry toluene (to compensate for the loss of solvent) were added to the mixture every 15 min. After 3h, the reaction mixture was cooled to r.t. and stirred over night. The crude was subjected to column chromatography (silica gel, petroleum ether 100%→ petroleum ether /EtOAc 9.5/0.5) to give **2** (0.296 g, yield 56 %) as a light yellow oil.

f. 04. 2 Synthesis of compound 3

Bromoacetonitrile (0.101 ml, 1.46 mmol) was added to a dispersion of compound **2** (0.121 mg, 0.73 mmol) and Cs_2CO_3 (0.476g, 1.46 mmol) in dry DMF (5 mL), cooled at 0°C. Then the mixture was stirred at r.t. for 2h, filtered through celite and DMF was removed under vacuum. The crude was purified by flash chromatography (silica gel, isocratic elution with DCM/ EtOAc 1:1). The resulting product appeared as a yellow oil (0.11 g, yield 74%).

f. 04. 3 Synthesis of compound 4

$LiAlH_4$ in THF 1M (1ml, 1 mmol) was added under N_2 drop by drop to a solution of compound **3** (0.102 g, 0.5 mmol) in dry THF (5 ml), cooled at 0°C. After that the reaction was mixed at r.t. for 30 min and then stopped by the addition, at 0°C, respectively of water (0.038 ml), 15% NaOH (0.038 ml) and again water (0.0114 ml), in order to induce the precipitation of lithium salts. Then the dispersion was stirred at r.t. for 15 min, dried with anhydrous Na_2SO_4, filtered off and the solvent was finally removed by evaporation. The crude was purified by chromatography (silica gel, EtOAc/ MeOH 9/ 1 + 1% NH_3), (0.05 g, yield 48%).

f. 04. 4 Synthesis of compound 5

A solution of compound **4** (0.044g, 0.21 mmol) in anydrous DCM (2 mL) was additioned dropwise to a solution of Malhex-NH-PEG-O-C_3H_6-CONHS (0.891g, 0.18 mmol) in dry DCM (2 mL) refrigerated at 0°C. The mixture was stirred at r.t. for 3h. Then the product was precipitated by adding diethyl ether (84 ml), stirred at r.t for 1h, collected by filtration and washed with fresh diethyl ether. In order to remove the fraction of Malhex-NH-PEG-O-C_3H_6-CONHS that did not react, the crude was solved in DCM and treated with PS-NMM (Biotage®, 0.2g, 0.36mmol)e PS-NH_2 (Biotage®, 0.24g, 0.36mmol).(0.458 g, yield 68%).

f. 04. 5 Synthesis of compound 6

A water solution (10 ml) of compound **5** (0.445 mg, 0.09 mmol) was treated with HCl 6N (3 μl), heated to reflux for 2h under magnetic stirring. Subsequently the reaction was cooled at r.t, and water was removed by evaporation affording the desired product SS33 (**6)** (0.421 g, yield 95%). ^1H NMR (400 MHz, MeOD , 25 °C): δ = 8.1 (m, 1H, CONH-Ar), 7.95 (m, 1H, maleimide-CONH),

6.84 (s, 2H, maleimide H) 6.68 (d, 1H, aromatic ring H), 6.45 (d, 1H, aromatic ring H), 6.30 (dd, 1H, aromatic ring H), 3.97- 3.94 (m, 2H, Ar-OC<u>H</u>$_2$), 3.66 (PEG chain), 2.35-2.31 (m, 2H, C<u>H</u>$_2$CONH-Ar) 2.23-2.19 (m, 2H, maleimide-C<u>H</u>$_2$CONH) 1.90-1.87 (m, 2H, C<u>H</u>$_2$CH$_2$CONH-Ar), 1.69-1.59 (m, 4H, maleimide-C<u>H</u>$_2$CH$_2$C<u>H</u>$_2$CH$_2$CONH), 1.36-1.30 (m, 2H, maleimide-CH$_2$C<u>H</u>$_2$CH$_2$ CH$_2$CONH).

f. 05. Synthesis of the catechol-PEG5000 co-surfactant (SS20_A)

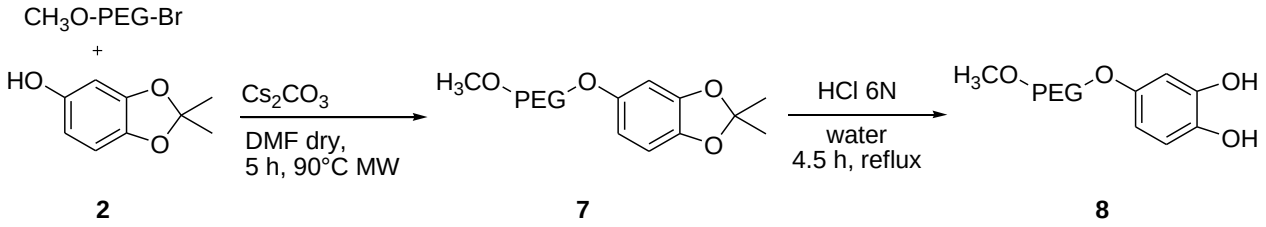

2 **7** **8**

*Scheme 2. Synthetic pathway leading to the SS20_A (**8**).*

f. 05. 1 Synthesis of compound 7

CH_3O-PEG-Br (0.74g, 0.15 mmol) was added to a mixture of compound **2** (0.027g, 0.16 mmol) and Cs_2CO_3 (0.053g, 0.16 mmol) in dry DMF (7 mL). The reaction was heated by a microwave to 90°C. After 5h, the dispersion was filtered through celite and the solvent was evaporated. The crude was precipitated by treatment with small amount of EtOAc, and then collected by centrifugation; the purified product appeared as light brown solid (0.65g, yield 83%).

f. 05. 2 Synthesis of compound 8

A water solution (6 ml) of compound **7** (0.648 mg, 0.13 mmol) was treated with HCl 6N (3 μl) in order to remove protecting group acetonide, and heated up at reflux for 5 h. Then water was evaporated and the residue was crystallized twice with methanol/ diethyl ether leading to the desired product SS20_A (**8**) (0.401 g, yield 61%). Additional 0.046 g of product **8** were recovered from the crystallization water by precipitation with diethyl ether and subsequent filtration thus increasing the isolated yield to an overall 68%. ^{1}H NMR (400 MHz, MeOD , 25 °C): δ = 6.68 (d, 1H, aromatic ring H), 6.45 (d, 1H, aromatic ring H), 6.30 (dd, 1H, aromatic ring H), 4.05- 4.02 (m, 2H, Ar-OC<u>H</u>$_2$), 3.66 (PEG chain), 3.38 (s, 3H, OC<u>H</u>$_3$).

f. 06. Synthesis of the catechol (c) co-surfactant: synthesis of the brominated PEG derivative 12

We obtained the compound **12** following the procedure reported in literature by Cozzi et al[21] and as we have already described in our previous work[22]. PEG samples were melted at 100°C in vacuum for 1h before their employment in order to remove traces of moisture. At the end of the reaction, we roughly purified PEG derivates by evaporating the solvent in vacuum, solving the residue in a small volume of CH_2Cl_2 and adding diethyl ether (around 100 mL/g of polymer), under stirring and at 0°C. Then the precipitate was filtered and the solid was repeatedly washed with fresh diethyl ether.

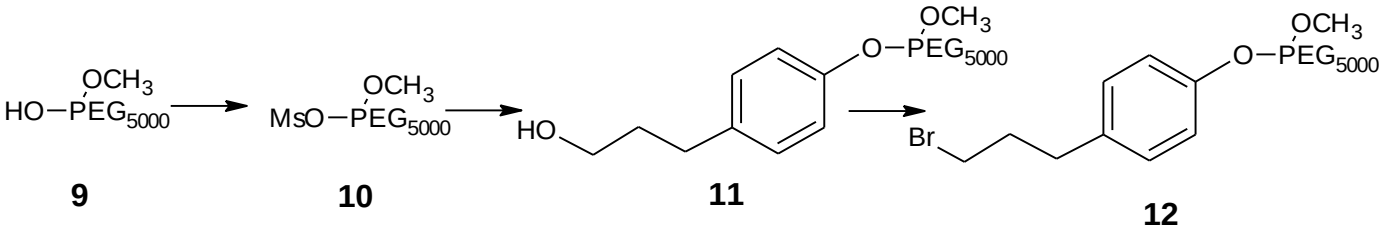

*Scheme 3: Preparation of the brominated PEG derivative **12**.*

f. 06. 1 Synthesis of compound 10

Mesyl chloride (93 μl, 1.2 mmol) dissolved in dry DCM (3 ml) was added dropwise to a solution of methoxy-PEG5000 commercially available (2g, 0.4 mmol) and trioctylamine (700 μl, 1.6 mmol) in 3 ml of dry DCM, cooled to 0°C. The reaction was stirred for 15 min at this temperature, then left overnight at RT (quantitative yield). ^{1}H NMR (400 MHz, CDCl3, 25 °C) : δ = 4.40 (m, 2H, C$\underline{H}_2$OMs), 3.66 (PEG chain), 3.38 (s, 3H, OC$\underline{H}_3$), 3.08 (s, 3H, C$\underline{H}_3SO_3$).

f. 06. 2 Synthesis of compound 11

The methoxy-PEG5000 mesylate **10** (10.49 g, 2.07 mmol) was treated with the commercially available 3-(4-hydroxyphenyl)-1-propanol (629 mg, 4.13 mmol) in anhydrous DMF and in the presence of K_2CO_3 (1.43 g, 10.35 mmol).The reaction was heated up to 70°C for 20 h affording the compound **11** (yield 92%). ^{1}H NMR (400 MHz, MeOD , 25 °C) : δ = 7.07 (d, 2H, aromatic ring H), 6.82 (d, 2H, aromatic ring H), 4.10 (m, 2H; PEGCH_2C$\underline{H}_2$OAr), 3.66 (PEG chain), 3.57 (m, 2H, $CH_2CH_2C\underline{H}_2$OH), 3.38 (s, 3H, OC$\underline{H}_3$), 2.63 (t, 2H, ArCH_2), 1.82 (m, 2H, $CH_2C\underline{H}_2CH_2$).

f. 06. 3 Synthesis of compound 12

The compound **11** (1g, 0.195 mmol) was solved in 5 ml of anhydrous DCM in the presence of triethylamine (81 μl, 0.584 mmol) and cooled to 0°C with an ice-bath. Then PBr_3 (55 ml, 0.584 mmol) was added in small portions under magnetic stirring. The reaction was left at r.t. overnight leading to the desired derivative **12**. In this case, in addition to diethyl ether precipitation and washing, the product was also purified with HPLC using a C18 reverse column. We applied the following HPLC eluant conditions: from 85% H_2O/ 15% CH_3CN to 100% CH_3CN with a flow rate 15 ml/min (yield 70%).^{1}H NMR (400 MHz, MeOD , 25 °C) : δ = 7.15 (d, 2H, aromatic ring H), 6.75 (d, 2H, aromatic ring H), 4.10 (m, 2H, PEG$CH_2C\underline{H_2}$OAr), 3.66 (PEG chain), 3.42 (m, 2H, CH_2Br), 3.36 (s, 3H, $OC\underline{H_3}$), 2.73 (t, 2H, $ArCH_2$), 2.12 (m, 2H; $CH_2C\underline{H_2}CH_2$).

f. 06. 4 Synthesis of the mono-catechol (c) co-surfactant (16)

We reported in the *Scheme 4* below the synthetic pathway that we wanted to follow in order to produce the derivative **16.** It is an example of type- (II) procedure where the PEG chain is bound to a mono- or di-catechol-diamine fragment, already obtained.

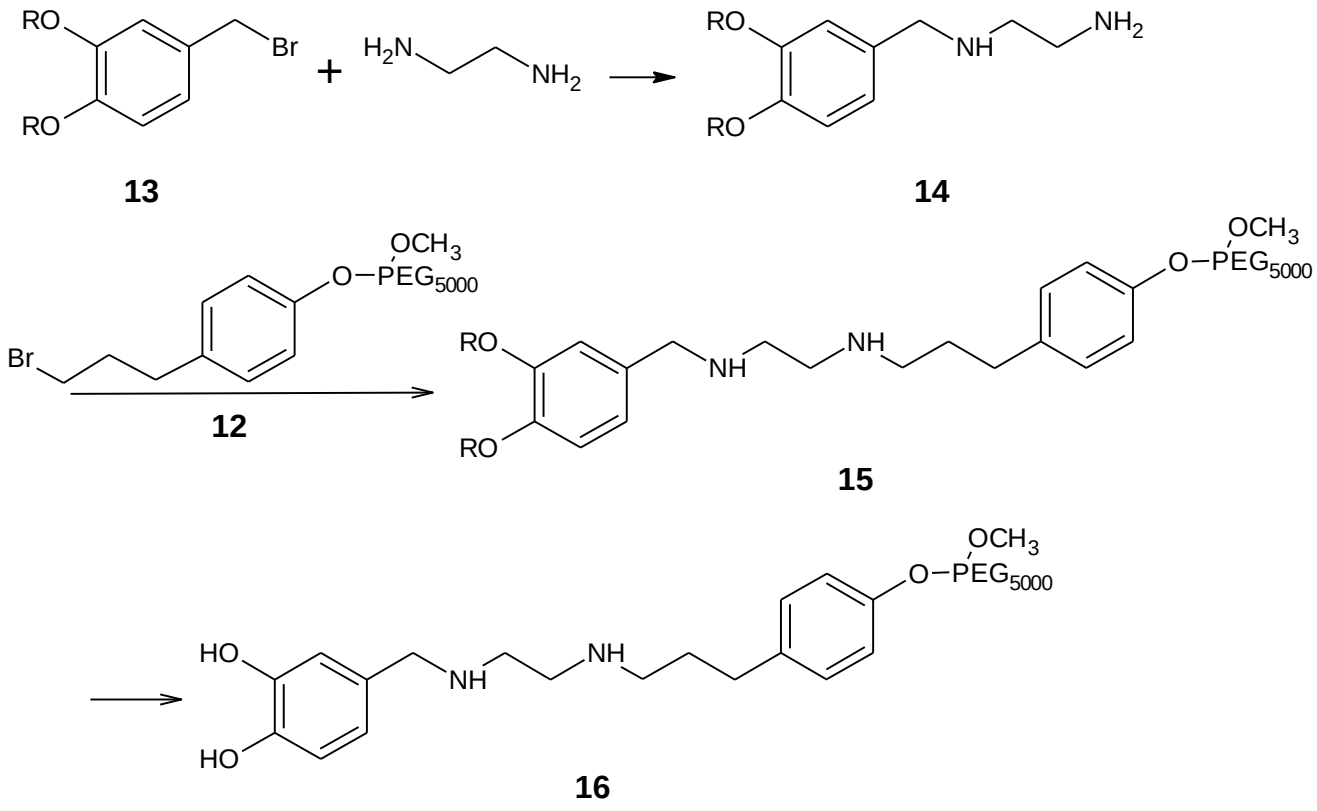

*Scheme 4: General preparation of the desired mono-catechol **16**.*

f. 06. 5 Synthesis of the mono-catechol (c) co-surfactant: *tert*-butyldimethylsilyl (TBDMS) ether protecting group

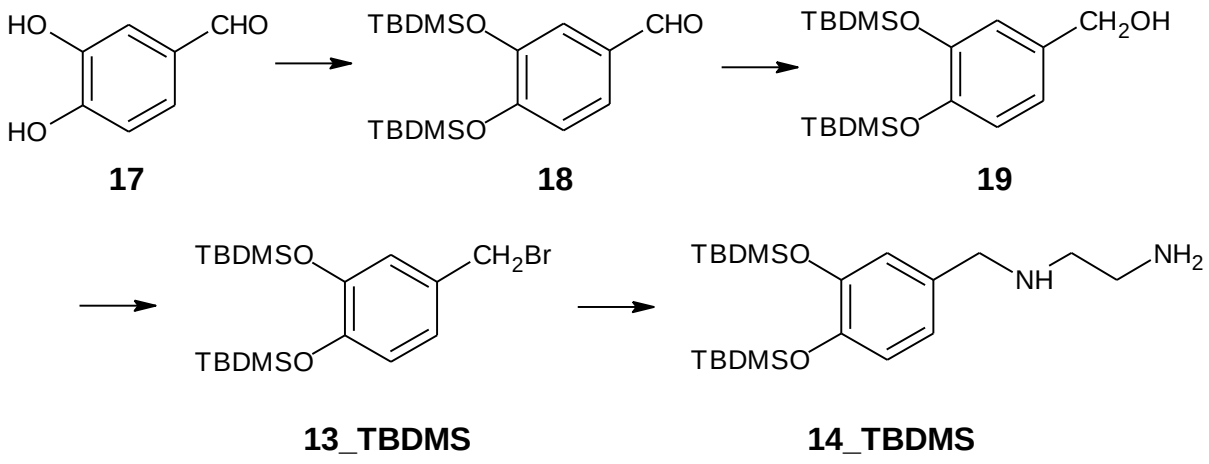

*Scheme 5: Preparation of the derivative 14 with **TBDMS** protecting group.*

f. 06. 6 Synthesis of compound 18

The product **18** was achieved according with a method reported in literature[25] starting from the commercially available 3,4-dihydroxybenzaldehyde **17** (100 mg, 0.72 mmol), solved in dry DCM (4 ml) in the presence of TEA (400 μl, 2.88 mmol). The reaction was cooled to 0°C and then a solution of TBDMS-chloride in a few ml of anydrous DCM was added to the system. After the addition, we needed to join dry THF to increase the reaction solubility. The mixture was stirred for 4 h at r.t. and evaporated. The residue was treated with water and extracted with diethyl ether. The organic phase was washed with brine, dried with anydrous Na_2SO_4, filtered off and finally evaporated. The crude was subjected to column chromatography (silica gel, hexane/EtOAc 95/5) to give **18** (0.194 g, yield 74 %).^{1}H-NMR (400 MHz, $CDCl_3$, 25 °C): δ = 9.71 (s, 1H, CHO), 7.28-7.26 (dd, 1H, aromatic ring H), 7.17 (d, 1H, aromatic ring H), 6.86- 6.84 (d, 1H, aromatic ring H), 0.90 (s, 18H, 2 × (C$\underline{H}_3$)$_3$ of TBDMS), 0.14 (s, 6H, (C$\underline{H}_3$)$_2$ of TBDMS), 0.13 (s, 6H, (C$\underline{H}_3$)$_2$ of TBDMS).

f. 06. 7 Synthesis of compound 19

$NaBH_4$ (32 mg, 0.85 mmol) was added in small portions to a solution of compound **18** (0.2501 g, 0.683 mmol) in dry THF (5 ml), refrigerated at 0°C thanks to an ice-bath. The reaction was stirred for 2h and thirty at r.t., but we evaluated by monitoring the reaction with TLC that it did not go to completeness, so we joined additional $NaBH_4$ (7 mg, 0.17 mmol). Finally we treated the mixture with dilute HCl and extracted the product with AcOEt. The organic layer was washed with water until neutral pH, then dried with anydrous Na_2SO_4 and evaporated in vacuum.(0.2258 g, yield 90%).^{1}H-NMR (400 MHz, $CDCl_3$, 25 °C): δ = 6.87-6.82 (m, 3H, aromatic ring H), 4.57 (s, 2H, C$\underline{H}_2$OH), 1.01 (s, 18H, 2 × (C$\underline{H}_3$)$_3$ of TBDMS), 0.22 (s, 12H, 2 × (C$\underline{H}_3$)$_2$ of TBDMS).

f. 06. 8 Synthesis of compound 13_TBDMS

We achieved the product **13_TBDMS** drawing inspiration from a synthetic pathway reported in literature[26]. PBr_3 (132 μl, 1.22 mmol) was added dropwise to a solution of **19** (226 mg, 0.62 mmol) in dry DCM (2 ml) at 0°C. After 30 min, the mixture was warmed to r.t. and magnetically stirred for 1 h. The crude was poured on ice and extracted three times with Et_2O; the organic phase was dried with Na_2SO_4 and evaporated. (0.218 g, yield 82%). ^{1}H-NMR (400 MHz, $CDCl_3$, 25 °C): δ = 6.89-6.76 (m, 3H, aromatic ring H), 4.44 (s, 2H, C$\underline{H}_2$Br), 1.01 (s, 9 H, (C$\underline{H}_3$)$_3$ of TBDMS), 1.00 (s, 9 H, (C$\underline{H}_3$)$_3$ of TBDMS), 0.22 (s, 12H, 2 × (C$\underline{H}_3$)$_2$ of TBDMS).

f. 06. 9 Synthesis of compound 14_TBDMS

Also the product **14_TBDMS** was obtained drawing inspiration from a method already reported in literature[27]. To a solution of ethylenediamine (1.69 ml, 25.3 mmol) in toluene (5 mL) was added dropwise a solution of **13_TBDMS** (0.218g, 0.506 mmol) dissolved in toluene (1 mL) over a period of 25 min at r.t.. Then the reaction was heated up to reflux for 4 h followed by treatment of a water solution of NaOH (90 mg in 400 μL of H_2O). After that the solvent and excess diamine were evaporated in vacuum affording a residue which was taken up in DCM, washed with H_2O and dried on anhydrous Na_2SO_4.(0.1575 mg, yield 75%). ^{1}H-NMR (400 MHz, $CDCl_3$, 25 °C): δ = 6.78-6.76 (m, 3H, aromatic ring H), 3.68 (s, 2H, Ar-C$\underline{H}_2$NH), 2.83-2.80 (t, 2H, NHC$\underline{H}_2$), 2.69-2.63 (m, 2H, C$\underline{H}_2$NH$_2$), 0.98 (s, 9 H, (C$\underline{H}_3$)$_3$ of TBDMS), 0.97 (s, 9 H, (C$\underline{H}_3$)$_3$ of TBDMS), 0.18 (s, 12H, 2 × (C$\underline{H}_3$)$_2$ of TBDMS). ESI-MS: m/z 411.5 [M+H]+.

f. 06. 10 Synthesis of the mono-catechol (c) co-surfactant: investigation of reactivity of 14_TBDMS

We have designed the reaction reported in the *Scheme 6* to investigate in detail why the coupling between the compounds **14_TBDMS** and **12** did not afford derivative **16**.

.

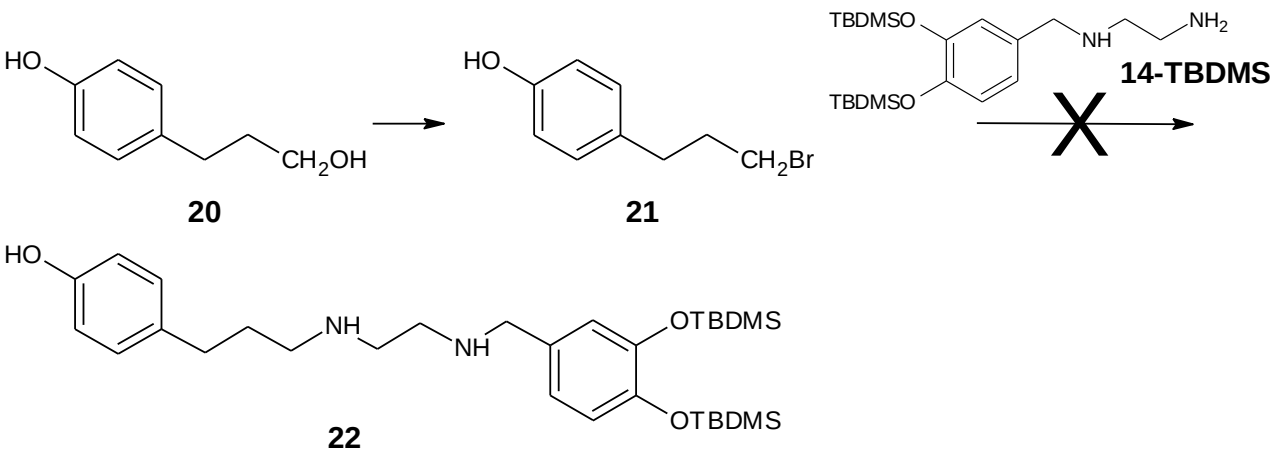

*Scheme 6: Preparation of the derivative **22**.*

f. 06. 11 Synthesis of compound 21

The product **21** was achieved following the procedure described in the literature to achieve 4-(2-Bromoethyl)phenol compound[28]. The commercially acquirable 3-(4-hydroxyphenyl)propanol (250 mg, 1.64 mmol) was dissolved in 48 wt % HBr (1.3ml) affording a orange solution that was heated up to 80°C and stirred for 16h. After that the reaction was warmed to r.t. and extracted with DCM. The organic phase was dried on anhydrous Na_2SO_4, filtered off and finally evaporated. (0.3551g, quantitative yield). ^{1}H-NMR (400 MHz, $CDCl_3$, 25 °C): δ = 7.09 (d, 2H, aromatic ring H), 6.80 (d, 2H, aromatic ring H), 3.41 (t, 2H; PEG$CH_2C\underline{H}_2OAr$), 2.73 (t, 2 H, $ArCH_2$), 2.19-2.10 (m, 2H, $CH_2C\underline{H}_2CH_2$).

f. 06. 12 Synthesis of the mono-catechol (c) co-surfactant: acetonide protecting group

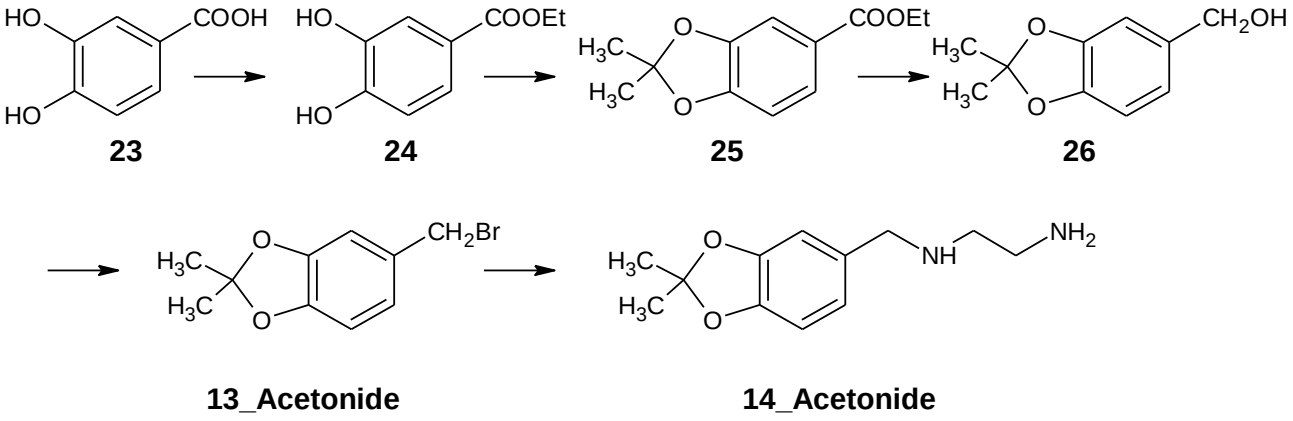

*Scheme 7: Preparation of the derivative **14** with acetonide protecting group.*

f. 06. 13 Synthesis of compound 24

We produced the compound **24** following the method reported in literature[29]. Concentrated H_2SO_4 (80 μl) was added dropwise to a solution of 3,4-dihydroxybenzoic acid (500 mg, 3.24 mmol) in EtOH (7ml). Then the reaction was heated to reflux for 4h. Since by monitoring with TLC, we have again observed the presence of starting material **23**, we added additional 5 drops of concentrated H_2SO_4 and we maintained the heating overnight. After evaporation of the solvent, the residue was treated with water and the product extracted with diethyl ether. The organic phase was washed with $NaHCO_3$ water solution, water and salt, dried on Na_2SO_4 and evaporated. (405 mg, yield 69%). ^{1}H-NMR (400 MHz, $CDCl_3$, 25 °C): δ = 7.26-7.23 (m, 2H, aromatic ring H), 6.63-6.61 (m, 1H, aromatic ring H), 4.13-4.05 (m, 2H, $OC\underline{H}_2CH_3$), 1.18-1.13 (m, 3H, $OCH_2C\underline{H}_3$).

f. 06. 14 Synthesis of compound 25

We have followed the procedure described on a patent[30]. A solution of **24** (200 mg, 1.10 mmol), DMP (271 μl, 2.20 mmol) and p-toluensolfonic acid as catalyst (8 mg) in dry toluene (15 ml) was heated to reflux for 20h. Then toluene was removed and the residue was extracted with AcOEt, washed respectively with a dilute water solution of $NaHCO_3$, water and salt, dried on Na_2SO_4 and evaporated. The crude was subjected to column chromatography (silica gel, hexane/EtOAc from 90/10 to 80/20) to give **25** as yellow solid (yield 49%).^{1}H-NMR (400 MHz, $CDCl_3$, 25 °C): δ = 7.63-7.60 (m, 1H, aromatic ring H), 7.41-7.39 (m, 1H, aromatic ring H), 6.77-6.72 (m, 1H, aromatic ring H), 4.36-4.30 (m, 2H, $COOC\underline{H}_2CH_3$), 1.70 (s, 6H, acetonide), 1.39-1.35 (m, 3H, $COOCH_2C\underline{H}_3$).

f. 06. 15 Synthesis of compound 26

According to the process detailed in the literature[31], a solution of compound **25** (140 mg, 0.63 mmol) in dry THF (3 ml) was added dropwise to a suspension of LiAlH4 (40 mg, 1.05 mmol) in dry THF (3 ml), under N_2, cooled at 0°C with an ice bath. Then the reaction was warmed to r.t. and stirred overnight. The reaction was quenched with AcOEt, filtered on celite and purified by chromatography (silica gel, hexane/EtOAc from 75/25 to 50/50), affording an oil (62.4 mg, yield 55%).^{1}H-NMR (400 MHz, $CDCl_3$, 25 °C): δ = 6.82-6.78 (m, 2H, aromatic ring H), 6.74-6.71 (m, 1H, aromatic H), 4.59 (s, 2H, $C\underline{H}_2OH$), 1.70 (s, 6H, acetonide).

f. 06. 16 Synthesis of compound 13_Acetonide

A solution of PBr_3 (150 μl, 1.58 mmol) in dry Et_2O (2 ml) was added during 15 min to a solution of **26** (0.26 g, 1.44 mmol) in dry Et_2O (3 ml) at 0°C. Then the reaction was warmed to r.t. and stirred for 30 min. The crude was poured on ice, quenched with water and stirred for 1h. Then the product was extracted with DCM and the organic phase was washed with salt, dried with Na_2SO_4 and evaporated. (0.278 mg, yield 79%). ^{1}H-NMR (400 MHz, $CDCl_3$, 25 °C): δ = 6.85-6.80 (m, 2H, aromatic ring H), 6.69-6.66 (m, 1H, aromatic H),4.49 (s, 2H, $C\underline{H}_2Br$), 1.70 (s, 6H, acetonide).

f. 06. 17 Synthesis of compound 14_Acetonide

A solution of **13-Acetonide** (50 mg, 0.21 mmol) in dry THF (210 μl) was added with a syringe pump (8 μl/min) to a solution of ethylenediamine (700 μl, 10.5 mmol) in dry THF (800 μl) at r.t. After 1h, since the reaction was complete as monitored by TLC, the mixture was treated with aqueous NaOH (10.4 mg, 0.26 mmol in 1 ml of water), and then extracted three times with DCM (3 × 3 ml). The organic phase was dried with with Na_2SO_4, filtered off and evaporated in vacuum. (33.6 mg, yield 72%). ^{1}H-NMR (300 MHz, $CDCl_3$, 25 °C): δ = 6.76-6.72 (m, 2H, aromatic ring H), 6.67 (d, 1H, aromatic ring H), 3.71 (s, 2H, Ar-C$\underline{H}_2$NH), 2.84-2.81 (t, 2H, NHC$\underline{H}_2$), 2.71-2.68 (m, 2H, C$\underline{H}_2$NH$_2$), 1.68 (s, 6H, acetonide).

f. 06. 18 Synthesis of the mono-catechol (c) co-surfactant: benzyl ether protecting group

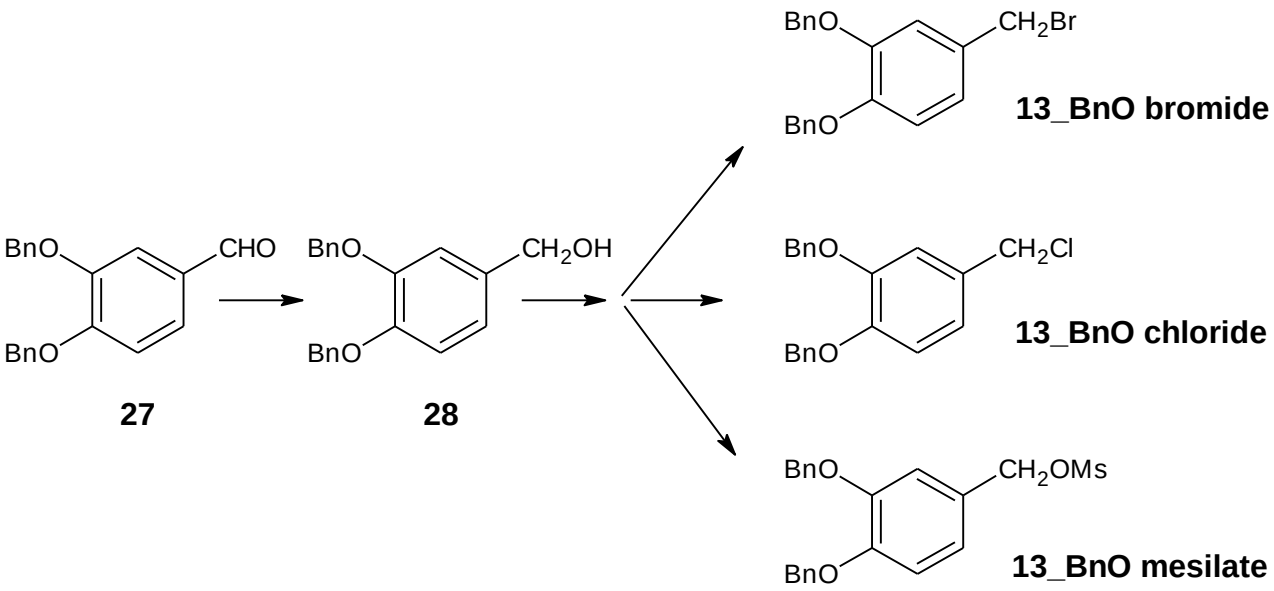

*Scheme 8: Preparation of different derivatives **13** with **benzyl ether** protecting group.*

The derivative **13_BnO bromide** was produced according with our previous work[22]. The treatment of compound **28** with $SOCl_2$ or mesyl chloride allowed us to achieve respectively **13_BnO chloride** and **13_BnO mesilate.**

f. 07. Preparation of PEG-ylated NPs

f. 07. 1 Preparation of PEG-ylated NPs from those obtained by hot-injection

We have prepared 3 different batches of PEG-ylated NPs starting from 9.6 nm iron oxide NPs prepared by hot-injection. A solution of PEG SS20_A or PEG SS33 (10.65 mg) or a mixture of both of them (5.33 mg each) in $CHCl_3$ (500 μl) was added to 500 μl of NP hexane solution (2.13 mg of iron oxide NPs). The NPs was heated to 70 °C for 2 days, then precipitated with hexane, collected by centrifugation and solved in deionized water (5 ml). The NPs were purified by dialysis for 2 days giving a little precipitate that was left in the tube.

f. 07. 2 Preparation of PEG-ylated NPs from those obtained by co-precipitation

3 ml of the water suspension of co-precipitated NPs (around 30 mg of Fe_3O_4) were treated with a mixture of PEG SS20_A and PEG SS33 (107 and 119 mg respectively). Then they were stirred and heated to 70 °C for 24h under N_2.Finally NPs were solved in deionized water(final volume of 36.9 ml) and purified by dialysis for 1 day, frequently changing water.

g. Characterization of PEG-ylated NPs

g. 01. DLS of PEG-ylated NPs

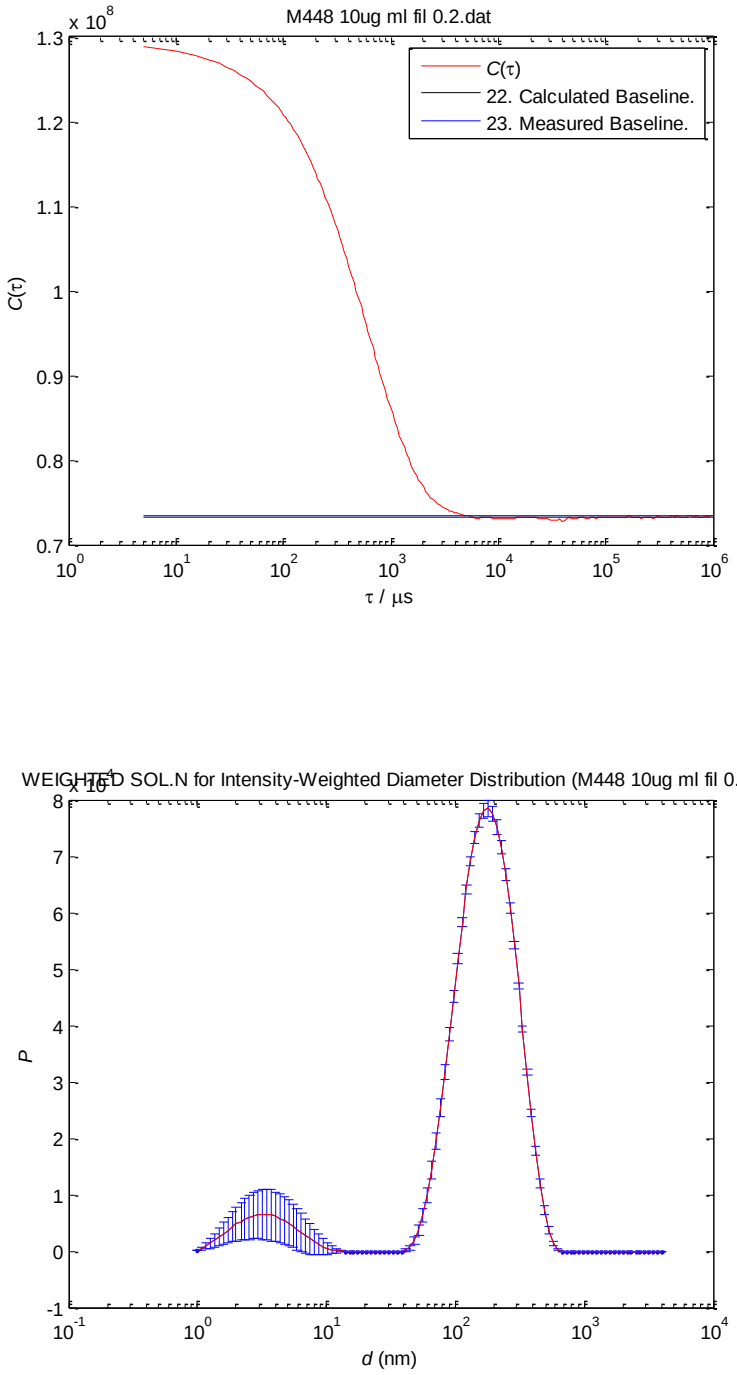

Fig 15. DLS autocorrelogram (top) and intensity-weighted diameter distribution (bottom) of co-precipitated NPs (M 448) coated with PEG SS20_A and PEG SS33. The mean diameter is 240 nm.

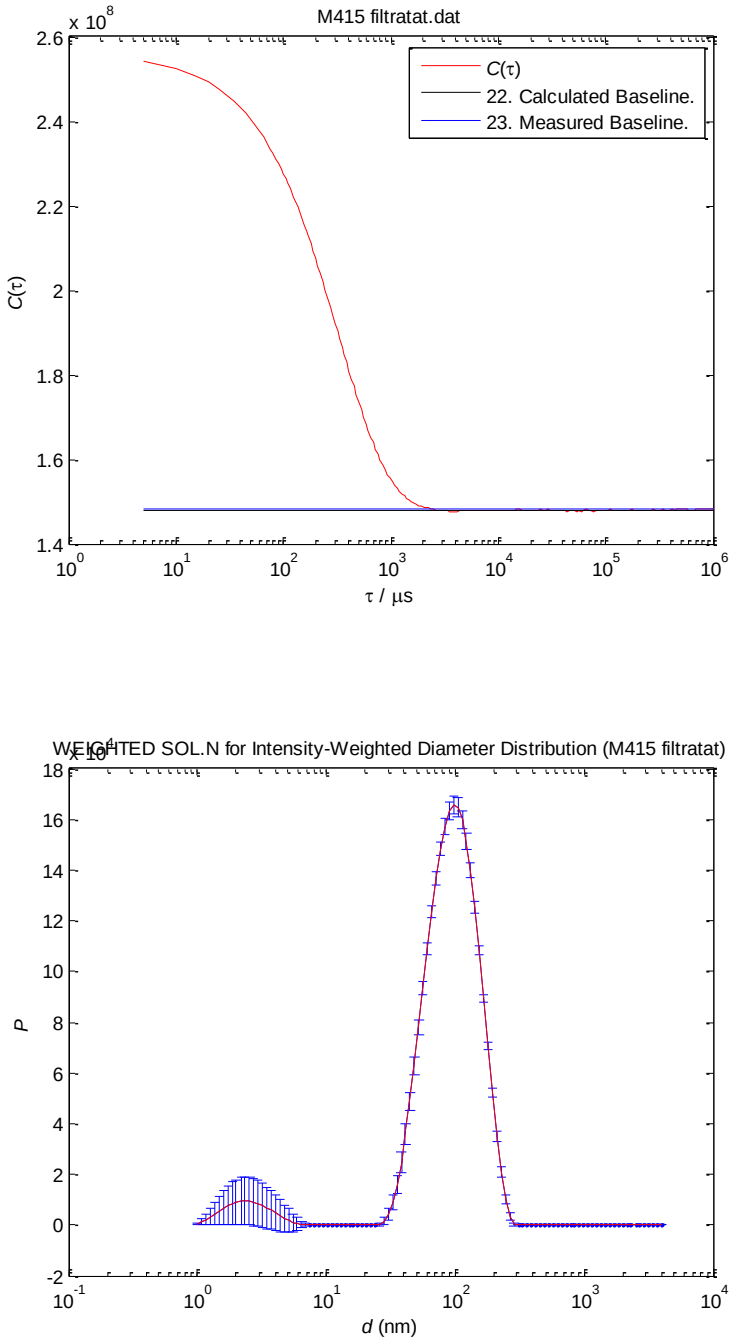

Fig 16. DLS autocorrelogram (top) and intensity-weighted diameter distribution (bottom) of solvothermal NPs (M 415) coated with PEG SS20_A and PEG SS33. The mean diameter is 120 nm.

g. 02. CHN analysis data

	Calculated	Experimental	
	MeO - SS20A	**M415**	*% organic in the NPs*
C	54,85%	**40,41%**	*74%*
H	9,09%	**6,48%**	*71%*
N	0%	**0,09%**	
O	36,06%		

	Maleimm - SS33	**M420**	*% organic in the NPs*
C	55,08%	**32,87%**	*60%*
H	8,93%	**5,21%**	*58%*
N	0,77%	**0,51%**	*66%*
O	35,22%		

	Maleimm - SS33 & MeO - SS20A	**M448**	*% organic in the NPs*
C	55,08%	**50,62%**	*92%*
H	8,93%	**7,73%**	*87%*
N	0,77%	**0,33%**	*43%*
O	35,22%		

Fig 17. Results of the CHN analysis for solvothermal NPs (M415 and M420) and for co-precipitated NPs (M 448) coated with PEG SS20_A and PEG SS33.

g. 03. Fluorescent assay to quantify maleimide groups

We reported in the Fig. 16 an example of calibration curve used to quantify maleimido groups by fluorescence measurement.

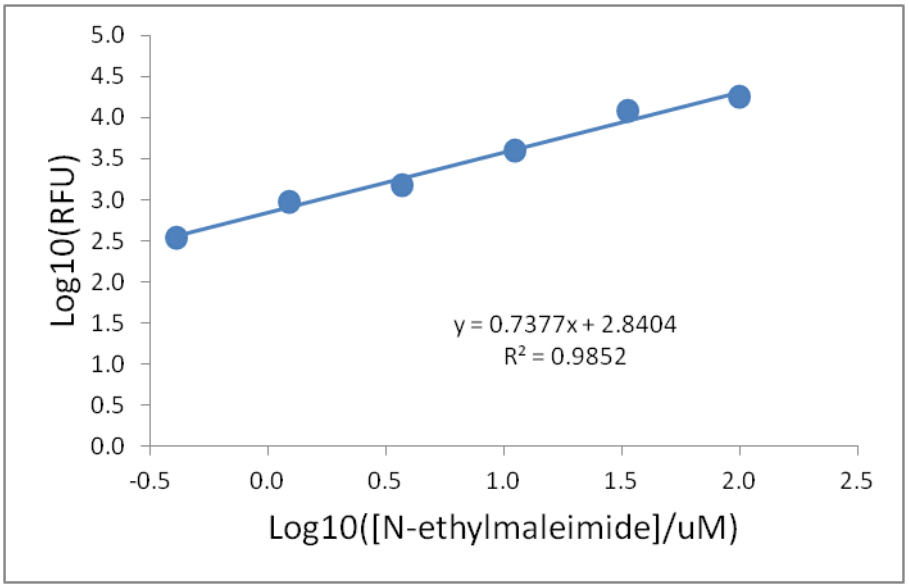

Fig 18. Maleimide calibration curve

h. Characterization methods and instruments

^{1}H-NMR spectra were registered with a Bruker Avance spectrometer in (^{1}H: 400 MHz or 300 MHz). ^{1}H-NMR of PEG derivatives (around 10 mg of solid in 0.4 ml of deuterated solvent) were collected with 32 scan and a recycle delay (D1 time parameter) of 10 s. HPLC purification was performed by BiotageTM C18 reverse phase chromatography. Transmission electron microscopy (TEM) images were taken with a Zeiss LIBRA 200FE microscope (Carl Zeiss AG, Oberkochen, Germany). The TEM sample was achieved by evaporating in air a drop of diluted NP solution on a carbon covered copper grid. FTIR spectra were registered with a Thermo Nicolet NEXUS 670 FTIR spectrometer (Thermo Fisher Scientific, Waltham, MA, USA). The sample for FTIR was produced by grinding and pelleting dry NPs with KBr (NP:KBr 1:100 w/w). Hydrodynamic diameter was measured employing a BI 90 Plus (Brookhaven Instruments Corporation, Holtsville, NY, USA) at $\theta = 90°$. Fluorescence measures were registered by a Synergy 2 Biotek Instrument.

References

[1] Karakoti , A. S., Das , S., Thevuthasan , S., Seal , S., PEGylated Inorganic Nanoparticles, *Angew. Chem. Int. Ed.*, **2011** , 50 , 1980-1994.

[2] Malmsten, M., Emoto, K., Van Alstine, J. M., Effect of Chain Density on Inhibition of Protein Adsorption by Poly(ethylene glycol) Based Coatings, *J. Colloid Interface Sci.*, **1998**, 202, 507-517.

[3] Howard, M. D., Jay, M., Dziublal, T. D., Lu, X. L., PEGylation of nanocarrier drug delivery systems: State of the art, *J. Biomed. Nanotechnol.*, **2008**, 4, 133-148.

[4] Choi , H. S., Ipe , B. I., Misra , P., Lee , J. H., Bawendi , M. G., Frangioni , J. V., Tissue- and Organ-Selective Biodistribution of NIR Fluorescent Quantum Dots, *Nano Lett.*, **2009** , 9 , 2354-2359.

[5] Zhang, G. D., Yang, Z., Lu, W., Zhang, R., Huang, Q., Tian, M., Li, L., Liang, D., Li, C., Influence of anchoring ligands and particle size on the colloidal stability and in vivo biodistribution of polyethylene glycol-coated gold nanoparticles in tumor-xenografted mice, *Biomaterials*, **2009**, 30, 1928- 1936.

[6] Eck, W., Craig, G., Sigdel, A., Ritter, G., Old, L. J., Tang, L., Brennan, M. F., Allen, P. J., Mason, M. D., PEGylated Gold Nanoparticles Conjugated to Monoclonal F19 Antibodies as Targeted Labeling Agents for Human Pancreatic Carcinoma Tissue, *ACS Nano*, **2008**, 2, 2263-2272.

[7] Amstad, E., Zurcher, S., Mashaghi, A., Wong, J.H., Textor, M., Reimhult, E., Surface Functionalization of Single Superparamagnetic Iron Oxide Nanoparticles for Targeted Magnetic Resonance Imaging, *Small*, **2009**, 5, 1334-1342.

[8] Amstad, E., Gillich, T., Bilecka, I., Textor, M., Reimhult, E., Ultrastable iron oxide nanoparticle colloidal suspensions using dispersants with catechol-derived anchor groups, *Nano Lett.*, **2009**, 9, 4042–8.

[9] Li, Z., Wei, L., Gao, M. Y., Lei, H., One-pot reaction to synthesize biocompatibile magnetite nanoparticles, *Adv. Mater.*, **2005**, 17, 1001-1005.

[10] Jun, Y-w., Lee, J.-H., Cheon, J., Chemical design of nanoparticle probes for high-performance magnetic resonance imaging, *Angew. Chem. Int. Ed.*, **2008**, 47, 5122-5135.

[11] Peng, S.,Wang, C., Xie, J., Sun, S., Synthesis and Stabilization of Monodisperse Fe Nanoparticles *J. Am. Chem. Soc.* **2006,** 128, 10676-10677.

[12] Na, H.B., Palui, G.,Rosenberg, J.T., Ji, X., Grant; S.C., Mattoussi, H., Multidentate Catechol-Based Polyethylene Glycol Oligomers Provide Enhanced Stability and Biocompatibility to Iron Oxide Nanoparticles, *ACS Nano*, **2012**, 6, 389-399.

[13] Kim, S.-W., Kim, S., Tracy, J. B., Jasanoff, M., Bawendi, M., Phosphine Oxide Polymer for Water-Soluble Nanoparticles, *J. Am. Chem. Soc.*, **2005**, 127, 4556-4557.

[14] Xu, C., Xu, K., Gu, H., Zheng, R., Liu, H. , Zhang, X,, Guo, Z., Xu, B., Dopamine as a robust anchor to immobilize functional molecules on the iron oxide shell of magnetic nanoparticles, *J. Am. Chem. Soc.*, **2004**,126 9938–9939.

[15] Xie., J, Xu., C, Kohler., N, Hou, Y., Sun, S., Controlled PEGylation of monodisperse Fe_3O_4 nanoparticles for reduced non-specific uptake by macrophage cells, *Adv. Mater.*, **2007**, 19, 3163–3166.

[16] Calcagnile, P., Fragouli, D., Bayer, I. S., Anyfantis, G. C., Martiradonna, L., Cozzoli, P. D., Cingolani, R., Athanassiou, A., Magnetically Driven Floating Foams for the Removal of Oil Contaminants from Water, *ACS Nano*, **2012**, 6, 5413–5419.

[17] Mondini, S., Ferretti, A. M., Puglisi, A., Ponti, A., Pebbles and PebbleJuggler: Software for Accurate, Unbiased, and Fast Measurement and Analysis of Nanoparticle Morphology from Transmission Electron Microscopy (TEM) Micrographs, *Nanoscale*, **2012**, 4 , 5356–5372. PEBBLES is freely available from the authors, http://pebbles.istm.cnr.it.

[18] Massart , R., Preparation of aqueous magnetic liquids in alkaline and acidic media, *IEEE Trans. Magn.*, **1981** , 17 , 1247-1248.

[19] Ling, D., Hyeon, T, Chemical Design of Biocompatible Iron Oxide Nanoparticles for Medical Applications, *Small*, **2013**, 9, 1450-1466.

[20] Hao, R., Xing, R., Xu, Z., Hou, Y., Gao, S., Sun, S., Synthesis, Functionalization, and Biomedical Applications of Multifunctional Magnetic Nanoparticles, *Adv. Mater.*, **2010**, 22, 2729-2742.

[21] Annunziata, R., Benaglia, M., Cinquini, M., Cozzi, F., Soluble-Polymer-Supported Synthesis of β-Lactams on a Modified Poly(ethylene glycol), *Chem. Eur. J.*, **2000**, 6, 133–8.

[22] Mondini, S., Drago, C., Ferretti, A. M., Puglisi, A., Ponti, A., Colloidal stability of iron oxide nanocrystals coated with a PEG-based tetra-catechol surfactant, *Nanotechnology*, **2013**, 24, 105702-105716.

[23] Yu, S-Y, Zhang, H-J., Yu, J.-B., Wang, C., Sun, L. N., Shi, W. D., Bifunctional Magnetic-Optical Nanocomposites: Grafting Lanthanide Complex onto Core-Shell Magnetic Silica Nanoarchitecture, *Langmuir*, **2007**, 23, 7836-7840

[24] Fujiwara, K., Sato, T., Sano, Y., Norikura, T., Katoono, R., Suzuki, T., Matsue, H., Total Synthesis of Thelephantin O, Vialinin A/Terrestrin A, and Terrestrins B–D, *J. Org. Chem.*, **2012**, 77, 5161-5166.

[25] Lee, C. Y., Sharma, A., Cheong, J. E., Nelson, J. L., Synthesis and antioxidant properties of dendritic polyphenols, *Bioorg. Med. Chem. Lett.*, **2009**, 19, 6326-6330.

[26] Brun, K. A., Linden, A., Heimgartner, H., New Optically Active 2H-Azirin-3-amines as Synthons for Enantiomerically Pure 2,2-Disubstituted Glycines: Synthesis of Synthons for Tyr(2Me) and Dopa(2Me), and Their Incorporation into Dipeptides, *Helvetica Chimica Acta*, **2002**, 85, 3422-3443.

[27] Hamada, A., Yaden, E. L., Horng, J. S., RuffoloJr. , R. R., Patil, P. N.,Miller D. D., N-Substituted imidazolines and ethylenediamines and their action on α- and β-adrenergic receptors, *J. Med. Chem.*, **1985**, 28, 1269-1273.

[28] Grice, C. A., Tays, K. L., Savall, B. M., Wei, J., Butler, C. R., Axe, F. U., Bembenek, S. D., Fourie, A. M., Dunford, Paul J., Lundeen, K., Coles, F., Xue, X., Riley, J. P., Williams, K. N., Karlsson, L., Edward, J. P., Identification of a Potent, Selective, and Orally Active Leukotriene A4 Hydrolase Inhibitor with Anti-Inflammatory Activity, *J. Med. Chem.*, **2008**, 51, 4150-4169.

[29] Verma, A. K., Singh, H., Satyanarayana, M., Srivastava, S.P., Tiwari, P., Singh, A. B., Dwivedi, A. K., Singh, S. K., Srivastava, M., Nath, C., Raghubir, R., Srivastava, A. K., Pratap, R., Flavone-Based Novel Antidiabetic and Antidyslipidemic Agents, *J.of Med. Chem.*, **2012**, 55, 4551-4567.

[30] Tachdjian, C., Tang, X.Q., Karanewsky, D. S., Servant, G., Li, X., Zhang, F., Chen, Q., Zhang, H., Davis, T., Darmohusodo, V., Wong, M., Selchau, V., Novel flavors, flavors modifiers, tastants, taste enhancers, umami or sweet tastants, and/or enhancers and use thereof., *Patent*, International Publication Number **WO 2005/041684 A2**.

[31] Kita,Y., Arisawa, M., Gyoten, M., Nakajima, M., Hamada, R., Tohma, H.,Takada,T., Oxidative Intramolecular Phenolic Coupling Reaction Induced by a Hypervalent Iodine(III) Reagent: Leading to Galanthamine-Type Amaryllidaceae Alkaloids, *JOC*, **1998**, 63, 6625-6633.

o Aknowledgments

Considero questo dottorato la conclusione di un periodo di ricerca iniziato 11 anni fa.
Da un punto di vista lavorativo un doveroso grazie va quindi in primis al Dott. Alessandro Ponti che, in tutti questi anni trascorsi al CNR, è stato il mio responsabile scientifico.
Grazie anche alla Dott.ssa Alessandra Puglisi che, dopo un periodo trascorso lavorando assieme, ha accettato da ricercatrice universitaria di svolgere il ruolo di mio tutor per questo dottorato.
Grazie agli "studiosi di scienza" con cui ho condiviso parte di questi anni in laboratorio: Alberto, Alessandro, Anna, Claudio, Laura, Marcello, Marta, Primiano e Sandro.

E poi … grazie ai miei genitori … di tutto.

Grazie alle persone che in questi anni hanno fatto positivamente parte della mia vita.
Alle amiche storiche Gill e Marina.
A Silvia, che ha creduto ed investito nella nostra amicizia dimostrando che può nascere ovunque.
Alle amiche che ho conosciuto durante questi anni di lavoro: a Serena, la prima persona che vidi nel sottoscala di via Golgi, lei che ancora spera che io sappia prendere la vita con più leggerezza e la smetta di farle fare code in viaggio.
A Giusy, una forza della natura, che ogni volta mi ricorda che nella vita bisogna perseverare per ottenere ciò che si vuole.
Ad Elena, (al grido di: "è viola,è viola!"), che mi ha voluto bene nonostante la sgridassi un giorno sì e l'altro pure (e che forse ora non ne ha davvero più bisogno).
A Cristina, carattere tosto sì , un po'come me, ma con un cuore grande e sincero.
A chi, se lo vorrà, entrerà davvero a far parte della mia vita …

Voi mi avete accompagnato in questi anni e spero continuerete a farlo: nei momenti belli ed in quelli difficili che ci sono stati.
Voi mi avete fatto capire che l'amicizia, quella vera, resiste e che sono le persone, quelle speciali come voi, che fanno la differenza e per cui vale la pena di impegnarsi, confrontandosi ogni giorno per crescere assieme.
Vi voglio bene.

Sara

Ed ora, non potendo più storicamente ricoprire il ruolo di faraone e neanche (per ora) quello di Papa, permettetemi almeno di "fare la faraona"…

Example of final recipe:

Roast guinea fowl with chestnut, sage & lemon stuffing

Ingredients

- 1 small guinea fowl, about 1kg
- 8 rashers streaky bacon
- 50g soft butter
- 1 onion, unpeeled and thickly sliced
- 2 tbsp plain flour
- 350ml strong chicken stock
- cranberry sauce, roast potatoes and vegetables, to serve

For the stuffing

- 1 onion, chopped
- 25g butter
- 1 tbsp chopped sage
- 50g walnut, finely chopped
- 50g breadcrumb
- zest 2 lemons
- ¼ tsp ground mace
- 100g cooked chestnut, quartered
- 1 medium egg, beaten with a fork

Method

1. First make the stuffing. Soften the onion in the butter very gently, then stir in the sage and cook for 2 mins more. Scrape into a bowl with the chopped walnuts, breadcrumbs, lemon zest, mace, chestnuts and egg and mix together well. Season generously.
2. For the guinea fowl, wash and wipe out the inside cavity. Mix the butter with some seasoning, then push and spread some under the skin over the breasts, and rub the rest over the legs. Lay the bacon across the breasts, smoothing over, and season with some more pepper. Push the stuffing into the cavity (any extra can be rolled into balls and baked in the oven for the last 20 mins cooking time). You can cover and chill the guinea fowl now for up to 24 hours.
3. To roast, bring the bird out of the fridge 30 mins before. Heat oven to 200C/180C fan/gas 6. Sit the bird in a snug roasting tin with the sliced onion underneath. Roast for 15 mins, then lower the oven to 180C/160C fan/gas 4 and roast for a further 35-45 mins for a 1kg bird (or longer if bigger – use the timings for a roast chicken). Check the bird is done by piercing the inside of the thigh with a knife and making sure the juices are clear, not bloody. Lift the guinea fowl off the onions, onto a platter. Loosely cover with foil, top with a towel (to keep it warm), and rest while you make the gravy.
4. Pour off the juices from the roasting tray into a jug or bowl, and allow to settle. Spoon a tbsp of the fat on top back into the roasting tray, pop on the hob over a low heat (make sure your roasting tray is suitable or transfer contents to a pan), and stir in the flour until it isn't dusty anymore. Gradually stir in the stock, plus any meat juices after you've discarded the rest of the fat, and bubble gently until thickened. Season with salt, pepper, and pinches of sugar if it needs it, then strain into a gravy jug and discard the onions. Serve with the guinea fowl, spooning out the stuffing as you carve, plus cranberry sauce and plenty of vegetables.